UV-induced DNA Damage Detection in Long Oligonucleotide Sequences using EvaGreen®

by

Ebuka Penticost Ikegwuonu

A thesis submitted in partial fulfillment of the requirements for the degree of

Master of Science

Department of Chemistry
University of Alberta

Abstract

The exposure of DNA to UV radiation can lead to deletions, strand breaks or base modifications such as the formation of cyclobutane pyrimidine dimers (CPDs), [6-4] pyrimidine-pyrimidinones, and photohydrates, which may then lead to skin cancer. Different methods have been developed for the detection of UV-induced DNA damage, including molecular beacons, smart probes, mass spectrometry, high-performance liquid chromatography, comet assays, and electrophoresis. However, these methods have disadvantages, such as rigorous or cumbersome sample preparation procedures which may further damage the DNA, are sequence dependent, and/or are expensive. Recent studies have shown that EvaGreen® (EG®), a DNA intercalating dye, can be used to detect UV-induced DNA damage in short oligonucleotide sequences. In this study, we show a simple mix-and-read method of detecting UV-induced DNA damage using calf thymus DNA (ct-DNA), salmon sperm DNA (ss-DNA) and *E. coli* DNA samples. The ss-DNA and ct-DNA were approximately 2000 base pairs long. Samples were irradiated anoxically individually and later simultaneously with UVC lamps emitting at 254 nm with a power density of 75 W m^{-2}. Irradiated DNA samples were then hybridized with EG® after various irradiation times and the fluorescence measured using a plate reader at room temperature. The results obtained show that the fluorescence intensities decrease with increasing irradiation time, consistent with EG® being released in its lower fluorescent-intensity form from the damaged DNA. Therefore, EG® is a potential tool for the detection of UV-induced DNA damage in long oligonucleotide sequences, and further shows good prospects of potentially up to and including genomic DNA. Under these conditions for the individual irradiation experiments of ct-DNA and ss-DNA, ct-DNA with an Adenine-Thymine base pair percentage composition (AT %) of 58.1 % is damaged at a faster rate than the ss-DNA of AT % composition of 56.9 %, with average damage time constants of 82 ± 13 min and 143 ± 43 min, respectively.

In the simultaneous irradiation experiments of ss-DNA and ct-DNA under the same conditions, ss-DNA although with a lower AT% composition showed similar average damage time constant of 112 ± 25 min with ct-DNA of an average damage time constant of 101 ± 24 min within experimental errors. The simultaneous UVC irradiation of extracted cellular *E. coli* DNA, ss-DNA and ct-DNA showed that *E. coli* DNA with an AT% composition of 49.2 which is lower than that of both ss-DNA and ct-DNA showed a higher average time constant. Results from the simultaneous irradiation of *E. coli* DNA and ss-DNA showed that *E coli* DNA had a damage time constant of 69 ± 11 min while 63 ± 6 min was obtained for ss-DNA which are similar within statistical analysis, although *E. coli* DNA showed an observed higher average damage time constant of 105 ± 29 min when irradiated simultaneously with ct-DNA of average damage time constant 66 ± 12 min, which is consistent with results obtained from previous studies. Finally, the systematic and human error analysis associated with this method was evaluated in this study.

Preface

This thesis is an original work by Ebuka Penticost Ikegwuonu, under the supervision of Dr. Loppnow. No part of this thesis has been previously published.

Dedicated to

God almighty, humanity and everyone working in the field of skin cancer research.

Acknowledgement

I would firstly like to thank God almighty whom without His grace I would not have gotten this far.

My sincere appreciation and gratitude go to my graduate supervisor in the person of Dr. Glen Loppnow whose support and guidance were both crucial and decisive in making this research work a success.

I would like to thank the past members of the Loppnow research group in the persons of Dr. Sindhu Nair and Amira El-Yabzi for their inestimable contributions which in many ways shaped this research work.

I also want to thank my parents Mr. and Mrs. Leonard Ikegwuonu, and my siblings Ugochukwu, Ebele, Amara, Chukwuma, Chibuzor, Chidindu, and Wealth for their immense support, prayers and well wishes throughout my studies. I won't fail to show my gratitude to Gareth Lambkin of the Biological Sciences facility whose help was instrumental in getting this work completed.

My love goes to my friends Chisom, Jennifer, Emeka, Kunle, Valentine, Innocent, Jean Paul, Isaac, Nathaniel, Ebenezer Obiorah and his family, members of the DLCF campus fellowship, and so many others whose names are not written here for their love and encouragement which were both very necessary and important to the success of my graduate studies.

Finally, I would like to thank the members of my supervisory committee James Harynuk and Jon Veinot for their supervision, Dr. Ratmir Derda and his research group for allowing me to

use their lab, and the entire faculty of the chemistry department of University of Alberta who might have instructed and in one way or the other influenced the success of this work.

I will also be quick to admit that this research work wouldn't have been possible without the funding of the Department of Chemistry, University of Alberta.

Table of Contents

List of Tables

List of Figures

List of Abbreviations

2AP	2-aminopurine
6-4 PPs	6-4 pyrimidine-pyrimidinone dimers
6-CF	6-carboxyfluorescein dye
A	adenine
C	cytosine
ct-DNA	calf thymus DNA
CFCs	chlorofluorocarbons
CPD	cyclobutyl pyrimidine dimers
DNA	deoxyribonucleic acid
dsDNA	double stranded DNA
EG	EvaGreen®
EDTA	ethylenediaminetetraacetic acid
ELISA	enzyme-linked immunosorbent assay
FISH	fluorescence in-situ hybridization
FITC	fluorescein isothiocyanate
FAM	6-carboxyfluorescein
G	guanine
GC	gas chromatography
HPLC	high performance liquid chromatography
IHC	immunohistochemical assay

LC-ESI-MS	liquid chromatography electrospray ionization tandem mass spectrometry
LMPCR	ligation mediated PCR
LC	liquid chromatography
LOD	limit of detection
LOQ	limit of quantification
MB	molecular beacon
MB ch	chimeric molecular beacon
mtDNA	mitochondrial DNA
mRNA	messenger RNA
MS	mass spectrometry
PAGE	polyacrylamide gel electrophoresis
PCR	polymerase chain reaction
qPCR	quantitative polymerase chain reaction
RT-PCR	real time polymerase chain reaction
ROS	reactive oxygen species
RNA	ribonucleic acid
SDS-PAGE	sodium-dodecyl sulfate-polyacrylamide gel electrophoresis
ss-DNA	salmon sperm DNA
SNP	single nucleotide polymorphism
ssDNA	single stranded DNA
SP	smart probe

T	thymine
Tb^{3+}	terbium probe
U	uracil
UV	ultraviolet
UVA	ultraviolet A (315-400 nm)
UVB	ultraviolet B (280-315 nm)
UVC	ultraviolet C (200-280 nm)

Chapter one

Detection of UV-Induced DNA Damage with EvaGreen®

General Introduction

1.1 The DNA molecule and its double helical structure

In 1953, James Watson and Francis Crick correctly predicted the structural nature of the deoxyribonucleic acid (DNA) molecule. Each subunit of DNA is known as a nucleotide[1]. These nucleotides are composed of a 5-carbon sugar, either 2'-deoxyribose (DNA nucleotide) or ribose (ribonucleic acid (RNA) nucleotide), a phosphate group on either the 3' or 5' carbon and a nitrogenous nucleobase[1]. The DNA molecule is made up of four nucleobases namely thymine (T), adenine (A), guanine (G) and cytosine (C); uracil (U) is only found in RNA. From here on in this thesis, only the DNA nucleotides will be considered. These nucleobases can be divided into two groups, the pyrimidines and the purines.

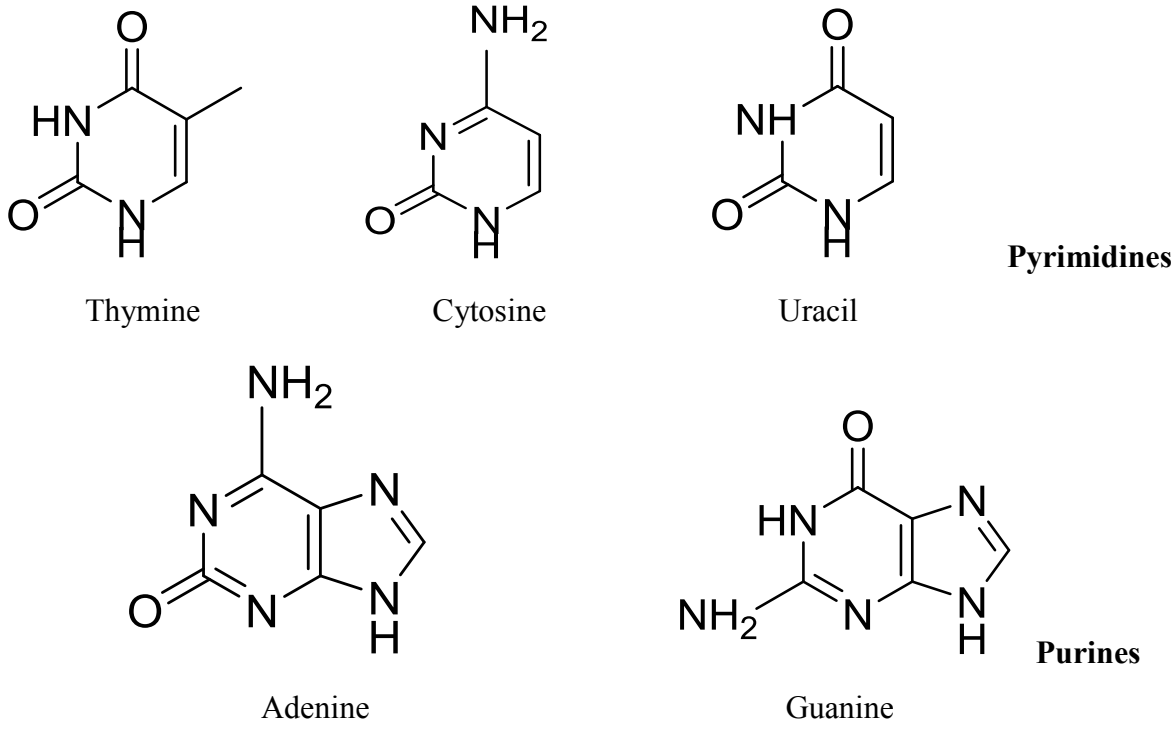

Figure 1.1: Chemical structures of the five nucleobases which make up both the DNA and RNA.

Thymine and cytosine are pyrimidine nucleobases, while adenine and guanine are purine nucleobases. Each base is distinctively complementary to only one of the other three nucleobases: adenine only base pairs to thymine with two hydrogen bonds, while guanine

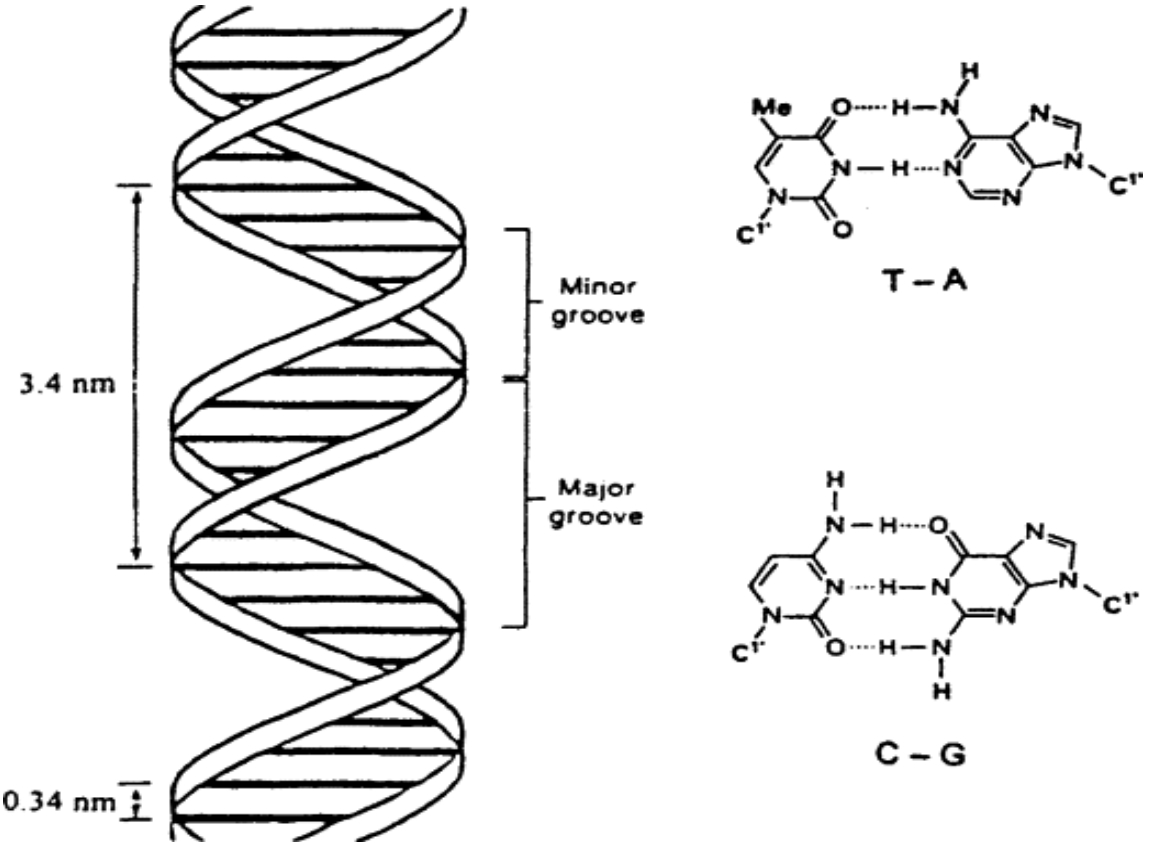

Figure 1.2: DNA structure. Shown are the DNA double helical structure with significant distances indicated, and a schematic of the hydrogen bonding in polynucleotide DNA.
Note: The schematic representation of double-stranded DNA. Reprinted with permission from Electrochemistry of DNA In *Applications of Kinetic Modelling*, pp 91–119 by Oliveira Brett, A. M.; Serrano, S. H. P.; Piedade, A. J. P., 1999, Compton, R. G., Hancock, G. B. T.-C. C. K., Eds.; Elsevier.

only base pairs to cytosine with three hydrogen bonds. These nucleotides together with the complementary binding of the nucleobases form the double helical structure of DNA. The DNA molecule consists of two strands which are joined to form the double helix. Each strand has a 5′-phosphate group at one end and a 3′-hydroxyl at the other end[2] with sugars linked by the phosphate groups via phosphodiester bonds. The sugar-phosphate chain acts as the structural

backbone[1,3]. This double helix consists of two grooves which are not identical[1], the major groove which is wider and the narrower minor groove[1]. In cellular organisms like *E. coli*, information can only be stored correctly in the DNA in the double helix form[1]. It is important to note that the missing 2′-hydroxyl group in DNA gives its phosphate esters resistance to hydrolysis and hence, much more stability to the DNA compared to RNA.

1.2 DNA role in cells

The major roles DNA plays in cells are replication, encoding information, mutation/recombination, and gene expression[1,2]. These four processes are vital for the overall well-being of cells, optimal performance of cellular activities and accurate storage and transfer of hereditary traits in organisms. This section will discuss those roles in detail.

Replication can be simply defined as the process whereby the DNA molecule makes a copy of itself during cell division[2]. Each of the DNA single strands serve as templates from which new DNA strands can be copied[2]. The newly synthesized strands are known as complementary strands. An enzyme known as the DNA polymerase is responsible for the copying of the new strands. The synthesis of the new strands occurs in the 5′→ 3′ direction along a localized Y-shaped region known as the replication fork[2]. This replication process is the basis for the accurate transfer of hereditary traits from parents to offspring as each daughter replicate consists of one strand of the template and a newly synthesized complementary strand[2]. The 3'-5'-endonuclease activity of the polymerase ensures proofreading, ensuring that incorrect base pairs are not incorporated during the transcription process, while the 5'-3'-exonuclease activity of the polymerase cuts off unwanted fragments from the growing chain.

Encoding of information seems to be the most important role that DNA plays in cells. Information stored by DNA is used for the synthesis of other essential biomolecules such as proteins and RNA. This information is stored in a region of the DNA known as the gene and is dependent on the arrangement of the nucleotides along each strand[2]. The gene is the basic functional unit of heredity that is transferred from the parents to the offspring. In eukaryotes (multicellular organisms), DNA is stored in the cell nucleus while in prokaryotes (unicellular organisms), DNA is stored in the cytoplasm of the cell[2]. The gene constitutes of units of A-T and

G-C which lie along a DNA strand. Each sequence of these three bases constitutes a "codon". A codon constitutes of three bases which corresponds to an amino acid through a process known as gene translation[2,3]. This therefore implies that the sequence of bases of the DNA determines the amino acid content of proteins in a cell which carry out the processes and functions in a cell[2].

Mutation can be defined as an alteration to the original order of nucleotide arrangement in any region of the genomic DNA[4]. These mutations can be in the form of strand breaks during growth[5] or rearrangement of base pairs in the form of insertions or deletions[4]. Mutations can arise from errors during replication or when DNA is exposed to damage inducing species such as chemicals or UV radiation[3]. Recombination refers to the process which involves the transfer of genetic materials between chromosomal regions and this helps to maintain the fidelity of the genomic material through repair of damaged DNA sites[4,6,7.] This process can either be a homologous or a non-homologous recombination[6,7]. An example of this process can be observed during meiosis in which there is an effective shuffling of maternal and paternal DNA to create new variant daughter cells.

Proteins and functional RNA are synthesized from a gene [3]. This unique process proceeds via four steps. First, a new RNA strand is synthesized from a DNA strand known as the template, and this process is known as transcription [2,3]. The newly synthesized RNA is known as the mRNA (messenger RNA) which is the template for protein synthesis[3]. The mRNA is then transported to the cytoplasm of the cell where the protein synthesis occurs[3]. Finally, in the cytoplasm the mRNA binds to ribosomes and a protein is synthesized with the help of the tRNA (transfer RNA) which decodes the sequence of the mRNA in a process known as translation[3].

1.3 UV spectrum and UV-induced DNA damage

UV radiation is a part of the electromagnetic spectrum which can damage DNA. This spectrum consists of three regions UVA, UVB, and UVC. Each region possesses different DNA damage capabilities, and each can lead to a different set of photoadducts. These various photoadducts are formed through different mechanisms depending on the UV source being used.

Solar energy is transmitted to the earth's surface in the form of electromagnetic waves. The ultraviolet spectrum which makes up less than 10% of the incident radiation reaching the earth's surface, ranges[8] from a wavelength of about 100 - 400 nm. This spectrum is further sub-divided into three categories[8] namely UVC which ranges between 100 - 280 nm, UVB which ranges between 280 - 315 nm and UVA which ranges between 315 - 400 nm. These three distinct regions of the ultraviolet spectrum induce DNA damage via different mechanisms with varying impact[9]. While exposure to solar radiation might have its health benefits such as vitamin D synthesis, prevention of diseases such as diabetes type 1 and osteoporosis[8], and aesthetic benefits such as skin tanning, excessive exposure to solar radiation can however be very harmful and can lead to all sorts of problems ranging from skin cancer conditions such as melanoma, sunburn, eye defects such as cataracts and pterygium, premature aging and non-melanoma skin cancers[10-13].

While the UVC part of the spectrum is absorbed by the ozone layer and oxygen in the atmosphere, the use of chemicals such as chlorofluorocarbons (CFCs) which destroy ozone molecules may increase the amount of UVC radiation (100-280 nm) reaching the earth's surface[41]. This seemingly anticipated increase in UVC radiation that is possible to reach the earth's surface is of worrying concern as this radiation is of the shortest wavelength in the UV spectrum which makes it the most energetic and dangerous compared to the other parts of the spectrum. Also, DNA's maximum absorption (260 nm) is well within the UVC range[47]. The absorption of UVC radiation also leads to the formation of cyclobutane pyrimidine dimers (CPDs) and 6-4 pyrimidine-pyrimidinone dimers (6-4 PPs). Also, some CPD lesions in aqueous solutions can be detected using UVC radiation[17,24]. Dunkern and Kaina have also studied and observed UVC-induced DNA double strand breaks resulting from replication of damaged DNA[17]. UVC is mostly used in laboratory and sterilization procedures and as such remains a very important component of the UVR spectrum that needs to be studied.

UVB radiation (280-315 nm) is the most biologically effective part of the UV spectrum, and can be absorbed directly by skin DNA which may lead to skin cancer upon excessive exposure[29,30]. Although the ozone layer plays a vital role in shielding wavelengths that are shorter than 290 nm from getting to the earth's surface, any adverse changes in environmental

conditions might alter this protection, paving the way for these short wavelengths to penetrate to the terrestrial environment which can have potential harmful effects[29]. Skin conditions such erythema, elastosis, actinic keratosis and telangiectasis have all been linked to UVB radiation absorption[31,32]. The negative impact of UVB on the survival abilities, fertility and the distribution of sex ratios of copepods *Tigriopus Californicus* found in intertidal environments have already been extensively studied[17,33]. Cellular DNA can potentially absorb UVB radiation and this poses harmful implications to living systems such as bacteria[30,34], cyanobacteria[17,35], phytoplankton[17,36], macroalgae[17,37], plants[17,38], animals and humans[39-41]. UVB-induced chemical modifications in DNA lead to dimerization of the nucleobases, thereby altering its molecular structure.

It is important to also note that the absorption of UVB radiation potentially leads to the formation of three major photoproducts, namely CPDs, 6-4PPs, and their corresponding Dewar isomers, with the last formed upon further exposure to UVA or UVB radiation[17,42]. In cells, DNA strand breaks have been observed upon exposure to UVB radiation, and UVB-induced ROS (reactive oxygen species) intermediates together with CPDs and 6-4 PPs can also lead to strand breaks which makes UVB a serious mutagen[17,43,44]. These photoproducts are potentially responsible for the strand breaks that occur at sites of collapsed replication forks during replication or transcription which can lead to mutations along DNA strands, and in severe cases can lead to skin cancer [17,45-47]. Frauk et al., have studied the survival strategies in UV-screening and non-screening Chlorophyta upon exposure to UVB radiation and photosystem II damage in two intertidal macroalgae[48]. Also, Roxanne et al., have studied the tolerance and persistence of the human genome to excessive exposure of UVB radiation[49]. UVB wavelengths have shown to be the most cytotoxic of the three distinct portions of the UV spectrum.

The UVA region of the ultraviolet spectrum occupies a longer wavelength range than UVC and UVB and will be poorly or unlikely absorbed by DNA. However, it can form reactive singlet oxygen species ($^1O_2$) when O_2 interacts with light and this species can indirectly damage DNA through photoactivated reactions[14,15]. These reactive oxygen species form products such as 8-oxo-7,8-dihydro-2'-deoxyguanosine (8-oxoGua), oxidized pyrimidines, strand breaks and

DNA-protein crosslinks which are photoproducts also formed from ionizing radiation[16,17]. This poses a lesser threat to DNA damage when compared to the other regions of the spectrum.

Although the UVA region has been mentioned to be less harmful as compared to the other regions of the UV spectrum, recent studies have shown that it can contribute to actinic premature aging of the skin, skin dryness, unwanted exfoliation, and can also lead to skin cancer[18-20]. UVA radiation has also been found to lead to the formation of CPDs in bacteria, eukaryotic cells and skins [17,21-23]. Other studies have also shown that CPD photolesions were formed in a higher magnitude than 8-oxoGua, which happens to be the most easily induced UVA mediated photoproduct, and strand breaks[17,24,25]. Malignant mutation fingerprints, which exist in the form of cytidine-to-thymidine transitions that has long been linked with UVB radiation, have been found in mice when they were exposed to UVA radiation[26,27]. Studies have also shown that this mutation which has also been found in the *Tp53* of keratosis and skin tumors in humans, is also present in the *Tp53* gene of hairless mice when they were exposed to UVA radiation[26,28]. Daoudi et al., have also confirmed that reactive oxygen species (ROS) which are produced by UVA radiation in tandem with benz(e)acephenanthrylene were cytotoxic to A375 cells, by using a comet assay[50]. In all, UVA through the formation of radical intermediates in the form of ROS, CPDs and other possible photolesions is deleterious and can lead to various unwanted outcomes which can impact the health of both humans and other organisms negatively.

1.4 Photochemistry of DNA

When DNA absorbs UV light, it is excited via $\pi\pi^*$ transitions to short-lived excited states with low quantum yields for photochemistry[51,52.] Internal conversion and subsequent vibrational relaxation brings most of the excited population back to its ground state[51]. Different photoproducts, which are precursors of cancer, can be formed upon irradiation of DNA, depending on exposure conditions such as in the absence or presence of oxygen and depending on the radiation source[51,53,54]. The most characterized photoproducts include CPDs, 6-4 PPs and photohydrate lesions, all formed in the absence of oxygen[52-56]. Other photoproducts in the presence of oxygen include 8-oxoGua (see Figure 1.3), oxidized pyrimidines, strand breaks and DNA-protein crosslinks[16,17].

Much work has been done to understand CPDs and they are the most characterized photoproducts in DNA[52]. CPDs are formed through dimerization between pyrimidine bases which exist next to each other in a sequence, with the most common dimers formed between thymine-thymine (T<>T), thymine-cytosine (T<>C), cytosine-thymine (C<>T), and cytosine-cytosine (C<>C)[52]. CPD formation (see Figures 1.4-1.6) upon UV irradiation proceeds via ($2\pi+2\pi$) cycloaddition of the double bond that occurs between C5-C6 of adjacent pyrimidine bases[52]. Previous studies have shown that CPDs formed in dilute solutions are mainly due to thymine and uracil derivatives in triplet state and that the quantum yield is dependent on the size and concentration of stacked aggregates[52]. When a monomer unit of a base is subjected to photolysis, four isomeric dimers are produced, namely, *cis-syn*, *cis-anti*, *trans-syn*, and *trans-anti*, however, in double-stranded DNA (dsDNA) only the *cis-syn* CPD isomer forms due to the rigid conformation of the double helix, although the *trans-syn* isomer can be formed in single-stranded DNA (ssDNA) as it affords more structural flexibility[52]. The pyrimidine nucleobases are more susceptible to UV damage and hence have greater quantum yields than the purine nucleobases which are more photostable.

The [6-4]-photoadducts, just like the CPDs, are also formed from [$2\pi+2\pi$] photocycloaddition (see Figure 1.4) but this proceeds via the instantaneous rearrangement of initially formed oxetane and azetidine intermediates from the photocycloaddition of the imino or carbonyl of the 3'-pyrimidine base onto the 5' carbon of an adjacent pyrimidine base[52,57]. Photohydrates are formed through the addition of water to C6 of an intermediate derived from the excited singlet state of a pyrimidine base[52]. In DNA and polynucleotides, the quantum yield of photohydrates is low, as this is not a favorable product due to their stacked structures[52]. Uracil which is a component of RNA is much more prone to form stable photohydrates.

Finally, adenine, which is one of the purine bases, has been found to undergo photocycloaddition (see Figure 1.6) reactions with thymine in dinucleotides, polynucleotides and DNA through the formation of a cyclobutane linkage between the C6-C5 of the thymine and C6-C5 of the adenine to give a photodimer[52,58-60]. The dimer formation is highly sequence specific and is a product of an excited singlet state in adenine[52]. Previous studies have indeed shown that photodimerization of adjacent adenine bases in oligomers and polymers in deoxyadenylic acid

exists with relatively high quantum yield[52,61]. The photoadduct in this case is formed through the rearrangement of the azetidine intermediate that leads to the addition of the N7-C8 double bond of the 5' adenine across the C5-C6 bond of the 3' adenine[52]. This adenine photoadduct is, however, of little importance for UVB radiation as adenine barely absorbs in that region.

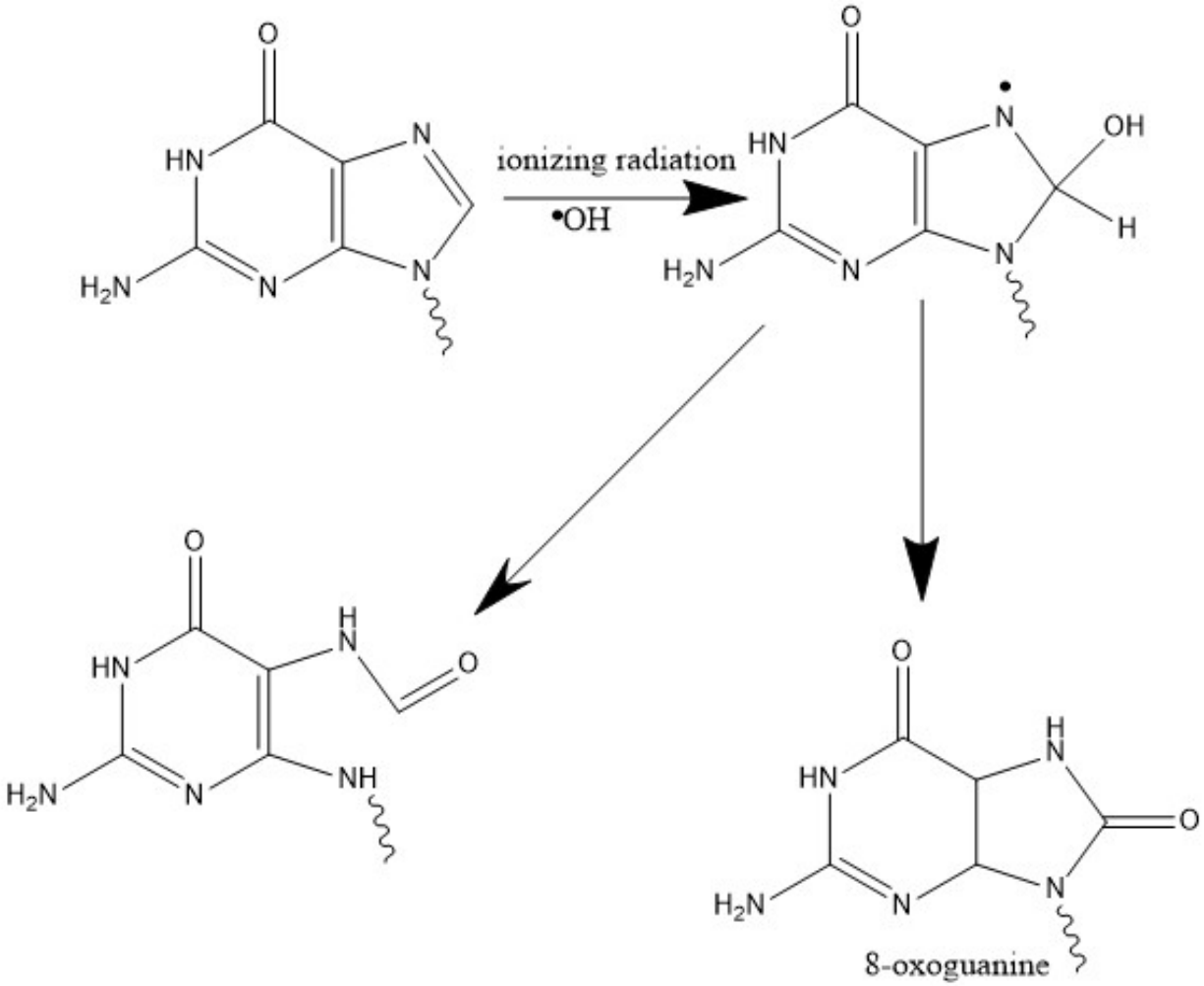

Figure 1.3: Chemical structures of photoadducts generated from UV irradiation, for the formation of 8-oxoGua via reactive oxygen species.

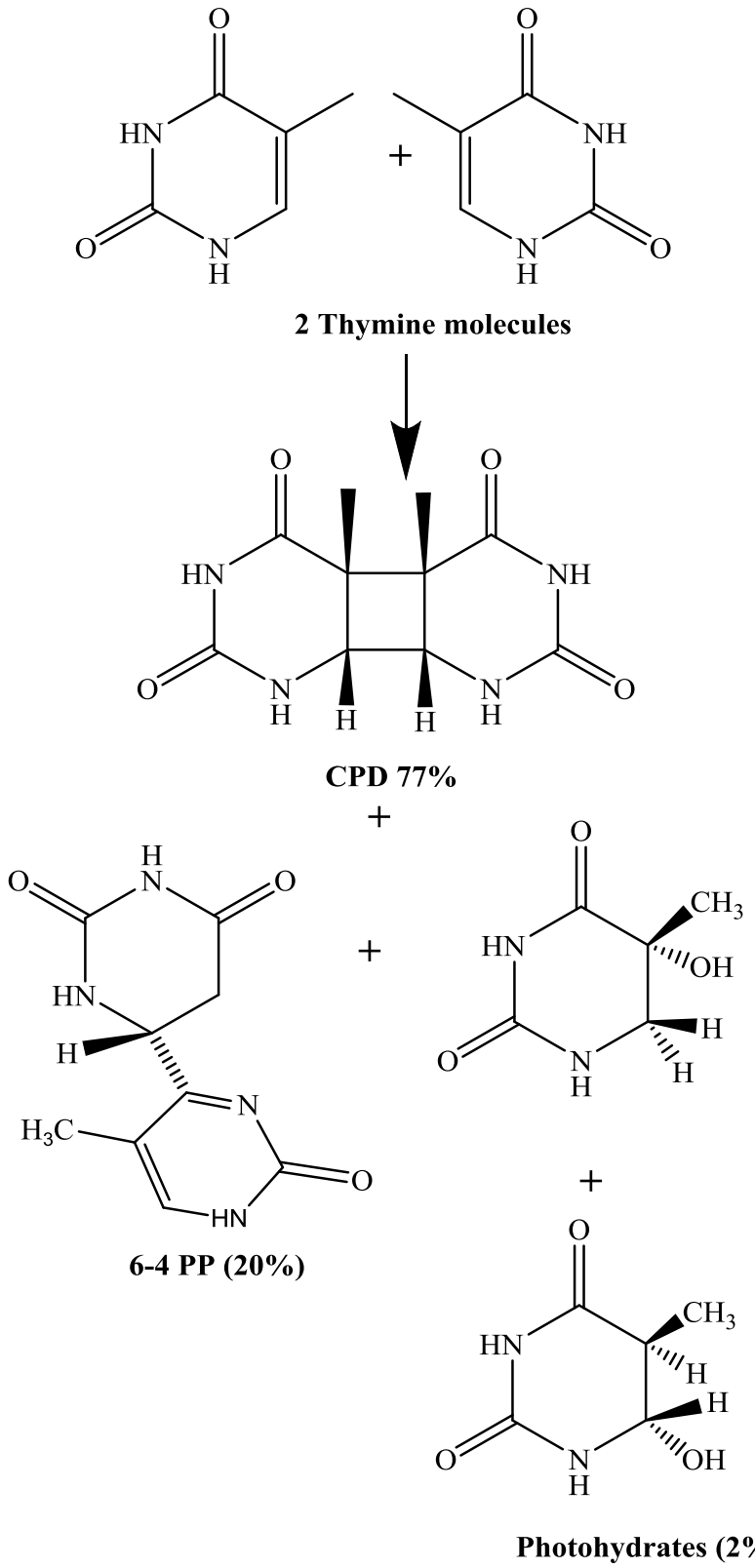

Figure 1.4: Chemical structures of thymine photoproducts via UV irradiation, with percentage quantum yields indicated in parentheses.

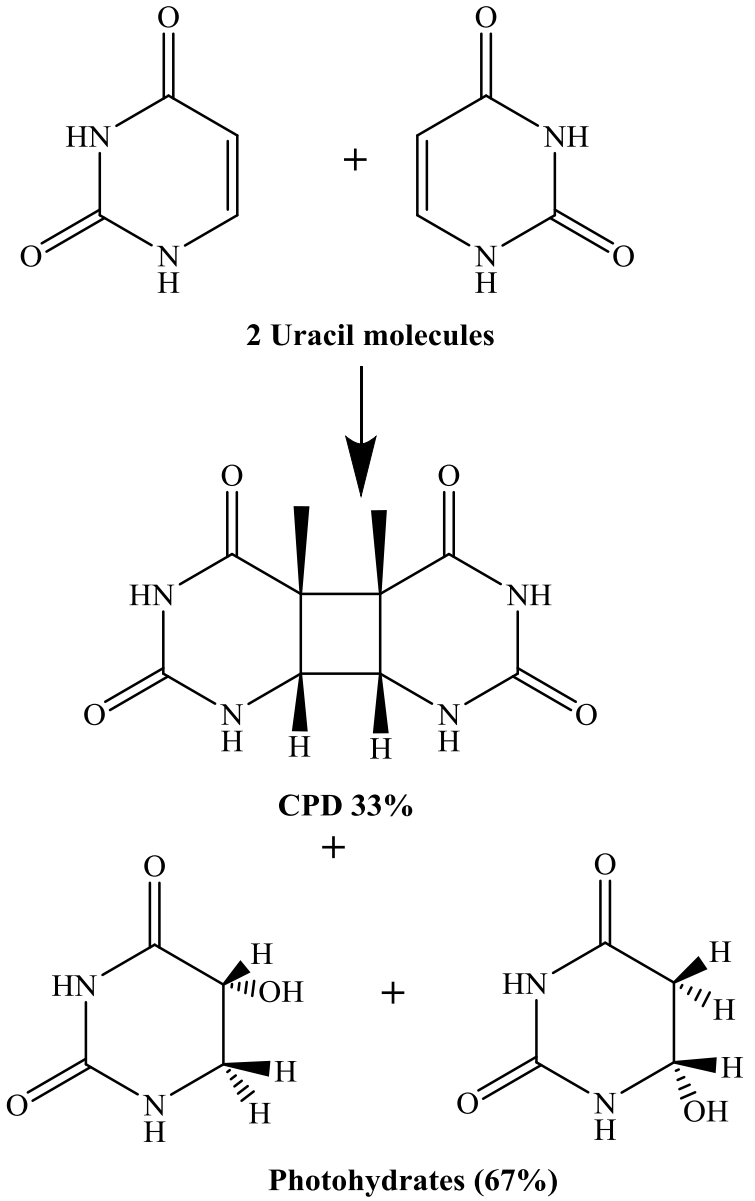

Figure 1.5: Chemical structures of uracil photoadducts generated from UV irradiation, with their percentage quantum yields indicated in parentheses.

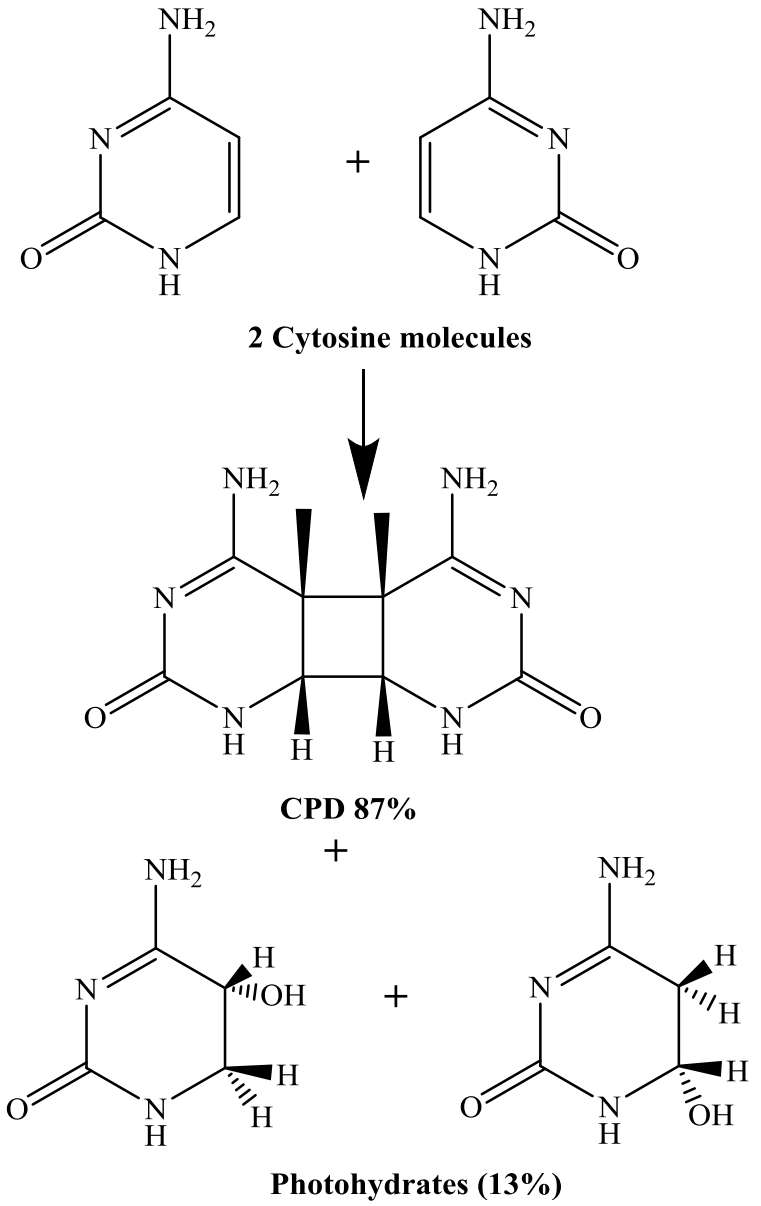

Figure 1.6: Chemical structures of cytosine photoadducts generated from UV irradiation, with their percentage quantum yields indicated in parentheses.

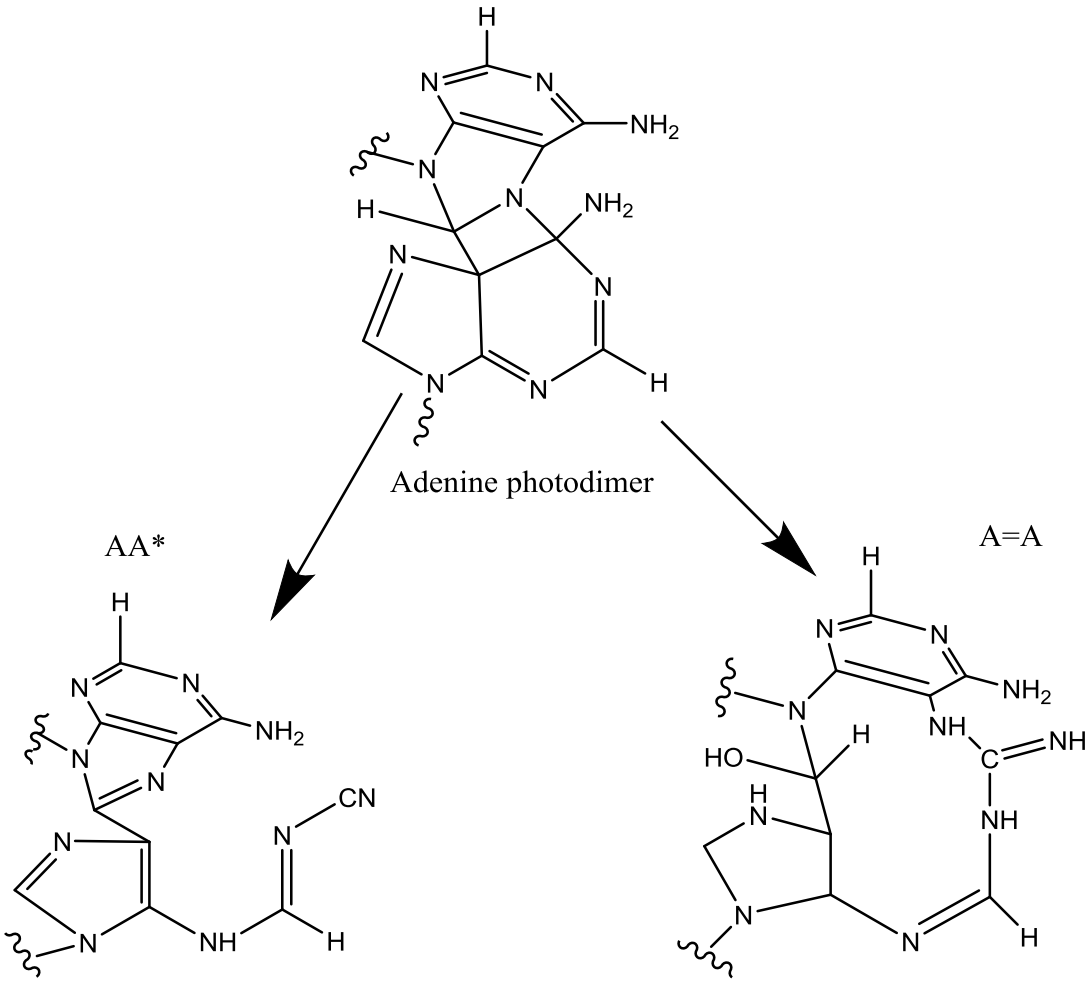

Figure 1.7: Chemical structures of adenine photoadducts generated from UV irradiation, where AA* and A=A are the various forms of photoproducts.

1.5 DNA damage detection

The fidelity in the conformation and base pair representation along the DNA double strand during replication and other life processes such as cell division is not only vital to the overall well-being of the cell but ensures that information encoded in the form of base pair matches which are translated to proteins are kept intact. Any mutation incurred or induced by either endogenous or exogeneous factors must therefore need to be detected in the best possible way. Since studies have revealed the importance in maintaining the base pair configuration in DNA and the adverse effects this poses to health, researchers have delved into finding better and more accurate ways of detecting DNA damage. Recently, several more assays and techniques to detect DNA damage have been discovered. DNA damage which can occur as strand breaks, insertion

or deletion of bases, formation of photoadducts which also involves base modifications and mismatches is a precursor to many diseases such as cancer.

Several methods for DNA damage detection exist, with each method having its advantages and shortcomings. These methods include but are not limited to polymerase chain reaction; a technique well documented and established for the amplification of DNA. Other methods include chromatographic techniques such as gas chromatography and liquid chromatography electrospray tandem mass spectrometry and gel electrophoresis. Immuno-based assays such as enzyme-linked immunosorbent assay and immunohistochemical assay techniques that are dependent on inducing a response from specific antibodies are also one of the methods that have also been developed for detecting DNA damage. Fluorescence-based detection methods such as hairpin probes, their analogues (smart probes and molecular beacons) and intercalators which include major groove binders such as EvaGreen® and terbium have also been developed to detect UV-induced DNA damage. Other methods such as affinity capillary electrophoresis with laser-induced fluorescence detection (CE-LIF), and cellular DNA damage detection assays in the form of comet and halo assays will also be discussed briefly in a bid to cover a full range of DNA damage detection techniques which have been developed over the years.

1.5.1 Polymerase Chain Reaction (PCR)

Over the years, PCR can be said to be one of the most established and frequently used method for

DNA damage detection. PCR is effective due to its specificity. The PCR is a DNA amplification method that involves the use of a primer to create exact copies of a DNA strand[62]. The DNA strand which is being copied is known as the template and the transcription is made possible by a polymerase known as the *taq* polymerase. The *taq* polymerase which propels the reaction is blocked from making further copies of the template once it encounters a region of damage on the strand, thereby limiting the quantity of the PCR product with the damaged sites[62]. Hence, it is both effective and relatively accurate. Quantitative PCR (qPCR), which is high molecular weight dependent, can be used to detect DNA damage in dsDNA[63] and has also been used to quantify both the quantity of damage in mitochondrial DNA (mtDNA) and the kinetics of damage

removal[63,64]. The qPCR technique has also been used to detect UV-induced photoproducts in 1.2kb fragments of the *LacI* gene from *Escherichia coli* (*E. coli*)[62], damage in mtDNA in *Schizosaccharomyces pombe* cells treated with hydrogen peroxide[62,65] and the frequency of cisplatin-induced lesions in fragments of the hamster *aprt* gene[62,66], just to name a few. Strand-specific qCPR detects DNA damage but is specific on a single strand, which infers more accuracy in both detecting DNA damage and gene repairs[63]. The single strand ligation-PCR offers the option of being able to detect lesions on a single strand in a single copy of a gene under more physiologically obtainable conditions and this makes it possible to detect antibodies of interest that are in any way associated with the DNA adduct under study [63]. Ligation mediated PCR (LMPCR) is a very sensitive assay which can be used to detect and repair of CPDs[67] and 6–4PPs[62] and is very useful when dealing with individual DNA photoproducts at low concentrations. LMPCR has also been used to study *in vivo* interactions of protein and DNA[68].

Other PCR methods include terminal transferase-dependent PCR, immuno-coupled PCR, PCR-based short interspersed DNA element. It can therefore be inferred that this method can be adapted in diverse ways depending on experimental objectives, analyte of interest or resources available to detect DNA damage in both ssDNAs and dsDNAs.

1.5.2 Gas Chromatography

Cells are the basic units of life and therefore being able to detect, characterize and quantify several cellular processes such as DNA damage, repair, and its biological significance becomes highly important. MS in tandem with GC presents a powerful analytical tool that can be used to proffer structural information involved in a chemical or biological analysis[62,69]. This technique can be used to measure a wide range of DNA damage products with the sensitivity as high as detecting a single DNA lesion in a system with multiple DNA damage products following an exogenous or endogenous induced damage[62,70]. This method involves hydrolyzing the DNA sample, derivatizing the hydrolysate, separation into various individual component using gas chromatography, and detection and quantification by MS[62,71]. GC-MS has been used *in vitro* to detect DNA-protein crosslinks which includes Thy-Gly, Thy-Ala and Cyt-Tyr in mammalian chromatin[62,72-74]. Oxygenated photoadducts formed through the reaction of DNA with reactive oxygen species can be detected using this method. GC-MS is widely used for the detection of

oxygen induced photoadducts due to the derivatization of the polar bases to give thermally stable substrates, although derivatization can sometimes lead to overestimation of oxidative products due an increase in the level of 8-OH-guanine, 8-OH-adenine and 5-OH-cytosine according to Jenner et al., 1998. This overestimation arises from the fact that derivatization of hydrolyzed DNA is done at high temperatures in the presence of air which is comprised of oxygen[75].

1.5.3 Liquid Chromatography Electrospray Ionization Tandem Mass Spectrometry (LC–ESI–MS)

LC-ESI-MS/MS method can be used to detect both UV and oxidatively-induced lesions in DNA[62]. The various monomer components of the sample are first separated into individual units by running the sample through a high-performance liquid chromatography (HPLC) column. This HPLC is then coupled with a MS/MS mass analyzer to detect the analyte of interest. This process involves the use of a soft ionization method operated in atmospheric pressure to generate gas phase ions through the application of a high voltage (2-5 kV). It is termed a soft ionization process since the molecular ions are not broken further down into fragments, thereby allowing for the detection of the molecular composition of the sample being investigated. A triple quadrupole mass analyzer is typically used for the detection of DNA adducts. In this triple quadrupole system, the first quadrupole (Q1) and the third quadrupole (Q3) are the mass filters.

The second quadrupole (Q2) is referred to as the collision cell in which the analyte ions experience collision-induced dissociation (CID) when they collide with an inert gas mostly argon and are separated from each other. There are often two types of detection methods used for detecting DNA adducts which are single ion monitoring (SIM) and multiple reaction monitoring (MRM) which is also known as selected reaction monitoring (SRM). In the SIM mode, only the ion of the analyte of interest is selected to pass through (Q1) and is detected. In the SRM mode, a precursor ion of the analyte of interest is selected to pass through Q1 and then goes into Q2. In Q2, it undergoes CID, and the ions are separated from each other and they go into Q3. In Q3, the analyte ions of interest are separated from the other ions and are detected. This method has been used to detect DNA adducts such as UV-induced pyrimidine dimer photoadducts[41] and has been in fact used to detect all possible 12 bipyrimidine photoproducts within isolated and cellular DNA arising from TT, TC, CT, and CC bipyrimidine sites[77]. Also, oxidative products such as

5,6-dihydroxy-5,6-dihydrothymidine, 5-hydroxy-2'-deoxyuridine, 5-(hydroxymethyl)-2'-deoxyuridine, 5-formyl-2'-deoxyuridine, 8-oxo-7,8-dihydro-2'-deoxyadenosine, 8-oxo-7,8-dihydro-2'-deoxyguanosine, 4,6-diamino-5-formamidopyrimidine, and 2,6-diamino-4-hydroxy-5-foramidopyrimidine have all been quantified within both isolated and cellular DNA upon exposure to γ-radiation using this method[78]. In all, this method has proven to be sensitive in the measurement of DNA adducts and the coupling of the liquid chromatography (LC) to other forms of mass analyzers[79] continues to be on the rise for the detection and quantification of DNA lesions.

1.5.4 Gel electrophoresis

The gel electrophoretic technique is based on the principle that negatively charged anions move downwards towards a positively charged anode[1]. This method largely depends on the size of the molecule moving through the gel, with the shape and size being important factors in the separation too. In the case of DNA, it means that shorter DNA strands will effectively move faster in the gel than the longer ones.

There are indeed three types of gel electrophoretic techniques, namely agarose gel electrophoresis, which is used to separate large pieces of DNA, polyacrylamide gel electrophoresis (PAGE) which is used for the sequencing of smaller pieces of DNA and sodium-dodecyl sulfate-polyacrylamide gel electrophoresis (SDS-PAGE) which is used for the separation of proteins. PAGE has now largely been replaced by the capillary electrophoretic method[1]. Ahmed and Setlow[80] have previously quantified single-strand breaks in pyrimidine dimers by using specific site-nicking enzymes, namely T4(T4-pdg) synthesized from bacteriophage and *Micrococcusluteu* in abasic conditions to create nicks in DNA strands by specifically cleaving the N-glycosyl bond of the 5' nucleotide which in turn cleaves the phosphodiester linkage and leaves a single-strand break at CPD sites of the dimer[80]. The DNA strands are then labelled with fluorophores (e.g., ethidium bromide), and then detected by exciting the fluorophore with ultraviolet light to measure the fluorescence intensity of the labelled DNA molecules before they leave the compartment. The reproducibility and sensitivity of this method is however low and makes use of standards that are relative to molecular weights[76].

Table 1.1: Different DNA damage detection techniques with their limits of detection, advantages and limitations.

Technique	Sensitivity	Advantages	Limitations
PCR		• Easily adaptable to increase sensitivity to other damage types • Versatile • Lower possibility of errors as regards base pair mismatches	• High cost of PCR kits • Primer is always required
Gas Chromatography		• Selective detection • Sensitive	• High instrumentation cost • Possibility of incurring further lesions during sample preparation • Sample preparation can be time consuming
LC-ESI-MS		• Sensitive • Can be used to detect damage in both isolated and cellular DNA • Selective detection • Adaptable to other mass analyzers thereby increasing sensitivity • Soft sample ionization process	• Expensive • Sample preparation involves many steps • Possible addition of lesions during sample preparation

Technique	Sensitivity	Advantages	Limitations
Alkaline Gel electrophoresis	• Tenths of fmol	• Can be used to analyze high molecular weight samples	• Limited to strand break detection • Requires fluorescent/radioactive reporter labelling
ELISA	0.9 fmol	• Simple • High selectivity to specific UV-damaged sites	• Antibody cross-reactivity issues • Expensive
IHC		• Can be used to directly detect cellular DNA damage • Does not require much sample volumes • Does not require DNA extraction	• Requires fluorescent/radioactive reporter labelling • Possible antibody cross-reactivity exists • Cells must be fixed
Molecular Beacon	DNA MB 4 pmol Ch MB 0.8 pmol	• Simple • Selective to overall damaged bases	• Nonselective to damage types • Labelling with quencher/fluorophore is required • Expensive synthesis
Smart probes		• Simple mix and read method • Relatively inexpensive	• Problem of inadequate quenching which leads to background fluorescence

Technique	Sensitivity	Advantages	Limitations
2AP probe	1 pmol		• Labelling with quencher/fluorophore is required • Not selective to damage types • Expensive synthesis
EvaGreen®		• Simple • Cost effective • Sensitive • Sequence independent • Fluorescent reporter labelling not needed	• Detection is limited to certain base pair lengths • Not selective to damage types
Tb^{3+}/hairpin probe	0.4 pmol	• Sensitive • Low cost • Selective to overall amount of damage • Simple • Fluorescent reporter labelling not needed	• Not selective to damage types
Immunoassay coupled with CE-LIF	3×10^{-21} moles	• Selective to specific type of DNA damage • Sensitive detection	• Fluorescent labelling is required • Cross reactivity of antibodies • Expensive Ab synthesis

Technique	Sensitivity	Advantages	Limitations
Comet assay		• Sensitive to damage types	• Limited to oxidative damage and strand breaks • Limited to single cell analysis • Fluorescent reporter labelling is required
Halo assay		• Fluorescent reporter labelling not required • Sensitive to damage types	• Limited to detecting chromatin fragility and single strand breaks • Limited to single cell

*In this table, abbreviations are, PCR: Polymerase chain reaction, LC-ESI-MS: Liquid chromatography electrospray ionization tandem mass spectrometry, ELISA: Enzyme-linked immunosorbent assay, IHC: Immunohistochemical assay, MB ch: Chimeric molecular beacon, 2AP: 2-Aminopurine probe, Tb^{3+}: Terbium probe, and CE-LIF: Capillary electrophoresis with laser induced fluorescence.

Note: Adapted from Detecting UV-Induced Nucleic-Acid Damage by El-Yabzi, A. F.; Loppnow, G. R. *Trends Anal. Chem.* **2014**, *61*, p.68.

1.5.5 Immunoassay

The term immunoassay generally can be used to refer to methods that use antibodies as tools to detect antigens. One of the flaws of this method is the cross reactivity of the antibodies with the DNA bases[75]. This method has been developed over the years and we will be looking at two types namely enzyme-linked immunosorbent assay (ELISA), and immunohistochemical assay. Immunoassays are based on inducing an immune response from specialized antibodies that respond to a stimulant which can be in form of chemicals or a biological anomaly. The idea behind the development of such assays is that in living systems such as humans, antibodies

which are a part of the immune system are triggered in response to any foreign material or influence which are not recognized by the cell machinery and are therefore seen as harmful to the body. These triggered responses lead to a chain or series of events that are geared to remove or in some cases repair any harm that has or potentially can be caused by such foreign material. In the case of UVC-induced photoproducts, antibodies which are sensitive to these photolesions can potentially be raised in a bid to detect these damages as we will be seeing in the discussion of such assays in the next sections.

1.5.5.1 Enzyme-linked immunosorbent assay (ELISA)

This is one of earliest and most common methods for detecting DNA damage[81], including its sensitivity to detect x-ray induced DNA damage[82]. In ELISA, a known amount of antigen of interest is immobilized on a surface (ELISA plate). Primary antibodies are then passed over the immobilized surface to bind to the antigen. Secondary antibodies linked covalently to enzymes are used to detect these primary antibodies. The enzyme substrate used in labelling the secondary antibody, such as a peroxidase or an alkaline phosphatase, absorbs strongly at visible wavelengths and hence is detected[76]. But it is important to mention that the conditions that favor the production of a photoproduct must be considered when using ELISA to achieve effective binding of the antibody as previous studies have shown that antibodies bind differently to bipyrimidine photoproducts[76,83-85]. ELISA has also been used to detect both the induction and repair of UV-induced damage[76,86]. Other labelling methods which are also used for ELISA include radiolabeling and fluorescein isothiocyanate (FITC) labelling.

1.5.5.2 Immunohistochemical assay (IHC)

This assay is usually performed on fixed or stationary cells and helps correct the deficiency of the cross-reactivity issues often encountered when using the ELISA method. The immunohistochemical assay makes use of RNase and protease for the effective removal of RNA and proteins that can interact with DNA[75]. The cells are counterstained with propidium iodide which facilitates the detection of the adducts through chemiluminescence. This assay can be used for detecting adducts in small sample volumes and does not require DNA extraction or hydrolysis[75]. IHC in combination with break-apart fluorescent in-situ hybridization (FISH) have been used to detect the ALK gene in non-small lung cancer cells [87]. IHC has also been used to detect both CPDs and 6-4PPs in irradiated bacteria cells[88]. In all, it is important to mention that

many monoclonal antibodies that bind specifically to several photoadducts have been developed thereby making this method increasingly interesting and more precise in detecting specific DNA photo lesions.

1.6 Fluorescence based DNA damage detection techniques

1.6.1 Hairpin probes

The hairpin probe as a detection technique for DNA damage basically involves a change in the fluorescence activity as a result of DNA damage. For example, for molecular beacons, the probe used in its native state does not emit fluorescence as the fluorophore and quencher lie near each other. As it binds to DNA, there is a separation between the fluorophore and the quencher and hence fluorescence is observed. The exponential increase of decrease in fluorescence can be attributed to the fact that a probe binds to DNA in a complementary manner in the absence of damage. As damage is introduced to a DNA strand, a change in the binding character of the probe is observed leading to an increase or decrease in fluorescence depending on the probe being used. Other hairpin probes such as the 2-amino purine (2AP) probes and smart probes suffer background fluorescence due to inadequate quenching. This pattern is, however, different when antibodies are used as the probes. An advantage to this method is the fact that some of these probes such as EvaGreen have little or no residual background fluorescence and hence offers better sensitivity for detection. Some of these techniques are discussed next.

Molecular beacons (MBs) are a fluorescence-based detection method for UV-induced DNA damage detection. The MB exist in the stem-loop structure in the absence of target DNA, in which one end of the loop contains a fluorophore and the other end a quencher[89-92]. The closeness in the proximity of the quencher and fluorophore mean that the MB shows little or no fluorescence activity[93]. When the MB hybridizes with complementary DNA target, a separation between the fluorophore and the quencher occurs and fluorescence is observed[76,94]. MB probes have been used to detect photoproducts in poly-dT and poly-rU strands with differences in their damage kinetics[94]. Yarasi et al., also demonstrated the use of MBs to detect photoadducts in thymine and uracil oligonucleotides. The inherent specificity of the MB makes it a very sensitive tool for DNA damage detection[76].

Although the MBs serve as both a sensitive and specific tool for DNA damage detection, its shortcomings have been well documented, with one being that designing the quencher and fluorophores can be very expensive and time consuming[76,95-98]. Another problem with this method is the residual background fluorescence due to inadequate quenching of the fluorophore[76,94]. Chimeric DNA-RNA molecular beacons have also been used to quantify nucleic acids, single nucleotide polymorphisms, and nucleic acid damage[99].

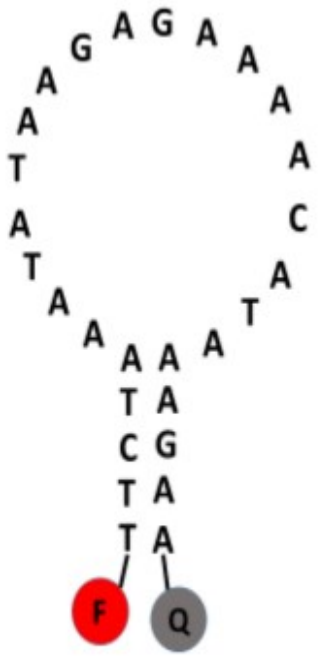

Figure 1.8: Schematic diagram of the hair pin structure of the molecular beacon where "F" is the fluorophore and "Q" is the quencher.

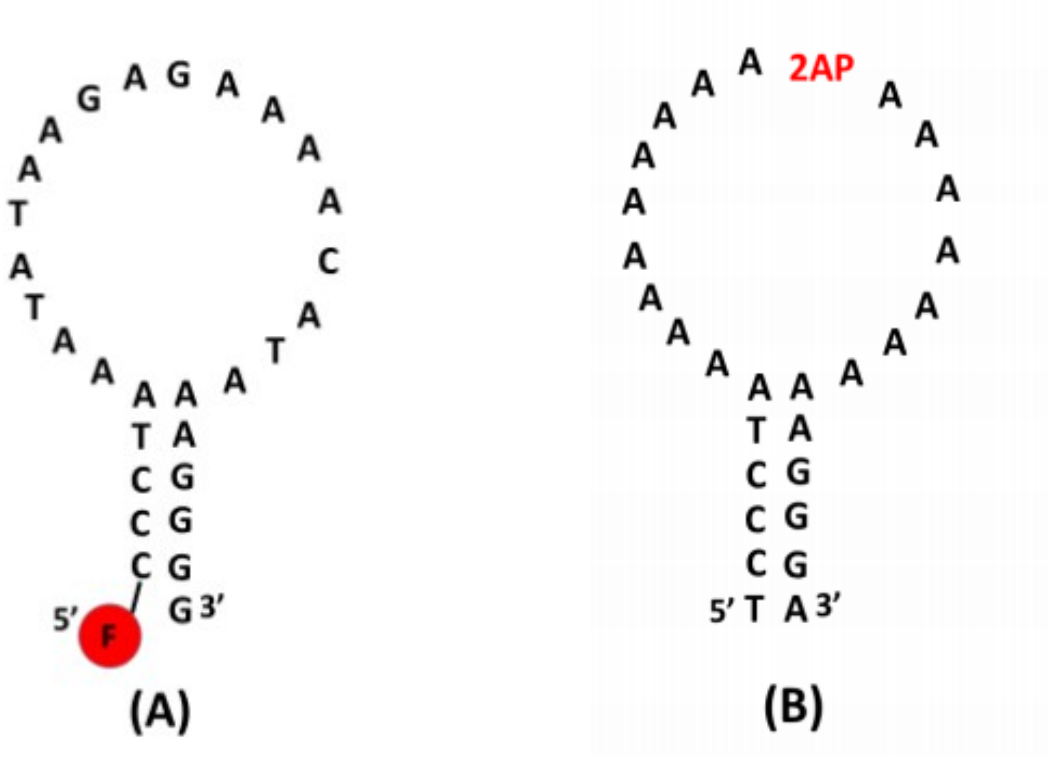

Figure 1.9: Schematic diagram of the stem-loop structure of (A) smart probe and (B) 2-aminopurine. Where "F" denotes fluorophore and "2AP" denotes 2-aminopurine.

Smart probes (SPs) are homologous to MBs in that they exist naturally in the same form. The difference is that the quencher in SPs is replaced with 2'-deoxyguanosine nucleotides and the quenching mechanism is photoinduced intramolecular electron transfer[76,97-98,100-101]. Nair et al., used a multiplexed method with SPs to detect photoinduced DNA damage in poly-dA oligonucleotide species and observed differences in damage kinetics which was dependent on the nature of nucleobases[94]. SPs have also been used to detect single base mismatches in DNA and DNA damage[102]. Although the use of SPs in DNA damage detection has shown to be both promising and interesting, it has similar flaws as 2AP, in that inadequate quenching persists.

Probes which consist of a hairpin containing a 2-aminopurine (2AP), an analog of adenine has also been used to detect DNA damage[103]. This probe fluoresces more in the presence of damaged DNA and its fluorescence is quenched when hybridized with the undamaged target[76,103]. This method can be said to give a positive signal as it fluoresces only when it binds to damaged DNA strands. This positive detection serves as an advantage for the use of 2AP probes

for DNA damage detection as it enhances specificity, although as mentioned earlier it suffers from background fluorescence and its synthesis can be quite expensive.

1.6.2 EvaGreen® and Tb^{3+} as methods of DNA damage detection

Some fluorescence techniques in the detection of DNA damage have been discussed extensively above, with each having its own merits and demerits. The ever-expanding field of DNA damage detection has led to the discovery of more probes for this same purpose, each of which possess its own uniqueness and advantages over the others. New fluorescent methods for detecting DNA damage will provide easier and cheaper ways of performing DNA damage detection with good reproducibility and convenience. Two such new methods are EvaGreen (EG®) and terbium (Tb^{3+}). EvaGreen dye (EG®) has been a well-known dye used for PCR and various other analysis. EG® has been shown to be compatible for qPCR analysis[104], direct quantification of DNA in microplates[102], in studying of Alu insertion polymorphisms[106] and RT-PCR analysis[107,108]. It has also been found to be stable to heat and hydrolysis[104]. The EG® dye is an intercalating dye, which binds to DNA in a non-sequence specific manner[104]. In the absence of dsDNA target, EG® consists of two chromophores in a stacked conformation and shows a weak fluorescence activity[109] due to intramolecular quenching. On hybridizing with dsDNA, the fluorophores separate from each other and hence fluorescence is observed. EG® binds complementarily to undamaged DNA, and hence there is an observed increase in fluorescence intensity; however, when damage is incorporated into the DNA helix, such as with increased UV irradiation (i.e., in the case of UV-induced DNA damage), a decrease in fluorescence intensity is observed as the EG®-dsDNA hybrid becomes unstable due to the induced lesions.

In the EG®-DNA hybridization assay for the detection of DNA damage, DNA samples of requisite concentrations are prepared and their absorbances are obtained using a UV spectrometer. The concentrations of the DNA samples are always prepared to be as close as possible and the resulting concentrations are calculated using the Beer-Lambert law: $A= \varepsilon bc$. Since the absorbed intensity I_A is related to the transmitted intensity, $I_A= I_0-I_t$, and is also related to the rate constant (k) through the quantum yield, ϕ, (which depicts the number of molecules that are damaged per photon absorbed from the UV light) and molar absorptivity, ε, $k= \sigma I_A \phi$ (where σ is the absorption cross section and is related to the molar absorptivity by a conversion

factor i.e. change in units), it is therefore important to ensure the absorbances of the sample solutions prepared are as close as possible during the sample preparation. Our group has demonstrated using this method that EG® can be used in detecting antiviral induced DNA damage[110] and recently for the detection of mutagenic hotspots in K-Ras and N-Ras proto-oncogenes for UVC-induced DNA damage[111]. Several other works are ongoing in the group using EG® as a tool to detect UV-induced DNA damage in longer nucleotide and extracted cellular DNA samples, as will be discussed in the later Chapters of this thesis.

Terbium chloride ($TbCl_3$) is a crystalline, water-soluble source of terbium. Terbium is a rare earth metal that has progressively been used in recent technologies[112]. Until a few decades ago, little was known of the biological effect of this compound[112]. It has mostly been used for metal and electrochemical analysis. Several studies have shown that Tb^{3+} can be used in detecting both DNA mismatches and UV-induced DNA damage[113,114]. El-Yabzi et al., went further to show that Tb^{3+} can also be used as a luminescent probe to show both location and number of mismatches in DNA sequences[114]. This method was found to be sensitive and showed good LOQ and LOD. Unlike other fluorescent probes, Tb^{3+} is inherently fluorescent in water due to the non-zero vibrational character of the coordinated water molecules[114]. The deprotonation of the oxygen on the phosphate backbone of DNA upon dissolution can dislodge one or more water molecules attached to Tb^{3+} when found in the same solution. However, no change is observed in the fluorescent activity of Tb^{3+} because coordination with the already paired nucleobases cannot occur, thereby limiting energy transfer[114,115]. However, Tb^{3+} forms a coordinate bond in the presence of an unpaired nucleobase in the damaged ssDNA and this enhances the fluorescence intensity of Tb^{3+} proportional to the extent of damage through ISC and radiationless energy transfer[114].

1.6.3 Affinity capillary electrophoresis with laser-induced fluorescence detection (CE-LIF)

With a LOQ[73] of 10^{-21} M in the detection of thymine glycols and the option of running analysis with small sample volumes, affinity capillary electrophoresis with laser-induced fluorescence (CE-LIF) has proven to be a powerful tool for bioanalysis. Although capillary electrophoresis (CE) can be adapted to mass spectrometry, UV and laser-induced fluorescence (LIF), LIF has become preferred due to its high selectivity and sensitivity.

This method offers the option for a faster separation process , and separation can be achieved in a matter of seconds. Jorgenson and Lukacs were the first to introduce this method in 1981[116] and since then, CE-LIF has gained a lot of recognition in biological assays. CE-LIF can be used for both homogeneous and heterogeneous matrices[116], and for homogeneous matrices, all reacting species are in the liquid phases. Two methods are used for the successful adaptation of CE with immunoreactions in the homogeneous assays. These two methods are namely competitive and non-competitive binding. For the non-competitive binding, either the antibody (Ab) or antigen (Ag) is in excess and the LIF signal for the immunocomplex formed is detected[116]. The problem with the non-competitive binding-based assay is that the signal of the immunocomplex formed between a small molecule like Ag and an Ab would be so small and hence poor sensitivity and low discrimination of LIF signals that is detected. However, the use of aptamers has really enhanced the non-competitive binding assay. In the competitive binding assay, fluorescently labelled Ab or Ag compete with unlabeled isotypes to bind to a known amount of reactant. These labelled and unlabeled isotypes react with the substrate of interest to give two LIF peaks, one of which corresponds to the immunocomplex formed and the other to the free unlabeled isotypes[116].

CE-LIF uses a laser-induced fluorescence detection technique. This means that a laser is used to excite the fluorophore during the analysis and the subsequent fluorescence signal is measured. Goulko et al., used CE-LIF to detect CPD photoproduct in human normal fibroblast CRL-2522 cells upon low UVB irradiation[117]. Although the specificity of this method to the detection of thymine glycols is yet to be validated, nevertheless it has been used to detect thymine glycols in irradiated A 549 cells[118]. While this method shows promise, high cellular DNA backgrounds can limit measurements of 6-4PP photoproducts using this method[76,117].

1.7 DNA damage detection in cellular DNA

Since DNA is found in cells, it is much easier and better to detect any form of damage directly from the cellular component of living organisms rather than going through the hassle of having to extract the DNA before checking for damage. As easy and important as this may sound, however, the challenges posed by having to develop a method that detects induced DNA damage in multiple cells simultaneously could well serve as a limiting factor in trying to develop a viable

method to do this. Because most of the assays employed in detecting cellular DNA damage require some form or application of electrophoretic technique, it means that it might be limited to detecting DNA damage in the form of strand breaks. We will be looking at some cellular DNA damage detection techniques in detail, namely the comet and halo assays. Both assays involve the staining of the sample with a fluorescent dye although the processes and shape of the analyte in both assays are quite different. The halo assay, which allows for an imaging technique seems to offer a more realistic option in detecting forms of DNA damage other than strand breaks. Both techniques will be discussed in detail in the next few paragraphs in order to fully understand their principles and limitations associated with studies that have been carried out using these methods.

The name comet assay was first introduced by Olive in 1991[75]. Comet assay is used to detect DNA damage on an individual cell basis and therefore is referred to as a single-cell gel electrophoresis assay. It is a very good method that can be used in detecting DNA strand breaks, crosslinks and alkali-labile sites in single cells. This technique is based on the micro-electrophoresis of cellular DNA content and like every other electrophoretic technique is size dependent. In the case of DNA, nicked strands travel much faster through the gel than undamaged strands[76]. In the sample preparation, the cells are carefully embedded in an agarose gel, lysed and then subjected to an electric field before being stained with a fluorescent dye. The damaged DNA, which are charged, migrate through the electric field in the form of the "tail of a comet" while the undamaged DNA migrate remaining in the "head of the comet". These comet tails increase in size as the damage in DNA increase. Images are captured using a fluorescence imaging microscope. Endonucleases, which are specific for different DNA damage sites, increase the specificity and sensitivity of this method. An example of this has been demonstrated in which T4 endonuclease V was used to enhance the detection of UVB-induced CPDs in keratinocyte cells[76,119]. Comet assays can be modified with the use of monoclonal antibodies to detect photoadducts like CPDs[76,120]. A combination of comet assay with FISH has been carried out to enhance its resolution in the detection of sequence-dependent DNA damage[121,122]. Comet assays are however more sensitive to strand breaks and are mostly used for dsDNA.

Another cellular detection technique is the halo assay. The procedure for this technique was first introduced by Vinograd et al., (1965) and was Later modified by Roti Roti and Wright

(1987)[75]. Halo assay is also a single-cell detection system and does not require the cells to be radiolabeled[75]. In this assay, the cells are first lysed and stained with propidium iodide (PI), a fluorescent intercalating dye. The intercalation of the PI with the DNA double helix alters the topology of the DNA coils and in doing so forms a fluorescent halo[75]. This halo in turn changes diameter which is proportional to the concentration of PI. Images of individual nucleotides are captured as 'halos', which are detected by an imaging system based on their chromatin fragility[75].

Malyapa et al in 1995, showed that halo assay can be used in the detection of base pair alterations in DNA sequences on an individual cell level[75]. Roti and Wright in 1987 showed that this assay can be employed in detecting rearrangements in DNA when irradiated with small doses of ionizing radiation (2 Gy) only when the DNA is unrepaired but on repair, the assay becomes insensitive[75] to detect DNA damages induced by ionizing radiation of doses lower than 10 Gy. To detect single strand breaks, after spreading the cells on an agarose gel and then on microscopic slides, this assay has been modified by incubating the cells firstly in a high-salt alkaline lye solution and afterwards in a second solution of lower alkalinity and finally stained with ethidium bromide[75]. Another version of this assay is one known as fast halo assay (FHA).

Other DNA damage detection methods exists which includes but not limited to terminal deoxyribonucleotidyl transferase mediated deoxyuridine triphosphate nick end labeling (TUNEL); high-performance liquid chromatography coupled to tandem mass spectrometry (HPLC-MS/MS); fluorescence in situ hybridization (FISH); flow cytometry (FCM); radio immunoassay (RIA); NMR: nuclear magnetic resonance spectroscopy were not mentioned in this Chapter as these have been covered in details in other review articles.

1.8 Aim and Summary of Thesis

The role of DNA and the importance of maintaining its structural and base pair integrity, in the optimal functioning of the cells and the entire system of a given organism cannot be over-emphasized. In the light of the above mentioned, it becomes imperative that any form of damage to DNA needs to be accurately and precisely measured, quantified and analyzed if the above-mentioned assertion is to hold true. From the various sections and paragraphs above, much work

has been put in to improve methods aimed at detecting various types of DNA damage and more continues to be done. It is in the need for the latter that we are trying to develop new, effective and cheaper ways of detecting UV-induced DNA photoadducts which are precursors to skin cancer. The use of EG® as a probe for DNA damage detection has since been receiving more attention but so far has only been used to detect DNA damage in short nucleotide sequences. Therefore, the necessity of this work arises from the idea that it is important to improve the EG®-DNA hybridization method in order to detect UV-induced DNA damage in long DNA sequences and in extracted cellular DNA. Also, comparing the damage profiles of different DNA samples being damaged via irradiation with UV light both individually and simultaneously will help shed more light on the understanding of the damage kinetics of various samples with respect to their base compositions when exposed to UV light.

Chapter 2 demonstrates the use of EG®-DNA hybridization technique to detect UV induced damage in individual DNA samples. Subjecting only a single sample does not take into consideration the systematic and human errors that might be associated with this method. In order to validate our method, two samples each of the same DNA sample were exposed to UV irradiation simultaneously using the cuvette method.

Chapter 3 of this thesis focuses on the comparative experiments between two different DNA samples exposed to UV irradiation simultaneously. Thus, *E. coli* DNA for example will be exposed to UVC irradiation at the same time with either calf thymus or salmon sperm DNA. The results obtained from the experiments will therefore go on to predict or show the differences in damage time constants corresponding to known G-C and A-T contents of the samples analyzed.

Finally, Chapter 4 will discuss the conclusion of this thesis and suggest future work that can be done to improve on the various modifications and adaptation we have made in this work. In all, this research work is aimed at adapting the EG®-DNA hybridization technique to the detection of UV induced DNA damage to both long nucleotide sequences and extracted cellular DNA and showing differences in damage kinetics as a function of percentage base pair concentration in different DNA samples.

Reference list.

(1) Vranken, D. Van; Weiss, G. *Introduction to Bioorganic Chemistry and Chemical Biology*; Scholl, S., Ed.; Garland Science, Taylor & Francis Group, LLC: New York, 2013; Vol. 36.

(2) Alberts, B.; Johnson, A.; Lewis, J.; Raff, M.; Roberts, K.; Peter Walter. *Molecular Biology of the Cell*, 4th ed.; Garland Science: New York, 2002.

(3) Berg, J. M.; Tymoczko, J. L.; Stryer, L. *Biochemistry*, 5th Revise.; W H Freeman & Co (Sd): New York, 2002.

(4) Brown, T. A. *Genomes*, 2nd ed.; Wiley-Liss: Oxford, 2002.

(5) Aylon, Y.; Kupiec, M. DSB Repair: The Yeast Paradigm. *DNA Repair (Amst).* **2004**, *3* (8–9), 797–815. https://doi.org/10.1016/j.dnarep.2004.04.013.

(6) Li, X.; Heyer, W. D. Homologous Recombination in DNA Repair and DNA Damage Tolerance. *Cell Res.* **2008**, *18* (1), 99–113. https://doi.org/10.1038/cr.2008.1.

(7) Barzel, A.; Kupiec, M. Finding a Match: How Do Homologous Sequences Get Together for Recombination? *Nat. Rev. Genet.* **2008**, *9* (1), 27–37. https://doi.org/10.1038/nrg2224.

(8) Corrêa, M. D. P. Amounts Observed in Brazil and South America *. **2015**, *90* (3), 297–310.

(9) Becker, M. M.; Wang, Z. Origin of Ultraviolet Damage in DNA. *J. Mol. Biol.* **1989**, *210* (3), 429–438. https://doi.org/10.1016/0022-2836(89)90120-4.

(10) Young, A. R. Acute Effects of UVR on Human Eyes and Skin. *Prog. Biophys. Mol. Biol.* **2006**, *92* (1), 80–85. https://doi.org/10.1016/j.pbiomolbio.2006.02.005.

(11) Chang, N. Bin; Feng, R.; Gao, Z.; Gao, W. Skin Cancer Incidence Is Highly Associated with Ultraviolet-B Radiation History. *Int. J. Hyg. Environ. Health* **2010**, *213* (5), 359–368. https://doi.org/10.1016/j.ijheh.2010.06.006.

(12) D'Orazio, J.; Jarrett, S.; Amaro-Ortiz, A.; Scott, T. UV Radiation and the Skin. *Int. J. Mol. Sci.* **2013**, *14* (6), 12222–12248. https://doi.org/10.3390/ijms140612222.

(13) Madan, V.; Lear, J. T.; Szeimies, R.-M. Non-Melanoma Skin Cancer. *Lancet (London, England)* **2010**, *375* (9715), 673–685. https://doi.org/10.1016/S0140-6736(09)61196-X.

(14) Alscher, R. G.; Donahue, J. L.; Cramer, C. L. Reactive Oxygen Species and Antioxidants: Relationships in Green Cells. *Physiol. Plant.* **1997**, *100* (2), 224–233. https://doi.org/10.1034/j.1399-3054.1997.1000203.x.

(15) Toyokuni, S. Oxidative Stress as an Iceberg in Carcinogenesis and Cancer Biology. *Arch. Biochem. Biophys.* **2016**, *595*, 46–49. https://doi.org/10.1016/j.abb.2015.11.025.

(16) Cooke, M. S.; Evans, M. D.; Dizdaroglu, M.; Lunec, J. Oxidative DNA Damage: Mechanisms, Mutation, and Disease. *FASEB J.* **2003**, *17* (10), 1195–1214. https://doi.org/10.1096/fj.02-0752rev.

(17) Rastogi, R. P.; Richa; Kumar, A.; Tyagi, M. B.; Sinha, R. P. Molecular Mechanisms of Ultraviolet Radiation-Induced DNA Damage and Repair. *J. Nucleic Acids* **2010**, *2010*, 592980. https://doi.org/10.4061/2010/592980.

(18) Hidaka, H.; Horikoshi, S.; Serpone, N.; Knowland, J. In Vitro Photochemical Damage to DNA, RNA and Their Bases by an Inorganic Sunscreen Agent on Exposure to UVA and UVB Radiation. *J. Photochem. Photobiol. A Chem.* **1997**, *111* (1–3), 205–213. https://doi.org/10.1016/S1010-6030(97)00229-3.

(19) Kligman, L. H. Photoaging. Manifestations, Prevention, and Treatment. *Dermatol. Clin.* **1986**, *4* (3), 517–528.

(20) Kligman, L. H.; Akin, F. J.; Kligman, A. M. The Contributions of UVA and UVB to Connective Tissue Damage in Hairless Mice. *J. Invest. Dermatol.* **1985**, *84* (4), 272–276. https://doi.org/10.1111/1523-1747.ep12265353.

(21) Kvam, E.; Tyrrell, R. M. Induction of Oxidative DNA Base Damage in Human Skin Cells by UV and near Visible Radiation. *Carcinogenesis* **1997**, *18* (12), 2379–2384. https://doi.org/10.1093/carcin/18.12.2379.

(22) Tyrrell, R. M. induction of Pyrimidine dimers in Bacterial DNA by 365 nm Radiation. *Photochem. Photobiol.* **1973**, *17* (1), 69–73. https://doi.org/10.1111/j.1751-1097.1973.tb06334.x.

(23) Perdiz, D.; Grof, P.; Mezzina, M.; Nikaido, O.; Moustacchi, E.; Sage, E. Distribution and Repair of Bipyrimidine Photoproducts in Solar UV-Irradiated Mammalian Cells. Possible Role of Dewar Photoproducts in Solar Mutagenesis. *J. Biol. Chem.* **2000**, *275* (35), 26732–26742. https://doi.org/10.1074/jbc.M001450200.

(24) Douki, T.; Reynaud-Angelin, A.; Cadet, J.; Sage, E. Bipyrimidine Photoproducts Rather than Oxidative Lesions Are the Main Type of DNA Damage Involved in the Genotoxic Effect of Solar UVA Radiation. *Biochemistry* **2003**, *42* (30), 9221–9226. https://doi.org/10.1021/bi034593c.

(25) Courdavault, S.; Baudouin, C.; Charveron, M.; Favier, A.; Cadet, J.; Douki, T. Larger Yield of Cyclobutane Dimers than 8-Oxo-7,8-Dihydroguanine in the DNA of UVA-Irradiated Human Skin Cells. *Mutat. Res. - Fundam. Mol. Mech. Mutagen.* **2004**, *556* (1–2), 135–142. https://doi.org/10.1016/j.mrfmmm.2004.07.011.

(26) El Ghissassi, F.; Baan, R.; Straif, K.; Grosse, Y.; Secretan, B.; Bouvard, V.; Benbrahim-Tallaa, L.; Guha, N.; Freeman, C.; Galichet, L.; Cogliano, V. A Review of Human Carcinogens--Part D: Radiation. *Lancet Oncol.* **2009**, *10* (8), 751–752. https://doi.org/10.1016/s1470-2045(09)70213-x.

(27) Ikehata, H.; Kawai, K.; Komura, J. I.; Sakatsume, K.; Wang, L.; Imai, M.; Higashi, S.; Nikaido, O.; Yamamoto, K.; Hieda, K.; Watanabe, M.; Kasai, H.; Ono, T. UVA1 Genotoxicity Is Mediated Not by Oxidative Damage but by Cyclobutane Pyrimidine Dimers in Normal Mouse Skin. *J. Invest. Dermatol.* **2008**, *128* (9), 2289–2296. https://doi.org/10.1038/jid.2008.61.

(28) Agar, N. S.; Halliday, G. M.; Barnetson, R. S.; Ananthaswamy, H. N.; Wheeler, M.; Jones, A. M. The Basal Layer in Human Squamous Tumors Harbors More UVA than UVB Fingerprint Mutations: A Role for UVA in Human Skin Carcinogenesis. *Proc. Natl. Acad. Sci. U. S. A.* **2004**, *101* (14), 4954 LP – 4959. https://doi.org/10.1073/pnas.0401141101.

(29) Urbach, F. Potential Effects of Altered Solar Ultraviolet Radiation on Human Skin Cancer. *Photochem. Photobiol.* **1989**, *50* (4), 507–513. https://doi.org/10.1111/j.1751-1097.1989.tb05556.x.

(30) Peak, M. J.; Peak, J. G.; Moehring, M. P.; Webb, R. B. Ultraviolet Action Spectra for DNA Dimer Induction, Lethality, and Mutagenesis in Escherichia Coli with Emphasis on the UVB Region. *Photochem. Photobiol.* **1984**, *40* (5), 613–620. https://doi.org/10.1111/j.1751-1097.1984.tb05349.x.

(31) Dylan Trotsek. *Sunscreen Photobiology.Molecular, Cellular and Physiological Aspects*; 2017; Vol. 110.

(32) Murphy, G. M. Sunblocks: Mechanisms of Action. **1999**, 34–36.

(33) Scott, L. C. Survival and Sex Ratios of the Intertidal Copepod, Tigriopus Californicus, Following Ultraviolet-B (290–320 Nm) Radiation Exposure. *Mar. Biol.* **1995**, *123* (4), 799–804. https://doi.org/10.1007/BF00349123.

(34) Peak, M. J.; Peak, J. G. Single-Strand Breaks Induced in Bacillus Subtilis DNA by Ultraviolet Light: Action Spectrum and Properties. *Photochem. Photobiol.* **1982**, *35* (5), 675–680. https://doi.org/10.1111/j.1751-1097.1982.tb02628.x.

(35) Sinha, R. P.; Dautz, M.; Häder, D. P. A Simple and Efficient Method for the Quantitative Analysis of Thymine Dimers in Cyanobacteria, Phytoplankton and Macroalgae. *Acta Protozool.* **2001**, *40* (3), 187–195.

(36) Buma, A. G. J.; De Boer, M. K.; Boelen, P. Depth Distributions of DNA Damage in Antarctic MarinE Phyto- and Bacterioplankton Exposed TO SUMMERTIME UV Radiation. *J. Phycol.* **2001**, *37* (2), 200–208. https://doi.org/10.1046/j.1529-8817.2001.037002200.x.

(37) Pakker, H.; Beekman, C.; Breeman, A. Efficient Photoreactivation of UVBR-Induced DNA Damage in the Sublittoral Macroalga Rhodymenia Pseudopalmata (Rhodophyta). *Eur. J. Phycol.* **2000**, *35* (2), 109–114. https://doi.org/10.1080/09670260010001735691.

(38) Quaite, F. E.; Sutherland, B. M.; Sutherland, J. C. Running Title: Gel Electrophoresis Assay for Pyrimidine Dimers in Plant DNA Key Words: Ozone Depletion, Ultraviolet Radiation, DNA, Pyrimidine Dimer, Gel Electrophoresis.

(39) Stein, B.; Rahmsdorf, H. J.; Steffen, A.; Litfin, M.; Herrlich, P. UV-Induced DNA Damage Is an Intermediate Step in UV-Induced Expression of Human Immunodeficiency Virus Type 1, Collagenase, c-Fos, and Metallothionein. *Mol. Cell. Biol.* **1989**, *9* (11), 5169–5181. https://doi.org/10.1128/mcb.9.11.5169.

(40) Lima-Bessa, K. M. de; Armelini, M. G.; Chiganças, V.; Jacysyn, J. F.; Amarante-Mendes, G. P.; Sarasin, A.; Menck, C. F. M. CPDs and 6-4PPs Play Different Roles in UV-Induced Cell Death in Normal and NER-Deficient Human Cells. *DNA Repair (Amst).* **2008**, *7* (2), 303–312. https://doi.org/10.1016/j.dnarep.2007.11.003.

(41) Sinha, R. P.; Häder, D.-P. UV-Induced DNA Damage and Repair: A Review. *Photochem. Photobiol. Sci.* **2002**, *1* (4), 225–236. https://doi.org/10.1039/B201230H.

(42) Taylor, J.-S.; Lu, H.-F.; Kotyk, J. J. Quantitative Conversion of the (6–4) photoproduct of TpdC to its Dewar Valence Isomer Upon Exposure to Simulated Sunlight. *Photochem. Photobiol.* **1990**, *51* (2), 161–167. https://doi.org/10.1111/j.1751-1097.1990.tb01698.x.

(43) Slieman, T. A.; Nicholson, W. L. Artificial and Solar UV Radiation Induces Strand Breaks and Cyclobutane Pyrimidine Dimers in <Em>Bacillus Subtilis</Em>

Spore DNA. *Appl. Environ. Microbiol.* **2000**, *66* (1), 199 LP – 205. https://doi.org/10.1128/AEM.66.1.199-205.2000.

(44) Nikandrova, Y.; Baumstark-Khan, C.; Horneck, G. Repair-Induced DNA Strand Breaks in UV-Irradiated Mammalian Cells. In *Fundamentals for the Assessment of Risks from Environmental Radiation*; Baumstark-Khan, C., Kozubek, S., Horneck, G., Eds.; Springer Netherlands: Dordrecht, 1999; pp 155–160. https://doi.org/10.1007/978-94-011-4585-5_20.

(45) Limoli, C. L.; Giedzinski, E.; Bonner, W. M.; Cleaver, J. E. UV-Induced Replication Arrest in the Xeroderma Pigmentosum Variant Leads to DNA Double-Strand Breaks, γ-H2AX Formation, and Mre11 Relocalization. *Proc. Natl. Acad. Sci.* **2002**, *99* (1), 233 LP – 238. https://doi.org/10.1073/pnas.231611798.

(46) Batista, L. F. Z.; Kaina, B.; Meneghini, R.; Menck, C. F. M. How DNA Lesions Are Turned into Powerful Killing Structures: Insights from UV-Induced Apoptosis. *Mutat. Res. - Rev. Mutat. Res.* **2009**, *681* (2–3), 197–208. https://doi.org/10.1016/j.mrrev.2008.09.001.

(47) Ichihashi, M. ; Ueda, M. ; Budiyanto, A. ; Bito, T. ; Oka, M. ; Fukunaga, M. ; Tsuru, K. ; Horikawa, T. UV-Induced Skin Damage. *Toxicology* **2003**, *189* (1–2), 21–39. https://doi.org/10.1016/s0300-483x(03)00150-1.

(48) Pescheck, F.; Lohbeck, K. T.; Roleda, M. Y.; Bilger, W. UVB-Induced DNA and Photosystem II Damage in Two Intertidal Green Macroalgae: Distinct Survival Strategies in UV-Screening and Non-Screening Chlorophyta. *J. Photochem. Photobiol. B Biol.* **2014**, *132*, 85–93. https://doi.org/https://doi.org/10.1016/j.jphotobiol.2014.02.006.

(49) Bérubé, R.; Drigeard Desgarnier, M.-C.; Douki, T.; Lechasseur, A.; Rochette, P. Persistence and Tolerance of DNA Damage Induced by Chronic UVB Irradiation of the Human Genome. *J. Invest. Dermatol.* **2017**, *138*. https://doi.org/10.1016/j.jid.2017.08.044.

(50) Ali, D.; Ray, R. S.; Hans, R. K. UVA-Induced Cytotoxicity and DNA Damaging Potential of Benz (e) Acephenanthrylene. *Toxicol. Lett.* **2010**, *199* (2), 193–200. https://doi.org/https://doi.org/10.1016/j.toxlet.2010.08.023.

(51) Loppnow, G. R.; Billinghurst, B. E.; Oladepo, S. A. *In Radiation Induced Molecular Phenomena in Nucleic Acids – A Comprehensive Theoretical and Experimental Analysis*

Series: Challenges and Advances in Computational Chemistry and Physics; Shukla, M. K. L., Ed.; Springer: Netherland, 2008.

(52) Horspool, M. W.; Song, P.-S. *CRC Handbook of Organic Photochemistry and Photobiology*, 1st ed.; Horspool, W., Song, P.-S., Eds.; CRC-Press: New york, 1995.

(53) Kundu, L. M.; Loppnow, G. R. Direct Detection of 8-Oxo-Deoxyguanosine Using UV Resonance Raman Spectroscopy†. *Photochem. Photobiol.* **2007**, *83* (3), 600–602. https://doi.org/doi:10.1562/2006-04-15-RA-876.

(54) Faichuk, M.; Mah, A.; Loppnow, G. R. Photochemistry of 5Fluorouracil Dideoxyribonucleoside Monophosphate. *Photochem. Photobiol.* **2007**, *83*.

(55) Horspool, L. Francesco, W. *CRC Handbook of Organic Photochemistry and Photobiology*; CRC Press: USA, 2003.

(56) Ravanat, J. L.; Douki, T.; Cadet, J. Direct and Indirect Effects of UV Radiation on DNA and Its Components. *J. Photochem. Photobiol. B.* **2001**, *63* (1–3), 88–102. https://doi.org/10.1016/s1011-1344(01)00206-8.

(57) Li, J.; Liu, Z.; Tan, C.; Guo, X.; Wang, L.; Sancar, A.; Zhong, D. Dynamics and Mechanism of Repair of Ultraviolet-Induced (6–4) Photoproduct by Photolyase. *Nature* **2010**, *466* (7308), 887–890. https://doi.org/10.1038/nature09192.

(58) Bose, S. N.; Davies, R. J.; Sethi, S. K.; McCloskey, J. A. Formation of an Adenine-Thymine Photoadduct in the Deoxydinucleoside Monophosphate d(TpA) and in DNA. *Science (80-.).* **1983**, *220* (4598), 723 LP – 725. https://doi.org/10.1126/science.6836308.

(59) Bose, S. N.; Kumar, S.; Davies, R. J.; Sethi, S. K.; McCloskey, J. A. The Photochemistry of d(T-A) in Aqueous Solution and in Ice. *Nucleic Acids Res.* **1984**, *12* (20), 7929–7947. https://doi.org/10.1093/nar/12.20.7929.

(60) Koning, T. M. G.; Davies, R. J. H.; Kaptein, R. The Solution Structure of the Intramolecular Photoproduct of d(TpA) Derived with the Use of NMR and a Combination of Distance Geometry and Molecular Dynamics. *Nucleic Acids Res.* **1990**, *18* (2), 277–284. https://doi.org/10.1093/nar/18.2.277.

(61) Pörschke, D. A Specific Photoreaction in Polydeoxyadenylic Acid. *Proc. Natl. Acad. Sci. U. S. A.* **1973**, *70* (9), 2683–2686. https://doi.org/10.1073/pnas.70.9.2683.

(62) Figueroa-González, G.; Pérez-Plasencia, C. Strategies for the Evaluation of DNA Damage and Repair Mechanisms in Cancer. *Oncol. Lett.* **2017**, *13* (6), 3982–3988. https://doi.org/10.3892/ol.2017.6002.

(63) Grimaldi, K. A.; McGurk, C. J.; McHugh, P. J.; Hartley, J. A. PCR-Based Methods for Detecting DNA Damage and Its Repair at the Sub-Gene and Single Nucleotide Levels in Cells. *Mol. Biotechnol.* **2002**, *20* (2), 181–196. https://doi.org/10.1385/MB:20:2:181.

(64) Santos, J. H.; Meyer, J. N.; Mandavilli, B. S.; Van Houten, B. Quantitative PCR-Based Measurement of Nuclear and Mitochondrial DNA Damage and Repair in Mammalian Cells. *Methods Mol. Biol.* **2006**, *314*, 183–199. https://doi.org/10.1385/1-59259-973-7:183.

(65) Senoo, T.; Yamanaka, M.; Nakamura, A.; Terashita, T.; Kawano, S.; Ikeda, S. Quantitative PCR for Detection of DNA Damage in Mitochondrial DNA of the Fission Yeast Schizosaccharomyces Pombe. *J. Microbiol. Methods* **2016**, *127*, 77–81. https://doi.org/10.1016/j.mimet.2016.05.023.

(66) De Boer, J. G.; Glickman, B. W. Mutations Recovered in the Chinese Hamster Aprt Gene after Exposure to Carboplatin: A Comparison with Cisplatin. *Carcinogenesis* **1992**, *13* (1), 15–17. https://doi.org/10.1093/carcin/13.1.15.

(67) Pfeifer, G. P.; Tornaletti, S. Footprinting with UV Irradiation and LMPCR. *Methods* **1997**, *11* (2), 189–196. https://doi.org/10.1006/meth.1996.0405.

(68) Strauss, E. C.; Orkin, S. H. Guanine-Adenine Ligation-Mediated PCR in Vivo Footprinting. *Methods* **1997**, *11* (2), 164–170. https://doi.org/10.1006/meth.1996.0402.

(69) Gowda, G. A. N.; Djukovic, D. Overview of Mass Spectrometry-Based Metabolomics: Opportunities and Challenges. *Methods Mol. Biol.* **2014**, *1198*, 3–12. https://doi.org/10.1007/978-1-4939-1258-2_1.

(70) Sato, K.; Greenberg, M. M. Selective Detection of 2-Deoxyribonolactone in DNA. *J. Am. Chem. Soc.* **2005**, *127* (9), 2806–2807. https://doi.org/10.1021/ja0426185.

(71) Dizdaroglu, M.; Coskun, E.; Jaruga, P. Measurement of Oxidatively Induced DNA Damage and Its Repair, by Mass Spectrometric Techniques. *Free Radic. Res.* **2015**, *49* (5), 525–548. https://doi.org/10.3109/10715762.2015.1014814.

(72) Gajewski, E.; Dizdaroglu, M. Hydroxyl Radical Induced Cross-Linking of Cytosine and Tyrosine in Nucleohistone. *Biochemistry* **1990**, *29* (4), 977–980. https://doi.org/10.1021/bi00456a020.

(73) Koivisto, P.; Peltonen, K. Analytical Methods in DNA and Protein Adduct Analysis. *Anal. Bioanal. Chem.* **2010**, *398* (6), 2563–2572. https://doi.org/10.1007/s00216-010-4217-3.

(74) Dizdaroglu, M.; Gajewski, E. Structure and Mechanism of Hydroxyl Radical-Induced Formation of a DNA-Protein Cross-Link Involving Thymine and Lysine in Nucleohistone. *Cancer Res.* **1989**, *49* (13), 3463–3467.

(75) Kumari, S.; Rastogi, R.; Singh, K.; Singh, S.; Sinha, R. DNA Damage: Detection Strategies. *Excli J* **2008**, *7*, 44–62.

(76) El-Yazbi, A. F.; Loppnow, G. R. Detecting UV-Induced Nucleic-Acid Damage. *TrAC Trends Anal. Chem.* **2014**, *61*, 83–91. https://doi.org/https://doi.org/10.1016/j.trac.2014.05.010.

(77) Douki, T.; Cadet, J. Individual Determination of the Yield of the Main UV-Induced Dimeric Pyrimidine Photoproducts in DNA Suggests a High Mutagenicity of CC Photolesions. *Biochemistry* **2001**, *40* (8), 2495–2501. https://doi.org/10.1021/bi0022543.

(78) Cadet, J.; Douki, T.; Frelon, S.; Sauvaigo, S.; Pouget, J.-P.; Ravanat, J.-L. Assessment of Oxidative Base Damage to Isolated and Cellular DNA by HPLC-MS/MS Measurement. *Free Radic. Biol. Med.* **2002**, *33* (4), 441–449. https://doi.org/10.1016/s0891-5849(02)00820-1.

(79) Singh, R.; Farmer, P. B. Liquid Chromatography-Electrospray Ionization-Mass Spectrometry: The Future of DNA Adduct Detection. *Carcinogenesis* **2006**, *27* (2), 178–196. https://doi.org/10.1093/carcin/bgi260.

(80) Bespalov, V. A.; Conconi, A.; Zhang, X.; Fahy, D.; Smerdon, M. J. Improved Method for Measuring the Ensemble Average of Strand Breaks in Genomic DNA. *Environ. Mol. Mutagen.* **2001**, *38* (2- 3), 166–174. https://doi.org/10.1002/em.1068.

(81) Santella, R. M. Immunological Methods for Detection of Carcinogen-DNA Damage in Humans. *Cancer Epidemiol. biomarkers Prev. a Publ. Am. Assoc. Cancer Res. cosponsored by Am. Soc. Prev. Oncol.* **1999**, *8* (9), 733–739.

(82) Waller, H.; Friess, E.; Kiefer, J. On the Immunological Detection of X-Ray Induced DNA Damage. *Radiat. Environ. Biophys.* **1981**, *19* (4), 259–264. https://doi.org/10.1007/BF01324091.

(83) L. Mitchell, D.; Clarkson, J. M. Use of Synthetic Polynucleotides to Characterise an Antiserum Made Against Uv- Irradiated Dna. *Photochem. Photobiol.* **1984**, *40* (6), 743–748. https://doi.org/10.1111/j.1751-1097.1984.tb04646.x.

(84) J. Cadet, P. V. *The Photochemistry of Nucleic Acids*; Morrison, H., Ed.; John Wiley & Sons, Ltd: New York, 1990.

(85) Cuquerella, M. C.; Lhiaubet-Vallet, V.; Cadet, J.; Miranda, M. A. Benzophenone Photosensitized DNA Damage. *Acc. Chem. Res.* **2012**, *45* (9), 1558–1570. https://doi.org/10.1021/ar300054e.

(86) Mizuno, T.; Matsunaga, T.; Ihara, M.; Nikaido, O. Establishment of a Monoclonal Antibody Recognizing Cyclobutane-Type Thymine Dimers in DNA: A Comparative Study with 64M-1 Antibody Specific for (6-4) Photoproducts. *Mutat. Res. Repair* **1991**, *254* (2), 175–184. https://doi.org/https://doi.org/10.1016/0921-8777(91)90009-E.

(87) Yatabe, Y. ALK FISH and IHC: You Cannot Have One without the Other. *Journal of thoracic oncology: official publication of the International Association for the Study of Lung Cancer*. United States April 2015, pp 548–550. https://doi.org/10.1097/JTO.0000000000000461.

(88) Peccia, J.; Hernandez, M. Rapid Immunoassays for Detection of UV-Induced Cyclobutane Pyrimidine Dimers in Whole Bacterial Cells. *Appl. Environ. Microbiol.* **2002**, *68* (5), 2542 LP – 2549. https://doi.org/10.1128/AEM.68.5.2542-2549.2002.

(89) Sokol, D. L.; Zhang, X.; Lu, P.; Gewirtz, A. M. Real Time Detection of DNA.RNA Hybridization in Living Cells. *Proc. Natl. Acad. Sci. U. S. A.* **1998**, *95* (20), 11538–11543. https://doi.org/10.1073/pnas.95.20.11538.

(90) Bonnet, G.; Tyagi, S.; Libchaber, A.; Kramer, F. R. Thermodynamic Basis of the Enhanced Specificity of Structured DNA Probes. *Proc. Natl. Acad. Sci.* **1999**, *96* (11), 6171 LP – 6176. https://doi.org/10.1073/pnas.96.11.6171.

(91) Leone, G.; van Schijndel, H.; van Gemen, B.; Kramer, F. R.; Schoen, C. D. Molecular Beacon Probes Combined with Amplification by NASBA Enable Homogeneous, Real-

Time Detection of RNA. *Nucleic Acids Res.* **1998**, *26* (9), 2150–2155. https://doi.org/10.1093/nar/26.9.2150.

(92) Beacons of Light. *Nat. Biotechnol.* **2006**, *24* (3), 303–304. https://doi.org/10.1038/nbt0306-303b.

(93) Yarasi, S.; McConachie, C.; Loppnow, G. R. Molecular Beacon Probes of Photodamage in Thymine and Uracil Oligonucleotides¶. *Photochem. Photobiol.* **2005**, *81* (2), 467–473. https://doi.org/10.1111/j.1751-1097.2005.tb00209.x.

(94) Nair, S. G.; Loppnow, G. R. Multiplexed, UVC-Induced, Sequence-Dependent DNA Damage Detection. *Photochem. Photobiol.* **2013**, *89* (4), 884–890. https://doi.org/10.1111/php.12066.

(95) Stöhr, K.; Häfner, B.; Nolte, O.; Wolfrum, J.; Sauer, M.; Herten, D.-P. Species-Specific Identification of Mycobacterial 16S RRNA PCR Amplicons Using Smart Probes. *Anal. Chem.* **2005**, *77* (22), 7195–7203. https://doi.org/10.1021/ac051447z.

(96) Knemeyer, J.-P.; Marmé, N.; Sauer, M. Probes for Detection of Specific DNA Sequences at the Single-Molecule Level. *Anal. Chem.* **2000**, *72* (16), 3717–3724. https://doi.org/10.1021/ac000024o.

(97) Heinlein, T.; Knemeyer, J.-P.; Piestert, O.; Sauer, M. Photoinduced Electron Transfer between Fluorescent Dyes and Guanosine Residues in DNA-Hairpins. *J. Phys. Chem. B* **2003**, *107* (31), 7957–7964. https://doi.org/10.1021/jp0348068.

(98) Misra, A.; Shahid, M. Immobilization of Self-Quenched DNA Hairpin Probe with a Heterobifunctional Reagent on a Glass Surface for Sensitive Detection of Oligonucleotides. *Bioorg. Med. Chem.* **2009**, *17* (16), 5826–5833. https://doi.org/10.1016/j.bmc.2009.07.015.

(99) El-Yazbi, A. F.; Loppnow, G. R. Chimeric RNA–DNA Molecular Beacons for Quantification of Nucleic Acids, Single Nucleotide Polymophisms, and Nucleic Acid Damage. *Anal. Chem.* **2013**, *85* (9), 4321–4327. https://doi.org/10.1021/ac301669y.

(100) Misra, A.; Kumar, P.; Gupta, K. C. Synthesis of Hairpin Probe Using Deoxyguanosine as a Quencher: Fluorescence and Hybridization Studies. *Anal. Biochem.* **2007**, *364* (1), 86–88. https://doi.org/10.1016/j.ab.2007.02.003.

(101) Kim, Y.; Yang, C. J.; Tan, W. Superior Structure Stability and Selectivity of Hairpin Nucleic Acid Probes with an L-DNA Stem. *Nucleic Acids Res.* **2007**, *35* (21), 7279–7287. https://doi.org/10.1093/nar/gkm771.

(102) Oladepo, S. A.; Loppnow, G. R. Self-Quenching Smart Probes as a Platform for the Detection of Sequence-Specific UV-Induced DNA Photodamage. *Anal. Bioanal. Chem.* **2010**, *397* (7), 2949–2957. https://doi.org/10.1007/s00216-010-3896-0.

(103) El-Yazbi, A. F.; Loppnow, G. R. 2-Aminopurine Hairpin Probes for the Detection of Ultraviolet-Induced DNA Damage. *Anal. Chim. Acta* **2012**, *726*, 44–49. https://doi.org/10.1016/j.aca.2012.03.021.

(104) Mao, F.; Leung, W.-Y.; Xin, X. Characterization of EvaGreen and the Implication of Its Physicochemical Properties for QPCR Applications. *BMC Biotechnol.* **2007**, *7*, 76. https://doi.org/10.1186/1472-6750-7-76.

(105) Ihrig, J.; Lill, R.; Mühlenhoff, U. Application of the DNA-Specific Dye EvaGreen for the Routine Quantification of DNA in Microplates. *Anal. Biochem.* **2007**, *359*, 265–267. https://doi.org/10.1016/j.ab.2006.07.043.

(106) González-Giraldo, Y.; Rodríguez-Dueñas, M.; Forero, D. A. Development of Novel High-Resolution Melting-Based Assays for Genotyping Two Alu Insertion Polymorphisms (FXIIIB and PV92). *Mol. Biotechnol.* **2016**, *58* (3), 197–201. https://doi.org/10.1007/s12033-016-9915-4.

(107) Wang, W.; Chen, K.; Xu, W. DNA Quantification Using EvaGreen and a Real-Time PCR Instrument. *Anal. Biochem.* **2006**, *356*, 303–305. https://doi.org/10.1016/j.ab.2006.05.027.

(108) Eischeid, A. C. SYTO Dyes and EvaGreen Outperform SYBR Green in Real-Time PCR. *BMC Res. Notes* **2011**, *4* (1), 263. https://doi.org/10.1186/1756-0500-4-263.

(109) Shoute, L. C. T.; Loppnow, G. R. Characterization of the Binding Interactions between EvaGreen Dye and DsDNA. *Phys. Chem. Chem. Phys.* **2018**, *20* (7), 4772–4780. https://doi.org/10.1039/C7CP06058K.

(110) El-Yazbi, A.; Loppnow, G. Probing DNA Damage Induced by Common Antiviral Agents Using Multiple Analytical Techniques. *J. Pharm. Biomed. Anal.* **2018**, *157*. https://doi.org/10.1016/j.jpba.2018.05.019.

(111) Nair, S. G.; Loppnow, G. R. Comparison of K-Ras and N-Ras Mutagenic Hot Spots for UVC Damage. *ACS Omega* **2019**, *4* (2), 3469–3475. https://doi.org/10.1021/acsomega.8b03017.

(112) Shimada, H.; Nagano, M.; Funakoshi, T.; Kojima, S. Pulmonary Toxicity of Systemic Terbium Chloride in Mice. *J. Toxicol. Environ. Health* **1996**, *48* (1), 81–92. https://doi.org/10.1080/009841096161483.

(113) Fu, P. K.-L.; Turro, C. Energy Transfer from Nucleic Acids to Tb (III): Selective Emission Enhancement by Single DNA Mismatches. *J. Am. Chem. Soc.* **1999**, *121* (1), 1–7. https://doi.org/10.1021/ja9826082.

(114) El-Yazbi, A. F.; Loppnow, G. R. Terbium Fluorescence as a Sensitive, Inexpensive Probe for UV-Induced Damage in Nucleic Acids. *Anal. Chim. Acta* **2013**, *786*, 116–123. https://doi.org/10.1016/j.aca.2013.04.068.

(115) El-Yazbi, A. F.; Wong, A.; Loppnow, G. R. A Luminescent Probe of Mismatched DNA Hybridization: Location and Number of Mismatches. *Anal. Chim. Acta* **2017**, *994*, 92–99. https://doi.org/10.1016/j.aca.2017.09.036.

(116) Nguyen, B. T.; Kang, M.-J. Application of Capillary Electrophoresis with Laser-Induced Fluorescence to Immunoassays and Enzyme Assays. *Molecules* **2019**, *24* (10). https://doi.org/10.3390/molecules24101977.

(117) Goulko, A. A. Development and Application of a Capillary Electrophoresis Immunoassay for DNA Lesions Induced by Ultraviolet Light; 2011.

(118) Le, X. C.; Xing, J. Z.; Lee, J.; Leadon, S. A.; Weinfeld, M. Inducible Repair of Thymine Glycol Detected by an Ultrasensitive Assay for DNA Damage. *Science* **1998**, *280* (5366), 1066–1069. https://doi.org/10.1126/science.280.5366.1066.

(119) Yarosh, D. B.; Boumakis, S.; Brown, A. B.; Canning, M. T.; Galvin, J. W.; Both, D. M.; Kraus, E.; O'Connor, A.; Brown, D. A. Measurement of UVB-Induced DNA Damage and Its Consequences in Models of Immunosuppression. *Methods* **2002**, *28* (1), 55–62. https://doi.org/10.1016/s1046-2023(02)00209-8.

(120) Sauvaigo, S.; Serres, C.; Signorini, N.; Emonet, N.; Richard, M.-J.; Cadet, J. Use of the Single-Cell Gel Electrophoresis Assay for the Immunofluorescent Detection of Specific DNA Damage. *Anal. Biochem.* **1998**, *259* (1), 1–7. https://doi.org/https://doi.org/10.1006/abio.1998.2628.

(121) Shaposhnikov, S.; Thomsen, P. D.; Collins, A. R. Combining Fluorescent in Situ Hybridization with the Comet Assay for Targeted Examination of DNA Damage and Repair. *Methods Mol. Biol.* **2011**, *682*, 115–132. https://doi.org/10.1007/978-1-60327-409-8_10.

(122) Shaposhnikov, S.; Frengen, E.; Collins, A. R. Increasing the Resolution of the Comet Assay Using Fluorescent in Situ Hybridization—a Review. *Mutagenesis* **2009**, *24* (5), 383–389. https://doi.org/10.1093/mutage/gep021.

Chapter Two
UV-INDUCED DNA DAMAGE IN CALF THYMUS AND SALMON SPERM

2.1 Introduction

The exposure of DNA to exogeneous environmental factors such as UV radiation has been studied as a potential risk that can lead to serious health conditions such as skin cancer. The main photoproducts formed from UV-irradiation of DNA include cyclobutane pyrimidine dimers (CPDs), 6-4 pyrimidone photoproducts (6-4 PPs) and their Dewar isomers[1,2]. CPDs are the major UV-induced photo lesions and are formed between adjacent pyrimidine bases through a $2\pi+2\pi$ cycloaddition reaction of the two C5=C6 double bonds of neighboring pyrimidine bases to yield a four-membered ring product[1-4]. Depending on the nature of DNA being analyzed, CPDs of varying stereochemistry can be obtained. For example, in single-stranded DNA (ssDNA), only the *cis-syn* and to a lesser extent the *trans-syn* isomer conformation is formed while in double-stranded DNA (dsDNA) only the *cis-syn* isomer is possible due to the rigidity and steric hinderance that exists in dsDNA[3,4]. Studies[1,4,5,6] have shown that thymine-thymine (TT) and thymine-cytosine (TC) base pairs are more susceptible spots for CPD formation as compared to their other pyrimidine base pair counterparts cytosine-thymine (CT) and cytosine-cytosine (CC), due to the presence of an electron donating methyl group on thymine which inductively stabilizes the positive charge on the ring, a likely intermediate in the triplet state formation of CPDs. CPDs may also undergo the reverse reaction to regenerate the pyrimidine dimer via either electron transfer or photolysis[3,5]. This reverse reaction occurs best with irradiation at wavelengths within the UVC region or lower wavelengths because of the thymine-thymine dimer (T<>T) absorption profile[3]. Another important photoproduct from UV irradiation is the 6-4 PPs, which are formed through a non-cyclic spontaneous rearrangement reaction between the C6 and C4 of the reacting pyrimidines[1,2,3,4]. For 6-4 PPs, TC and CC are more reactive sites than TT or CT base pairs[3]. Because of the presence of the 2-pyrimidone chromophore in 6-4 PPs, 6-4 PPs are converted to Dewar isomers through the electrocyclization reaction of the pyrimidone[1,3] upon absorption of radiation in the near UV region (312-327 nm).

Various methods have been developed over the years as potential tools for the detection of UV-induced DNA damage, such as the use of molecular beacons, smart probes, mass

spectrometry, high-performance liquid chromatography, comet assays, and electrophoresis[7]. The chromatographic methods, however, require derivatization either by acidic hydrolysis or some enzymatic digestion which can introduce more lesions to the DNA samples, expensive, and the sample preparation can be both tedious and time-consuming[7-9]. The electrophoresis and comet assay methods are more sensitive to strand breaks and therefore are not as appropriate to quantify or detect sequence-specific UV-induced DNA damage. Molecular beacons (MBs) and smart probes (SPs), which are analogues of MBs, have been used for the detection of sequence-specific damage and single nucleotide polymorphisms in DNA[10,11]. SPs and MBs exist normally as hairpin structures of DNA with a fluorophore (F) and quencher (Q) at each end. Because of the proximity that exists between F and Q, there is little or no observed fluorescence due to Förster resonance energy transfer (FRET). However, upon binding with a complementary DNA target, the hairpin becomes linear, and the F and Q become separated and fluorescence is observed. As damage is introduced into the DNA strands via UV irradiation, the DNA-MB/SP hybrid becomes less stable and lower fluorescence intensity is observed. In this way, damage is detected by decreasing fluorescence intensity with increased exposure to some damage initiator, such as UVC light[7,10,11]. Although MBs and SPs show a lot of promise, they both suffer the same disadvantages, which are that they are sequence specific, they have appreciable background fluorescence, and they are expensive to design and use[7]. These problems associated with the above-mentioned methods of DNA detection all point to the necessity of having a mild, cost-effective, easy and sequence-independent DNA damage detection technique.

Recent studies[12] have shown that EvaGreen® (EG®), a DNA intercalating dye, can be used to detect UV-induced DNA damage in short oligonucleotide sequences in a mild, easy, inexpensive, and sequence-independent way. EG® predominantly exists as two acridine orange (AO) moieties that are joined by a linker[13]. EG® dye in solution (closed form) is weakly fluorescent because the two AO chromophores are stacked together but in the presence of dsDNA, the two chromophores intercalate between the base pairs stacked along the DNA strand. The intercalation separates the two AO moieties and results in highly fluorescent monomeric AOs still connected by the linker[12,13]. However, EG® has not yet been adapted to detect UVC-induced damage in more realistic samples i.e., long oligonucleotide or genomic sequences. In this study, we demonstrate the use of EG® as a prospective tool for the detection of UVC-induced

DNA damage using calf thymus DNA (ct-DNA) and salmon sperm DNA (ss-DNA) samples of approximately 2000 base pairs long. Their susceptibilities to UVC-induced damage using a high-throughput 96-well plate assay were compared as a function of their AT % compositions. Also, the magnitude of instrumental and pipette errors was measured directly from fluorescence intensities of fluorescein. Our results show good correlation of damage with the AT % compositions of the DNA, with ct-DNA damaging at a faster rate than the ss-DNA. The error analysis confirmed that over 90% of the propagated error in the UVC-induced DNA damage fluorescence intensity measurements were from sources other than pipetting and instrumental sources. These results are discussed in the context of DNA damage mechanisms and method development.

2.2 Experimental

2.2.1 Materials

6-carboxyfluorescein dye (6-CF) and deoxyribonucleic acid sodium salt fiber from ct-DNA (Sigma-Aldrich, Inc., Oakville, ON, Canada), UltraPure™ ss-DNA solution (8 μM, ThermoFischer Scientific, Waltham MA, USA), and 26.6 μM EG® (Biotium, Inc, Fremont, CA, USA) were all used as received without further purification. DNA samples were stored at -20 ˚C upon receipt and until needed. 5 μM EG® was prepared by pipetting and dissolving 2842 μL of the 26.6 μM EG® stock solution in a 50 mL falcon tube and diluted to a final volume of 15120 μL with (10 mM Tris, 10 mM NaCl, 1 mM EDTA, pH ~ 7.4) using a 1000 μL pipette.

2.2.2 UVC irradiation

Please note that all concentrations described throughout this thesis Chapter are per DNA strand, not per DNA base. A 3.02 μM ct-DNA stock solution was prepared by dissolving 0.0393 g of the DNA salt fiber in nanopure water at room temperature (Barnsted Nanopure, Boston, MA, USA) in a 10.0 mL volumetric flask. This solution was diluted to a 0.152 μM solution with an extrapolated Beer-Lambert law absorbance of 4.00. The dissolved solution was left overnight to allow for adequate dissolution of the DNA fiber. The stock solution was then further diluted to 0.038 μM as calculated from the measured absorbance of 0.990 by using the Beer-Lambert expression (ε of 2.64×10^7 cm^{-1} M^{-1} assuming 2000 base pairs per DNA strand). Similarly, for ss-DNA, a 0.06 μM solution with a measured absorbance of 1.585 (ε of 2.64×10^7 cm^{-1} M^{-1}

assuming 2000 base pairs per DNA strand) was prepared by diluting 189 μL of the 8 μM stock solution to 25.0 mL in a volumetric flask. Samples were vortexed, pipetted into 5 mL cuvettes, purged with nitrogen gas for 20 min and stoppered tightly using a septum. UV light from UVC lamps emitting at 254 nm with a power density of 75 W m^{-2} was used for the irradiation of the samples. The UVC lamps were switched on 20 min before each experiment to ensure a stable light source. The cuvettes containing the nitrogen-purged DNA samples were clamped vertically, placed in a water bath and were positioned equidistant from the irradiating lamps in a Luzchem (Ottawa, ON, Canada) DEV photoreactor. The photoreactor atmosphere was kept anoxic by constant purging of the chamber with nitrogen gas; this also kept ozone from being generated by the lamps. The water bath was used to maintain constant temperature during the experiment and all samples were constantly stirred in the cuvette to maintain homogeneity throughout the irradiation process. Irradiated and control samples were subjected to all the same procedures, except that the control samples were never exposed to UVC light. At each time point, three aliquots of 50 μL (for a total volume of 150 μL for each), each taken through the septum so as not to disturb the atmosphere of the control and irradiated nitrogen-purged samples, were removed from the cuvettes and pipetted into 0.6 mL Eppendorf tubes.

2.2.3 Absorbance and fluorescence measurements

Absorption spectra were measured on a Shimadzu (Kyoto, Japan) UV-1280 absorption spectrophotometer with a set maximum wavelength of 260 nm and a path length of 1 cm. Nanopure water was used as a blank for all absorbance measurements.

Earlier studies[12] have shown that dsDNA binds optimally with EG® in a ratio of 1 DNA bp: 1.33 EG® molecules, i.e., 4 molecules of EG® binds approximately to 3 bp of DNA, and that at a ratio above 1:1.4, new aggregate species are likely to be formed[13]. This therefore suggests that optimal concentrations of EG® are 120 μM (in the case of salmon sperm) or lower to avoid aggregate formation. In order to ensure optimal binding of the EG® with the dsDNA, calculations were done to obtain desired volumes and concentrations of both the dye and DNA for each experimental trial. An example of how this calculation was done can be seen in the case of 0.060 μM ss-DNA. The 0.06 μM was converted to its base pair equivalent by multiplying with the average base pair concentration i.e. 0.060 μM × 2000 bp = 120 μM. Since the volume for the

two ss-DNA replicates is 600 µL, then 120 µM × x/600 µL = 17 bp. This gives us a volume of 84 µL, 42 µL of ss-DNA for each of the two replicates. For EG®, a constant concentration of 5 µM was used. However, in order to achieve optimal binding for EG® using the ratio 1 bp DNA: 1.33 EG®, 5 µM × x/600 = 1.33, gives 159.6 µL, approximately 80 µL of EG® for each replicate. A 178 µL volume of buffer (10 mM Tris, 10 mM NaCl, 1 mM EDTA, pH ~ 7.4) was then added to these solutions for a final volume of 300 µL for each replicate. This same calculation was also used in the preparation of the ct-DNA solutions. All DNA bp and EG® concentrations were a fixed ratio of 1: 1.33.

The irradiated DNA solutions were mixed with EG® in the proportions described above to form the assay mixture and then hybridized by incubating in the dark at 37 ºC for 20 min using the plate reader at room temperature. Fluorescence intensity measurements were then performed by using the SpectraMax (Molecular Devices, San Jose, CA, USA) i3x plate reader with the excitation and emission wavelengths set at 485 and 535 nm, respectively.

2.2.4 Pipette and instrument error analysis

A stock solution of 100 µM 6-CF dye was prepared by dissolving 0.009 g of the dye in 250. mL water in a volumetric flask. Concentrations of 50 µM, 30 µM, 5.0 µM, 2.0 µM, 1.0 µM, 0.5 µM, 0.2 µM, and 0.1 µM of the 6-CF dye were prepared by serial dilution. Twelve 200-µL replicate volumes of each concentration were then pipetted into each row of the 96-well plate and the fluorescence intensities were measured using a SpectraMax i3x plate reader with the excitation and emission wavelengths set at 492 and 517 nm, respectively. The fluorescence measurement was taken three times for each well of the 96-well plate to ascertain consistency in measured fluorescence values.

2.3 Results and discussion

In this study, an assay to detect UVC-induced genomic DNA damage, namely EG® fluorescence detection, was extrapolated to very large strands of DNA, up to thousands of base pairs. Thus far, EG® has only been applied to DNA strands of at most 100 bp[12]. The DNA samples of ss-DNA and ct-DNA were chosen because each has approximately the same length (2000 bp long) and approximately the same molar mass (1.3×10^6 Da). In this method, EG® fluorescence decreases

with increasing DNA damage because the DNA becomes more flexible as the damage disrupts the double-strand base pairing, allowing the EG® to de-intercalate. The EG® fluorescence intensity decrease with time, indicative of DNA damage, for the samples will be compared and discussed in terms of DNA composition. Experiments to determine the effect of concentration on the observed damage and for determination of a complete error analysis are also discussed.

2.3.1 Error analysis

To measure the pipetting and instrumental errors, solutions of different concentrations of 6-CF dye were prepared through serial dilution, transferred carefully into different wells of a 96-well plate, with each row of wells representing one of the concentrations, and the fluorescence intensities were measured. The results are shown in Tables 2.1 and 2.2.

Table 2.1 shows the average fluorescence intensity, standard deviation and resulting error (the standard deviation divided by the mean) for each well in the 96-well plate after multiple measurements. Because the sample is unchanged during these measurements, the instrumental error alone can be obtained from the standard deviation over three experimental measurements. The individual standard deviations and mean values per well were then averaged over all the wells to obtain the subsequent average standard deviation and mean. The average standard deviation was then divided by the average mean to obtain the average instrumental error. The average instrument error obtained as shown in the Table 2.1 below is 2.039 %, which indicates a very negligible error. Also, the average fluorescent intensity decreased as expected with a decrease in 6-CF concentration, except for wells 13-24. Although the 6-CF concentration is approximately halved in these wells compared to wells 1-12, the mean fluorescence intensity does not decrease. This anomaly in mean fluorescence intensities can be attributed to the inner filter effect, a common problem with highly concentrated fluorophore solutions. The inner filter effect is caused by the attenuation of the excitation beam within the sample by the fluorophore molecules. This attenuation therefore leads to distorted readings by lowering the emitted fluorescence from what is expected and thus decreasing the fluorescence signal detected. This anomaly suggests the need to use lower fluorophore concentrations during the DNA analysis, which is consistent with earlier studies on the binding of EG® with DNA. The error per well shows a very small magnitude of error. Most of the Figures obtained from the error per well

analysis shows that the precision of the plate reader is ≥ 96% for all the readings obtained. Thus, the results obtained from this analysis shows that the SpectraMax i3x plate reader used for the measurement of the fluorescence intensities in this study and pipetting contributed to only a negligible amount of error in the results obtained.

Table 2.1 Instrumental (SpectraMax i3x plate reader) error analysis

Well No.	Mean (μ, counts)	SD (σ, counts)	Error (σ/μ)
1	3.247×10^{8}	1.724×10^{6}	0.005310
2	3.267×10^{8}	2.928×10^{6}	0.008962
3	3.232×10^{8}	3.197×10^{6}	0.009894
4	3.243×10^{8}	2.501×10^{6}	0.007713
5	3.305×10^{8}	1.940×10^{6}	0.005870
6	3.308×10^{8}	3.425×10^{6}	0.01035
7	3.312×10^{8}	4.018×10^{6}	0.01213
8	3.332×10^{8}	1.918×10^{6}	0.005756
9	3.298×10^{8}	1.960×10^{6}	0.005941
10	3.340×10^{8}	3.009×10^{6}	0.009009
11	3.319×10^{8}	2.860×10^{6}	0.008616
12	3.340×10^{8}	4.829×10^{6}	0.01446
13	4.098×10^{8}	1.493×10^{7}	0.03643
14	4.032×10^{8}	6.374×10^{6}	0.01581
15	3.607×10^{8}	9.548×10^{6}	0.02647
16	4.043×10^{8}	8.637×10^{6}	0.02136

17	4.038×10^8	9.967×10^6	0.02468
18	4.029×10^8	1.177×10^7	0.02923
19	4.061×10^8	7.544×10^6	0.01858
20	4.050×10^8	6.354×10^6	0.01569
21	4.007×10^8	9.574×10^6	0.02390
22	4.159×10^8	1.208×10^6	0.02905
23	4.129×10^8	9.562×10^6	0.02316
24	4.142×10^8	1.369×10^6	0.03306
25	1.777×10^8	6.430×10^6	0.03619
26	1.805×10^8	4.286×10^6	0.02374
27	1.827×10^8	4.419×10^6	0.02419
28	1.838×10^8	6.463×10^6	0.03517
29	1.841×10^8	4.882×10^6	0.02651
30	1.787×10^8	5.150×10^6	0.02882
31	1.693×10^8	4.553×10^6	0.02689
32	1.834×10^8	6.283×10^6	0.03426
33	1.888×10^8	6.031×10^6	0.03194
34	1.923×10^8	5.873×10^6	0.03053
35	1.914×10^8	6.849×10^6	0.03579
36	1.918×10^8	3.265×10^6	0.01702
37	7.946×10^7	2.581×10^6	0.03248
38	7.169×10^7	1.319×10^6	0.01840

39	7.575×10^7	1.184×10^6	0.01563
40	6.940×10^7	1.689×10^6	0.02434
41	7.617×10^7	1.827×10^6	0.02398
42	7.657×10^7	1.478×10^6	0.01930
43	7.601×10^7	2.093×10^6	0.02754
44	7.763×10^7	2.175×10^6	0.02802
45	7.857×10^7	1.757×10^6	0.02236
46	7.882×10^7	1.834×10^6	0.02327
47	7.948×10^7	2.152×10^6	0.02708
48	8.019×10^7	2.172×10^6	0.02709
49	3.991×10^7	1.422×10^6	0.03564
50	4.226×10^7	1.177×10^6	0.02784
51	3.654×10^7	1.110×10^6	0.03038
52	4.191×10^7	1.138×10^6	0.02716
53	4.249×10^7	8.740×10^6	0.02057
54	4.180×10^7	1.631×10^6	0.03902
55	4.172×10^7	9.184×10^6	0.02201
56	4.190×10^7	1.277×10^6	0.03047
57	4.300×10^7	1.164×10^6	0.02707
58	4.324×10^7	1.692×10^6	0.03912
59	4.736×10^7	1.290×10^6	0.02724
60	4.656×10^7	1.675×10^6	0.03598

61	2.642×10^7	4.530×10^5	0.01715
62	2.987×10^7	1.470×10^5	0.004920
63	2.934×10^7	2.456×10^5	0.008369
64	2.994×10^7	3.418×10^5	0.01142
65	2.937×10^7	4.508×10^5	0.01535
66	2.965×10^7	5.239×10^5	0.01767
67	2.953×10^7	5.932×10^5	0.02009
68	2.970×10^7	1.931×10^5	0.006501
69	3.063×10^7	6.485×10^5	0.02117
70	3.086×10^7	6.774×10^5	0.02195
71	3.100×10^7	4.886×10^5	0.01576
72	3.106×10^7	4.831×10^5	0.01555
73	1.164×10^7	1.664×10^5	0.01430
74	1332×10^7	3.093×10^5	0.02323
75	1.174×10^7	5.682×10^5	0.004839
76	1.206×10^7	1.019×10^5	0.008442
77	1.300×10^7	1.577×10^5	0.01213
78	1.225×10^7	1.262×10^5	0.01030
79	1.195×10^7	1.954×10^5	0.01635
80	1.316×10^7	1.915×10^5	0.01455
81	1.325×10^7	2.505×10^5	0.01891
82	1.314×10^7	3.134×10^5	0.02386

83	1.360×10^7	2.418×10^5	0.01779
84	1.342×10^7	1.780×10^5	0.01327
85	6.250×10^6	9.113×10^5	0.01458
86	5.974×10^6	1.124×10^5	0.01882
87	6.202×10^6	1.345×10^5	0.02169
88	6.332×10^6	7.028×10^5	0.01110
89	6.220×10^6	9.333×10^5	0.01501
90	6.520×10^6	6.793×10^5	0.01042
91	5.960×10^6	1.409×10^5	0.02364
92	6.035×10^6	1.172×10^5	0.01943
93	6.323×10^6	1.703×10^5	0.02693
94	6.385×10^6	1.117×10^5	0.01750
95	6.105×10^6	1.065×10^5	0.01745
96	6.669×10^6	1.292×10^5	0.01937
AVG	1.355×10^8	2.764×10^6	0.02039

In this table, the well no. indicates the individual numbering of the wells in the 96-well plate with wells 1-12 containing the 50 µM 6-CF dye solutions, wells 13-24 containing the 30 µM solution, etc., Mean and SD are the mean and standard deviation obtained over three experimental runs of each well, Error is the standard deviation divided by the mean, and AVG are the average values of these over all the wells. Concentrations of aqueous 6-CF dye used are 50 µM, 30 µM, 5 µM, 2 µM, 1 µM, 0.5 µM, 0.2 µM, and 0.1 µM.

It is important to note that the 6-CF dye used in this error experiment is different from the EG® used in the detection of UVC-induced DNA damage in the irradiated long oligonucleotide samples in this study and hence both dyes have different characteristics. That being stated, the

occurrence of the inner filter effect as seen in the higher concentration of 6-CF will not be a problem using EG® as EG® at higher concentrations forms intermediates and hence this can affect the sensitivity of the method. Therefore, lower concentration of EG® will be used in this study as will be seen in subsequent sections.

Table 2.2 Combined instrument and pipette error analysis

Concentration (μM)	Mean (μ, counts)	SD (σ, counts)	Error (σ/μ)
50	3.295×10^8	4.502×10^6	0.01366
30	4.033×10^8	1.631×10^7	0.04043
5	1.837×10^8	7.994×10^6	0.04351
2	7.664×10^7	3.527×10^6	0.04601
1	4.240×10^7	2.906×10^6	0.06856
0.5	2.978×10^7	1.261×10^6	0.04236
0.2	1.271×10^7	7.189×10^5	0.05657
0.1	6.248×10^6	2298×10^5	0.03677
Average	1.355×10^8	4.681×10^6	0.03453

In this table, the mean instrumental and pipette errors as a function of 6-CF concentration in μM are shown. Mean and SD are the mean fluorescence intensities and their standard deviation obtained over three measurements of all 12 wells containing a single 6-CF dye concentration. Errors are the mean fluorescence intensities obtained across twelve wells in each row of the 96 well plate representing each concentration divided by their standard deviation. Concentrations of aqueous 6-CF dye used are 50 μM, 30 μM, 5 μM, 2 μM, 1 μM, 0.5 μM, 0.2 μM, and 0.1 μM.

Table 2.2 shows the analysis of the combined instrument and pipette errors. The average combined instrument and pipette error was obtained by calculating the mean fluorescence intensities and their standard deviations in each row of the 96-well plate, representing a single

concentration of 6-CF. The individual means and standard deviations per concentration were then averaged to obtain the subsequent average mean and standard deviation. The average standard deviation was then divided by the average mean to obtain the average combined instrument and pipette error. As seen from Table 2.2, the average combined instrument and pipette error, as a percentage, obtained was 3.453%, which is a small percentage error. From Tables 2.1 and 2.2, the percentage average instrumental error was 2.039% while the average percentage combined instrument and pipette error 3.453%. The total error, $(\sigma/\mu)_T$, is related to the instrumental, pipette, and other errors by the expression $(\sigma/\mu)_T = \sqrt{\{(\sigma/\mu)^2_I + (\sigma/\mu)^2_P + (\sigma/\mu)^2_O\}}$ where the P, I and O subscripts indicate pipette, instrument and other sources, μ and σ are the mean and standard deviation, respectively. This therefore suggests that the error due to pipetting is 2.786%. It can therefore be inferred that error in experimental results larger than 3.453% will come from sources other than the pipette or the plate reader used in this study. Those other sources will be discussed in the appropriate section.

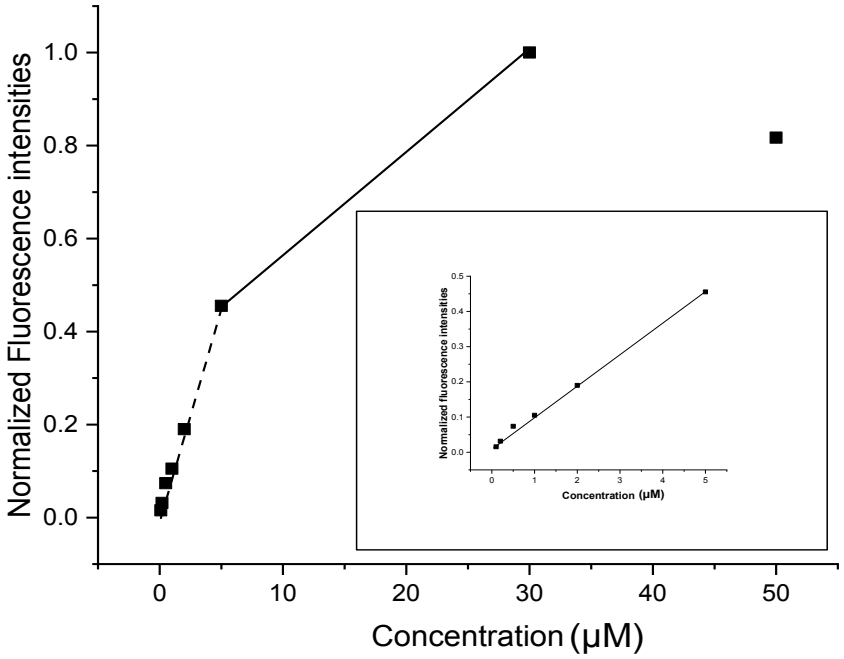

Figure 2.1: Normalized fluorescence mean intensities of various 6-CF fluorophore solutions (filled squares) as a function of their concentration. The values were obtained over three

experimental runs by exciting solutions of 6-CF in nanopure water at 492 nm and recording emission at 517 nm. The solid line through the points was obtained by a free-hand fit, omitting the 50 μM point due to the inner filter effect (see text). The concentrations of 6-CF for which their fluorescence intensities were measured are 50 μM, 30 μM, 5 μM, 2 μM, 1 μM, 0.5 μM, 0.2 μM, and 0.1 μM. The dashed line indicates the linear region of the graph as shown in the inset graph.

Figure 2.1 shows the average normalized fluorescence intensities of 6-CF solutions as a function of concentration using the data in Table 2.2. The plot shows a linear decrease (dashed line in Fig. 2.1 and inset) in fluorescence intensity as concentration decreases for concentrations below 30 μM. At concentrations above 30 μM, the inner filter effect leads to anomalous fluorescence intensities lower than would be expected from a linear dependence of intensity on concentration. As explained above, the inner filter effect will lead to lower-than-expected fluorescence intensity values.

2.3.2 Detection of UVC induced DNA damage in calf thymus and salmon sperm DNA

In this study, ct-DNA and ss-DNA solutions were irradiated with UVC light and the resulting damage detected by EG® fluorescence. In undamaged DNA, EG® intercalates in the DNA and forms a highly fluorescent complex. Increasing UVC-induced damage will lead to less rigid double-stranded DNA due to the disruption of the base pairing/hydrogen bonding. The consequently more flexible DNA will release EG® into solution where it is less fluorescent, and a resulting decrease in the sample fluorescence can be measured[12,13]. It is important to mention that EG® control only and the unirradiated DNA control only show no fluorescence activity. This means that any fluorescence activity observed for the DNA was due to its intercalation with EG®. Different concentrations were used in this study to also understand the effect of concentration on the damage time constants. The damage time constants of the samples for each trial were obtained by using the single exponential line fits for the plots. The reported average damage time constants for each sample was obtained by averaging the three individual damage time constant values obtained over three experimental trials. The possible explanations for the varying degrees of errors in the data points and in the damage time constants as will be seen in the plots are subsequently addressed in the appropriate sections of this Chapter. Because the

comparison of the damage kinetics of ct-DNA and ss-DNA have been extensively covered in Chapter 2, we will not be doing that in this section.

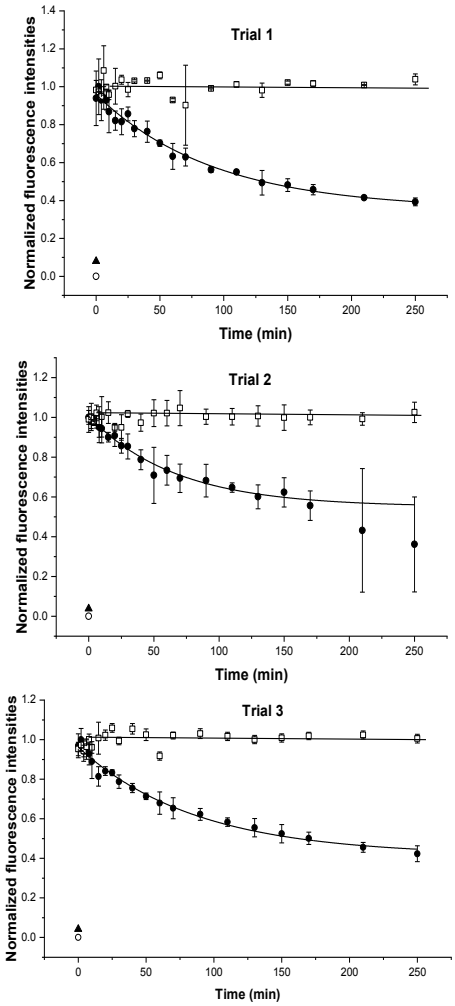

Figure 2.2: Normalized EG® fluorescence intensity as a function of UVC irradiation time for ct-DNA in Trial 1 (A), Trial 2 (B) and Trial 3 (C). EG® fluorescence detection of UVC-irradiated ct-DNA, (filled circles) and an unirradiated control (open squares) were obtained for the three experimental trials by exciting a hybridization mixture containing typically 0.0085 µM ct-DNA and 5 µM EG® in Tris buffer (10 mM Tris, 1 mM EDTA, 10 mM NaCl, pH~7.4) at 485 nm and recording emission at 535 nm. The solid lines through the points are single exponential fits to the equation, $I_F = I_0 + Ae^{-t/T}$, where I_F is the fluorescence intensity at time t, I_0 is the fluorescence intensity at t=0, A is the pre-exponential factor and T is the time constant. For the three ct-DNA

trials, T = 92 ± 6, 67 ± 9, and 87 ± 8, respectively, I_0= 0.3539 ± 0.01235, 0.5500 ± 0.02547 and 0.4156 ± 0.01887, respectively, and A= 0.5875, 0.5579, and 0.5707, respectively, for trials 1, 2 and 3. The solid lines through the control points are linear fits. Also shown are the fluorescence signals for EG® alone (filled triangles) and DNA alone (open circles). Irradiated DNA concentrations are 0.038 μM (A), 0.039 μM (B), and 0.051 μM (C)**.**

Fig. 2.2 shows the EG® fluorescence intensities obtained as a function of increasing UVC irradiation time for three samples of ct-DNA. Also shown are the fluorescence levels for the unirradiated control ct-DNA samples, and the fluorescence intensities of EG® and ct-DNA alone. Note that the fluorescence of EG® and ct-DNA alone are very low. Thus, any fluorescence above these levels comes from EG® intercalated in DNA. This is because DNA has no intrinsic fluorescence and EG® in solution without the presence of a complementary DNA target exists as two AO moieties fused together by a linker with a weak fluorescence, but upon intercalation between base pairs, these moieties are separated resulting to two fluorescent monomers that are still bound by the linker. Note also that the unirradiated samples show little or no fluorescence decrease with time, indicating that the EG® fluorescence intensity decrease in the irradiated samples comes from UVC-induced damage that leads to greater DNA flexibility, as described above. The last two data points in plot B appears to have larger errors when compared to the other points on the plot. A possible reason for this might be because some of the pipetted aliquots at this time points might have stuck to the walls of the wells during pipetting thereby leading to reduced volumes in the wells and hence errors in the fluorescence intensities obtained across these wells.

Ct-DNA solutions of concentrations 0.038 μM, 0.039 μM, and 0.051 μM were irradiated up to a maximum time of 250 min. The fluorescence intensity vs. time curves obtained, as seen in panels A, B, and C in Fig. 2.1, are similar and show an exponential decrease in fluorescence that is consistent with first-order kinetics. The time constants obtained from these single-exponential fittings are 92 ± 6 min, 67 ± 9 min, and 87 ± 8 min for irradiated ct-DNA solutions of 0.038, 0.039 and 0.051 μM concentrations, respectively. Appreciable decrease in fluorescence occurs until about the 170 min timepoint, where it levels off. The decrease in fluorescence intensities that occurs with increasing irradiation time is due to the de-intercalation of EG® from

the ct-DNA which is increasingly damaged. The de-intercalation is attributed to UVC-induced damage introduced in the dsDNA; as the UVC irradiation time increases, increased formation of photoproducts occurs. Although the aim of these experiments is not focused on determining the total time taken for DNA to fully damage as a result of UVC irradiation, a possible explanation for the levelling-off of the plot at the later time points might be as a result of the identity and position of the bases along the DNA double helix. It is well documented that UVC-induced DNA damage is sequence dependent, and that TT sequences are more photoreactive than their TC, CT and CC counterparts, and much more photoreactive than the other, photostable dinucleotide pairs possible[1,5,14]. This means that for all the 16 possible dinucleotide combinations along the dsDNA, only the TT dinucleotide is very photoreactive, with less photoreactivity in the TC, CT, and CC dinucleotides. The leveling off can therefore be due to EG® still intercalated at these less photoreactive dinucleotide combinations throughout the DNA, leading to a constant fluorescence intensity as observed at these later time points. This might suggest that at these later time points, all the photoreactive sites on the DNA strand are damaged. Also, earlier studies[1] have shown that photoproducts are formed readily at the flexible ends of oligonucleotides rather than at their more rigid centers, as demonstrated in poly (dA)-(dT) tracts. Therefore, the levelling-off of the fluorescence intensities observed at the later time points as seen in Fig. 2.2 and subsequent plots in this Chapter (see below) may also suggest that at those time points, the UVC-induced damage being observed might be occurring close to or at the more rigid sites of the DNA double helix.

Table 2.3 Damage time constants for ct-DNA

Trial	Concentration (mM)	Absorbance	Damage Time Constants (min)
1	0.038	0.992	92 ± 6
2	0.039	1.041	67 ± 9
3	0.051	1.355	87 ± 8

In this table, the UVC-induced damage time constants in minutes at various concentrations in μM and resulting absorbances of ct-DNA are shown. Results shown are means that have been averaged over three trials and the errors shown are one standard deviation.

Table 2.3 shows the UVC-induced damage time constants obtained from the three different samples of ct-DNA. The different concentrations resulted in somewhat different UVC-induced damage time constants with minimal errors. The UVC-induced damage time constant obtained from the irradiation of 0.039 μM (trial 2) gave the highest error. A possible reason for the higher error observed in trial B is the much larger error bars associated with the fluorescence intensities measured for the last two timepoints 210 min and 250 min. The inconsistencies in values observed for these two timepoints might be due to possible errors in pipetting during the transfer of replicate volumes into the wells of the 96-well plate. This may have led to unequal replicate volumes in the wells and could have led to errors in fluorescent intensity readings. Another possible reason for the larger errors on the last two time points in trial 2 is that the time lag between the exposure of the hybridized ct-DNA/EG® in the 96-well plate and its insertion into the molecular plate reader might vary between experimental trials and this can be a potential source of error. Also, improper mixing of the individual replicate representations in the 96-well plate can lead to errors in fluorescence intensity measurements. It is interesting to note that when the data obtained for these last two time points are removed and the curve is replotted, a damage time constant of 62 ± 7 min with a smaller error as compared to the 67 ± 9 min reported above is obtained. Although the irradiated ct-DNA solutions for trials 1 and 2 had almost similar concentrations, their UVC-induced damage time constants differ significantly, which shows that concentration might not be a determinant factor for the observed UVC-induced damage time constant differences. A plausible reason for the differences in the damage time constants obtained can be due to the possible dynamic transient conformational changes that occur in the DNA double helix. DNA conformation, dynamics and interactions in solutions have been extensively studied[15-20]. These studies suggest the possibility of some UVC-induced damage sites on the DNA poorly binding to EG® due to these continual short-lived changes in the structural pattern of the DNA double helix. Also, the fluorescence decay plots as seen in this Chapter only show the fitting errors, and other factors such as varying all the parameters in the fit can also be a reason for the differences in damage time constants obtained throughout this Chapter. It is important to mention that the damage time constants obtained for trials 1 and 3 are the same within experimental error even though the irradiated ct-DNA for these trials differ. Finally, it is important to note that other potential errors such as those involved in the experimental and assay

design as highlighted in earlier sentences which are not represented in the plots might also be a reason for the differences observed in damage time constants across individual trial runs.

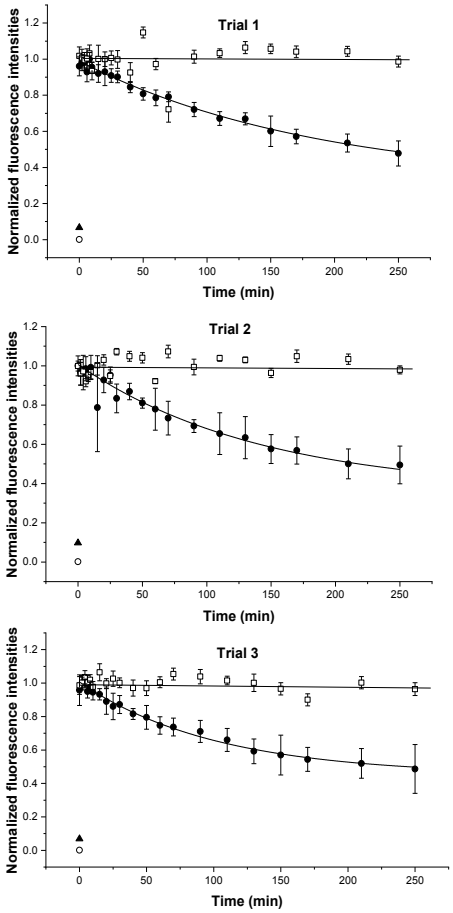

Figure 2.3. Normalized EG® Fluorescence intensity as function of UVC-irradiation time for ss-DNA in Trial 1 (A), Trial 2 (B) and Trial 3 (C). EG® fluorescence detection of UVC-irradiated ss-DNA, (filled circles) and an unirradiated control (open squares) were obtained for the three experimental trials by exciting a hybridization mixture containing typically 0.0085 μM ss-DNA and 5 μM EG® in Tris buffer (10 mM Tris, 1 mM EDTA, 10 mM NaCl, pH~7.4) at 485 nm and recording emission at 535 nm. The solid lines through the points are single exponential fits to the equation, $I_F = I_0 + Ae^{-t/T}$, where I_F is the fluorescence intensity at time t, I_0 is the fluorescence intensity at t=0, A is the pre-exponential factor and T is the time constant. For ss-DNA, T = 186 ± 37, 141 ± 26, 101 ± 12 for A, B and C, respectively, I_0= 0.3089 ± 0.08598, 0.3619 ± 0.0713, 0.4503 ± 0.03604, and A= 0.6395, 0.6090, and 0.4282, respectively for trials 1, 2, and 3. The solid lines through the control points are linear fits. Also shown are the fluorescence signals for

EG® alone (filled triangles) and DNA alone (open circles). Irradiated DNA concentrations are 0.060 μM (A), 0.060 μM (B), and 0.058 μM (C)**.**

Fig. 2.3 represents the fluorescence decay curves obtained from the irradiation of 0.060 μM, 0.060 μM, and 0.058 μM concentrations of ss-DNA with absorbances of 1.585, 1.585, and 1.536, respectively. The ss-DNA solutions were also irradiated up to a maximum time of 250 min. The resulting DNA damage constants are collected in Table 2.4 below. The fluorescence decay curves were obtained by the excitation of hybridization mixtures containing typically 0.0085 μM ss-DNA and 5 μM EG® μM in Tris buffer (10 mM Tris, 1 mM EDTA, 10 mM NaCl, pH~ 7.4) at 485 nm and emission recorded at 535 nm. Substantial changes in fluorescence intensity is observed until around the 170 min mark. After 170 min, the damage proceeds slowly until 250 min. The time constants obtained for trials 1, 2, and 3 using single exponential fittings were 186 ± 37 min, 141 ± 26 min, 101 ± 12 min respectively. The curves also show a continuous decrease in fluorescence until the 170 min time point where it levels off. In each trial, the unhybridized DNA alone and EG® alone samples show no fluorescence, as expected. The reason for the observed levelling-off of the fluorescence intensities at the later time points and the lack of fluorescence activity observed for both the unhybridized DNA and EG® have been discussed above.

Table 2.4 Damage time constants for ss-DNA

Trial	Concentration (μM)	Absorbance	Damage time constants (min)
1	0.060	1.585	186 ± 37
2	0.060	1.585	141 ± 26
3	0.058	1.536	101 ± 12

In this table, the UVC-induced damage time constants in minutes at various concentrations of irradiated ss-DNA in μM are shown, with their absorbance values. Results have been averaged over three trials.

Table 2.4 shows the damage time constants obtained from the three experimental trials of the ss-DNA, the respective absorbances and extrapolated Beer-Lambert concentrations of the irradiated ss-DNA solutions. UVC-induced damage time constant obtained from the first experimental trial 1 which involved the irradiation of 0.060 μM gave the most error. Although the irradiated ct-DNA solutions for trials 1 and 2 had the same concentrations, their UVC-induced damage time constants are the same within experimental error which confirms that concentration might be a determinant factor for the observed UVC-induced damage time constant differences. The possible reasons for both the large errors observed in the damage time constants and the differences in damage time constants obtained irrespective of concentration and absorbance has been explained in detail above.

Tables 2.3 and 2.4 shows that the UVC-induced damage time constants for ct-DNA and ss-DNA might not be dependent on concentration. Comparing the results from these two tables further shows some interesting relationship between the concentration of the irradiated DNA solutions and the damage time constants obtained. For the ct-DNA, trials 1 and 3 of different irradiated DNA concentrations showed similar damage time constants within experimental error, while for the ss-DNA, trials 1 and 2 of similar irradiated DNA concentrations showed similar damage time constants within the experimental error. However, it has been well established that the rate of reaction (k) for unimolecular reactions is independent of the concentration (c) of the reacting species. To further confirm that the concentration of the species had little or no effect on the rate constant, we can calculate the effect such concentration differences would have on the rate constant by using the equation, $k= \sigma I_A \phi$. Assuming that the quantum yield (ϕ) and the absorption cross section (σ) of each DNA sample were constant and solving for the rate constant ratios for two DNA samples we will have $k/k' = I_{A/} I_{A'}$. But $A=\log I_0/ I_t = \varepsilon bc$, and $I_A= I_0-I_t$. Therefore, solving for I_A as a function of concentration, we have that $A= \log (I_{A/} I_t)/I_t= \varepsilon bc$. Linearizing the equation ($10^{-x} \sim 1-x + x^2\ldots$), we have that $I_A/I_t + 1 \sim 1 + \varepsilon bc$. Substituting into the rate constant ratio equation, we arrive at $k/k' = c/c'$. Putting the concentrations and solving for the rate constant ratios for the two DNA samples used in this study, it gives approximate values of 1 and therefore it's safe to say that the rate constants in these reactions were not affected by concentration. The error observed in the UVC-induced damage time constants for the ss-DNA runs is higher than those of the ct-DNA.

Table 2.5 Average time constants of ct-DNA and ss-DNA, and their A-T % compositions.

Sample	AT composition (%)	Average Time constant (min)
ct-DNA	58.1	82 ± 13
ss-DNA	56.9	143 ± 43

In this table, the AT compositions of ct-DNA and ss-DNA in percentages and their average UVC-induced damage time constants in minutes are shown.

Table 2.5 shows the average time constants obtained over three experimental trial runs of ct-DNA and ss-DNA and their respective AT% compositions. Both ct-DNA and ss-DNA have molecular weights of 1.3×10^6 Da, with AT% compositions of 58.1 % for ct-DNA and 56.9 % for ss-DNA. ss-DNA was observed to have a slower average damage time constant of 143 ± 43 min than ct-DNA of average damage time constant of 82 ± 13 min over the three experimental runs. The slower rate of UVC-induced damage and hence the larger damage time constants observed with the ss-DNA, correlates as expected with its lower AT% composition of 56.9 % as compared to the ct-DNA. This is because studies have shown that TT sites are the most photoreactive. This therefore means that ct-DNA with a higher AT% composition with supposedly more TT dinucleotide bases, will have more photolabile sites and therefore is expected to damage faster upon sustained exposure to UVC irradiation as our results suggests. The above results consistently show a regular damage pattern with ct-DNA being more susceptible to UVC-induced damage as it has a higher AT% composition than ss-DNA.

From the data obtained from these experiments under the same conditions, it is clearly seen that ss-DNA with a higher GC composition had higher damage time constants of 186 ± 37 min, 141 ± 26 min, 101 ± 12 min while the ct-DNA had damage time constants of 92 ± 6 min, 67 ± 9 min, 87 ± 8 min over three experimental runs. Also, the kinetic fluorescence plots above show that EG® in the absence of dsDNA weakly fluoresces. The decrease in fluorescence with irradiation times, as seen in all the curves in Figures 2.2 and 2.3, shows the ability of the EG® dye to detect UVC-induced damage in both the ct-DNA and ss-DNA, which are averagely 2000 bp long. This exponential decrease in the fluorescence of EG® which can be seen from the plots

above with increased UVC irradiation time shows UVC-induced DNA damage/formation of photoproducts in both DNA samples used. The intercalation of EG® is not sequence-dependent and this makes it a better fluorescence technique when compared to other fluorescence probes such as MBs, SPs and terbium (Tb^{3+}) which are sequence dependence. Also, UVC-induced DNA damage detection using EG® as a probe provides a milder, cheaper and easier alternative than the use of MBs, Tb, SPs and chromatography-based methods. This therefore suggests that EG® can be used effectively to probe DNA damage in long nucleotide sequences up to genomic DNA damage as seen in the results obtained in this Chapter. Although this assay shows lots of promise, it is important to mention that this method is a negative DNA damage detection method that possesses an intrinsic disadvantage. This is because the undamaged DNA- EG® hybrid has a high fluorescence, with damage measured as a decrease in fluorescence intensity observed with increased irradiation time. Hence damage is measured as a function of the difference between large fluorescence values and its sensitivity might therefore be compromised. Also, the short time lag that exists between the exposure of the hybridized EG®/dsDNA in the 96-well plate and the subsequent slotting into the plate reader for fluorescence measurements is a potential source of error for this assay. The intrinsic property of EG®, having a weak background fluorescence and its ability to detect UV-induced damage in double stranded DNA makes it a more adaptable probe for the detection of UVC-induced DNA damage in realistic samples, and gives it an advantage over other fluorescence probes such as Terbium (Tb^{3+})[21] which is limited to single stranded DNA, MBs[7,8] and SPs[8] which are sequence dependent, and other DNA damage detection methods such as HPLC-MS[22,23] gel electrophoresis[24] and polymerase chain reaction (PCR)[25,26,27] which are limited to detecting only strand breaks and suffer from low sensitivity. This therefore shows that EG® is a prospective tool for UVC-induced DNA damage detection in long DNA sequences.

2.4 Conclusion

In summary, we have been able to demonstrate an assay that can detect UVC-induced DNA damage in large dsDNA sequences using ct-DNA and ss-DNA as targets with the hybridization of EG®. Our results show that the change in fluorescence intensities with increased irradiation time corresponds to the UVC-induced damage observed in these samples. The damage rates of the samples were found to be consistent with their AT % compositions with ct-DNA which has

an AT % composition of 58.1 % damaging at a faster rate than the ss-DNA with an AT % composition of 56.9 %. Although concentration is not a rate-determining factor in the reaction as expected for a unimolecular reaction, the position of the data points on each of the plots and the errors in fluorescence intensity values (which possibly came from well cross-talks) obtained for some time points influenced the damage time constants. Our results also showed that at time points from 170 min, there is little, or no damage observed which is likely because the photoreactive sites have all been damaged at this time. This assay therefore provides a cheap and sequence-independent method of detecting UVC-induced DNA damage which is an advantage as compared to earlier used DNA damage detection techniques such as HPLC-MS, MBs, SPs, and gel electrophoresis. As earlier results and discussion in this Chapter suggest, it is observed that a small variation in the AT % composition of these DNA samples alters their damage time constants in a very significant way with ct-DNA of a higher AT % composition damaging at a faster rate than the ss-DNA with both species having identical extinction coefficients and photochemical rate constants. Although this method shows great prospects for the detection of UVC-induced DNA damage in long nucleotide sequences, further analysis such as MS is still needed to both characterize and validate this method. Finally, the complete error analysis carried out showed that both the instrument a SpectraMax i3x plate reader used for the fluorescence measurements and pipetting involved in the transfer of sample aliquots contributed negligible errors to the experimental results obtained. Hence, most of the errors came from other sources.

Reference List

(1) Rastogi, R. P.; Richa; Kumar, A.; Tyagi, M. B.; Sinha, R. P. Molecular Mechanisms of Ultraviolet Radiation-Induced DNA Damage and Repair. *J. Nucleic Acids* **2010**, *2010*.

(2) Douki, T. The Variety of UV-Induced Pyrimidine Dimeric Photoproducts in DNA as Shown by Chromatographic Quantification Methods. *Photochem. Photobiol. Sci.* **2013**, *12* (8), 1286–1302.

(3) Horspool, M. W.; Song, P.-S. *CRC Handbook of Organic Photochemistry and Photobiology*, 1st ed.; Horspool, W., Song, P.-S., Eds.; CRC-Press: New York, 1995. 1297-1304

(4) Schreier, W. J.; Gilch, P.; Zinth, W. Early Events of DNA Photodamage. *Annu. Rev. Phys. Chem.* **2015**, *66* (1), 497–519.

(5) Law, Y. K.; Forties, R. A.; Liu, X.; Poirier, M. G.; Kohler, B. Sequence-Dependent Thymine Dimer Formation and Photoreversal Rates in Double-Stranded DNA. *Photochem. Photobiol. Sci.* **2013**, *12* (8), 1431–1439.

(6) Cadet, J.; Mouret, S.; Ravanat, J. L.; Douki, T. Photoinduced Damage to Cellular DNA: Direct and Photosensitized Reactions. *Photochem. Photobiol.* **2012**, *88* (5), 1048–1065.

(7) El-Yazbi, A. F.; Loppnow, G. R. Detecting UV-Induced Nucleic-Acid Damage. *TrAC - Trends Anal. Chem.* **2014**, *61*, 83–91.

(8) Cadet, J.; Weinfeld, M. Detecting DNA Damage. *Anal. Chem.* **1993**, *65* (15), 675–682.

(9) Cadet, J.; Sage, E.; Douki, T. Ultraviolet Radiation-Mediated Damage to Cellular DNA. *Mutat. Res. - Fundam. Mol. Mech. Mutagen.* **2005**, *571* (1-2 SPEC. ISS.), 3–17.

(10) El-Yazbi, A. F.; Loppnow, G. R. Chimeric RNA–DNA Molecular Beacons for Quantification of Nucleic Acids, Single Nucleotide Polymophisms, and Nucleic Acid Damage. *Anal. Chem.* **2013**, *85* (9), 4321–4327. https://doi.org/10.1021/ac301669y.

(11) Nair, S. G.; Loppnow, G. R. Multiplexed, UVC-Induced, Sequence-Dependent DNA Damage Detection. *Photochem. Photobiol.* **2013**, *89* (4), 884–890.

(12) Nair, S. G.; Loppnow, G. R. Comparison of K- Ras and N- Ras Mutagenic Hot Spots for UVC Damage. *ACS Omega* **2019**, *4* (2), 3469–3475.

(13) Shoute, L. C. T.; Loppnow, G. R. Characterization of the Binding Interactions between EvaGreen Dye and DsDNA. *Phys. Chem. Chem. Phys.* **2018**, *20* (7), 4772–4780.

(14) Khoe, C. V.; Chung, L. H.; Murray, V. The Sequence Specificity of UV-Induced DNA Damage in a Systematically Altered DNA Sequence. *J. Photochem. Photobiol. B Biol.* **2018**, *183* (March), 88–100.

(15) Patel, D. J.; Pardi, A.; Itakura, K. DNA Conformation, Dynamics, and Interactions in Solution. **1982**, *216* (May).

(16) Kastenholz, M. A.; Schwartz, T. U.; Hünenberger, P. H. The Transition between the B and Z Conformations of DNA Investigated by Targeted Molecular Dynamics Simulations with Explicit Solvation. *Biophys. J.* **2006**, *91* (8), 2976–2990.

(17) Charney, E.; Chen, H. H. Structure of A-DNA in Solution. *Proc. Natl. Acad. Sci. U. S. A.* **1987**, *84* (6), 1546–1549.

(18) Wood, B. R. The Importance of Hydration and DNA Conformation in Interpreting Infrared Spectra of Cells and Tissues. *Chem. Soc. Rev.* **2016**, *45* (7), 1980–1998.

(19) Svozil, D.; Kalina, J.; Omelka, M.; Schneider, B. DNA Conformations and Their Sequence Preferences. *Nucleic Acids Res.* **2008**, *36* (11), 3690–3706.

(20) Nielsen, P. E.; Møllegaard, N. E.; Jeppesen, C. DNA Conformational Analysis in Solution by Uranyl Mediated Photocleavage. *Nucleic Acids Res.* **1990**, *18* (13), 3847–3851.

(21) El-Yazbi, A. F.; Loppnow, G. R. Terbium Fluorescence as a Sensitive, Inexpensive Probe for UV-Induced Damage in Nucleic Acids. *Anal. Chim. Acta* **2013**, *786*, 116—123.

(22) Douki, T.; Court, M.; Sauvaigo, S.; Odin, F.; Cadet, J. Formation of the Main UV-Induced Thymine Dimeric Lesions within Isolated and Cellular DNA as Measured by High Performance Liquid Chromatography-Tandem Mass Spectrometry. *J. Biol. Chem.* **2000**, *275* (16), 11678–11685.

(23) Douki, T.; Cadet, J. Individual Determination of the Yield of the Main UV-Induced Dimeric Pyrimidine Photoproducts in DNA Suggests a High Mutagenicity of CC Photolesions. *Biochemistry* **2001**, *40* (8), 2495–2501.

(24) Vignard, J.; Mirey, G.; Salles, B. Ionizing-Radiation Induced DNA Double-Strand Breaks: A Direct and Indirect Lighting Up. *Radiother. Oncol.* **2013**, *108* (3), 362–369.

(25) Kumari, S.; Rastogi, R.; Singh, K.; Singh, S.; Sinha, R. DNA Damage: Detection Strategies. *Excli J* **2008**, *7*, 44–62.

(26) Tommasi, S.; Pfeifer, G. P. Sunlight Induces pyrimidine dimers preferentially at 5-methylcytosine bases**.** *Cancer Res,* **1997**, *57*, 4727–4730.

(27) Wang, G.; Hallberg, L. M.; Saphier, E.; Englander, E. W. Short Interspersed DNA Element-Mediated Detection of UVB-Induced DNA Damage and Repair in the Mouse Genome, in Vitro, and in Vivo in Skin. *Mutat. Res. - DNA Repair* **1999**, *433* (3), 147–157.

Chapter Three

Detection of UV-induced DNA damage in extracted cellular DNA and regular DNA samples

3.1 Introduction

The exposure of DNA to ultraviolet radiation (UVR) can lead to many potential health challenges such as aging[1], and in more serious cases skin cancer[2]. Over the years, various damage detection methods have been developed which include gel electrophoresis, mass spectrometry-based techniques, immunological techniques and others in order to detect UV-induced and other types of DNA damage[3]. While some of these methods boast good potential, they still possess some inherent properties that leaves a lot to be desired. Demerits such as low or lack of specificity towards some types of damages, poor result feedbacks, laborious sample preparation and high cost are some of the problems that are associated with some of these detection methods[4]. In order to address this, the use of the fluorescent dye EvaGreen® (EG®) as a potential tool for the detection of UVC-induced DNA damage becomes a very interesting option. With its ability to detect damage irrespective of base pair sequence and low cost, EG® provides a cost effective, easy and generalizable way of detecting UV-induced damage.

The potential use of fluorescence-based techniques in determining UV-induced DNA damage have been explored in the research literature. Fluorescence probes such as 2-aminopurine (2AP) and molecular beacons (MB) have been used in studies to detect UV-induced DNA damage[4,5]. El-Yazbi, et al. have also used chimeric RNA-DNA, analogues of MBs, to quantify nucleic acids, single nucleotide polymorphisms (SNP), and nucleic acid damage[6]. Smart probes, which are also analogues of MBs, have been used to detect UV-induced DNA damage in 96-well plates and in cuvettes[7]. Other MB analogues such as locked nucleic acid hairpin probes, and hypochromism probes have been used to detect UV-induced DNA damage[8-10]. These analogues have been found to be more cost effective than MBs with similar sensitivity to damage types in most cases, although they still suffer from demerits such as inadequate quenching that leads to background fluorescence, low sensitivities in the case of the hypochromism probes, and they are sequence specific. In other studies, other fluorescence probes such as terbium (Tb^{3+}) have both been used to detect nucleic acid damage mismatches in double stranded DNA (ds-

DNA)[11,12]. Other review articles have also highlighted the use of staining dyes as reporters in various methods used in detecting DNA damage[13,14]. Although much work continues to be done in the field of using fluorescence techniques to detect DNA damage, problems such as background fluorescence, poor selectivity based on the DNA sequence being analyzed, and the ability of the method to detect damage not just in single stranded DNA but also in double stranded DNA still persists. Also, the challenge of the cost associated with having to synthesize these probes could be overbearing and therefore leaves the researcher with a huge challenge to deal with. One of the major challenges therefore is to develop a method that is not only sequence independent but can be used to determine UV-induced damage in longer nucleotide sequence, one which will therefore have implications in trying to answer questions potentially posed in real world situations and not just confined to laboratory experiments.

The use of EG® as a potential tool for the detection of UV-induced nucleic acid damage has continued to attract numerous research interests. Interestingly, the binding interactions between EG® and DNA shows that EG® can be suitable for probing nucleic acid damage[15]. Nair, et al. have shown the differences in the mutation hotspots of the K-*Ras* and N-*Ras* using EG® as probe[16]. All of the research with EG has been done with sequences no longer than 20-30 base pairs. An open question is the applicability of this technique to longer DNA strands.

This study will investigate the potential of using EG® as a probe to detect UV-induced DNA damage in longer nucleotide sequences. The samples used in this study are DNA extracted from cultured *E. coli* cells, and DNA samples of salmon sperm (ss-DNA) and calf thymus (ct-DNA). Each DNA pair being investigated was exposed to UVC radiation simultaneously for a maximum time of 250 min at room temperature. To further confirm the results in Chapter 2, ss-DNA and ct-DNA were simultaneously exposed to UVC radiation. Because Chapter 2 has already discussed the comparison between ct-DNA and ss-DNA, this Chapter will be discussing the comparison of UVC-induced DNA damage observed from the simultaneous irradiation of the *E. coli* DNA sample with both the ct-DNA and ss-DNA as used in this study. The detection of UVC-induced DNA damage will be discussed as a function of the observed decrease in the fluorescence intensity of EG® with increased irradiation time. Also, the damage time constant results obtained for each DNA sample will be compared and discussed in correlation with their

respective AT% composition to determine UVC-induced damage susceptibilities as a function of nucleotide sequence. The supposed reasons for the errors and observed differences in the damage time constant obtained for each DNA sample across the experimental trials will not be covered in this Chapter as it has already been discussed in Chapter 2. Finally, the results obtained will show the potential of EG® as a cheap and simple method for the detection of nucleic acid damage in long nucleotide sequences.

3.2 Experimental

3.2.1 Materials

Deoxyribonucleic acid (DNA) sodium salt fiber from calf thymus (ct-DNA), protease from Streptomyces griseus, and ribonuclease (RNase, Sigma-Aldrich, Inc., Oakville, ON, Canada), 8 µM UltraPure™ salmon sperm (ss-DNA), sodium dodecyl sulfate (SDS), and buffer-saturated phenol DNA solution (ThermoFischer Scientific, Waltham MA, USA), and EvaGreen® dye solution (Biotium, Inc, Fremont, CA, USA) were all used as received without further purification. DNA samples were stored at -20 ˚C upon receipt and until needed.

3.2.2 *E. coli cell* culture growth and DNA extraction

The LB media was prepared by the combination of 10 g of tryptone, 5 g of yeast extract, 10 g of NaCl, and 1 liter of distilled water and the pH was adjusted to 7.0 with 1 N NaOH. The resulting mixture was distributed into four 250.0 mL volumetric flasks and autoclaved for 15 min at 121 °C. Upon cooling of the LB media, cells are scraped off the top of a glycerol cell stock and into the four flasks of LB media, and the cell culture was left to grow overnight at a temperature of 37 ˚C mixing at 225 revolutions per minute (RPM). A 10-fold dilution of the obtained cell culture is measured in a BioMate 3 spectrophotometer (Thermo spectronic, ThermoFischer Scientific, Waltham MA, USA) to obtain the optical density (OD) using LB media as blank. For a 250 mL cell culture, the typical OD_{600} was 3.08. Since 1 OD_{600} unit = 1×10^9 cells/mL, an *E. coli* cell culture with an OD_{600} of 3.08 will constitute 3×10^9 cells/mL.

For the *E. coli* DNA extraction, the *E. coli* cells were suspended in a Tris-EDTA (TE) (10 mM Tris, 1 mM EDTA, pH~7.6) solution and vortexed before the addition of 10% SDS solution. The 10% SDS stock solution was prepared by dissolving 10 g of SDS in 100 mL of ultrapure

water (Millipore Sigma, Burlington, MA, USA) and filtered to remove particulates. For each 250 mL *E. coli* cell culture, 20 mL of the TE buffer/SDS was used in the ratio 9:1 of buffer and SDS, respectively. 80 mg of protease was added to each cell suspension, incubated at 37 ˚C for about 3 hours and then sheared by repeatedly flowing in and out of an 18G1 needles and then a 26Gx1/2 needle. The needles were used to break up the long strands of DNA by first passing the *E. coli* cell culture through the larger 18G1 needles and finally through the 26Gx1/2 needles which are of smaller diameter to obtain smaller *E. coli* DNA fragments. The sheared *E. coli* DNA was then extracted using a 1:1 buffer-saturated phenol/chloroform mixture with the solutions continually mixed overnight using a mixer (ThermoFischer Scientific, Waltham MA, USA). The extracted mixture was spun in an Avanti J-26 XPI centrifuge (Beckman Coulter Life Sciences, Lakeview Parkway, IN, USA) using a SX 4400 rotor at 4700 RPM and 4 ˚C, and the top layer was carefully pipetted into clean falcon tubes for further extraction. This extraction was repeated at least 3 times. After extraction, 20 mL of chloroform solution was added to the extracted *E. coli* DNA to remove any phenols present. The *E. coli* DNA was precipitated by adding 5 mL of 5 M NaCl and 200 mL 95% ethanol to the aqueous solution and allowing to sit overnight at 4 ˚C. Upon precipitation, the *E. coli* DNA pellets were collected by spinning for 30 min in an Allegra X-30R centrifuge (Beckman Coulter Life Sciences, Lakeview Parkway, IN, USA) using a JLA 16-250 rotor at an RPM of 20,000g at 4 ˚C. After spinning, the ethanol/water supernatant was discarded, and the *E. coli* DNA pellets were left to sit and air dry in the fume hood for about 1 hr. Upon drying, 20 mL of TE buffer solution was added with 10 mg of RNase and the resulting mixture was mixed properly, and allowed to sit for 30 min at 37 ˚C. This was followed by the addition of 16 mL ammonium acetate and 10 mL of isopropanol, and the solution was left to sit for 10 min. The resulting solution was spun for 30 min in a JLA 16-250 rotor at an RPM of 20,000g at 4 ˚C. The solvents were discarded each time and the pellet washed twice with 200 mL 70% EtOH and spun each time for 30 min using a JLA 16-250 rotor at an RPM of 20,000g at 4 ˚C. The *E. coli* DNA pellets were left to dry overnight in a fume hood at room temperature. The dry *E. coli* DNA pellets were dissolved in TE buffer and stored at -20 ˚C until needed. To obtain the concentration of the extracted *E. coli* DNA, a 10× dilution was performed, with the absorbance (A_{260}) and concentration measured using a P360 Nanophotometer (Implen, Inc. Schatzbogen, Munich, Germany). The measured concentration of the *E. coli* DNA stock solution was 112 ng/μL with an A_{260} of 3.92, but because a 10× dilution was done, the actual

concentration of the stock solution was 1120 ng/μL. Nanopure water (Barnsted Nanopure, Boston, MA, USA) was used as a blank for all absorbance measurement with a path length of 1 mm.

3.2.3 UV irradiation (comparative experiment of ss-DNA and ct-DNA)

A 0.152 μM ct-DNA stock solution with an extrapolated Beer-Lambert law absorbance of 4.00 was prepared by dissolving 0.0393 g of the DNA salt fiber in nanopure water at room temperature in a 10.0 mL volumetric flask. A 3980 μL volume of the stock was dissolved in a 10.0 mL volumetric flask and made up to mark to give a measured absorbance of 1.597 and an extrapolated Beer-Lambert law concentration of 0.0605 μM using the expression $A = \varepsilon bc$ where ε is the molar absorptivity, b is the path length and c is concentration. For the ss-DNA, 756 μL of the 8 μM stock solution was diluted in a 10.0 mL volumetric flask to give an absorbance of 1.596 and an extrapolated Beer-Lambert law concentration of 0.0605 μM. All absorbance measurements were made at room temperature using a Shimadzu (Kyoto, Japan) UV-1280 with a path length of 1 cm and using nanopure water as blank. Samples were then vortexed pipetted into 5 mL cuvettes, irradiated and subjected to the same procedures as those used in the ct-DNA and ss-DNA comparative experiments as explained in Chapter 2.

3.2.4 UV irradiation (comparative experiment of *E. coli* DNA with ct-DNA and ss-DNA

For the *E. coli* DNA comparative experiments, a concentration of 50.0 ng/μL *E. coli* DNA solution with an A_{260} of 0.100 was prepared from the stock solution of concentration 1120 ng/μL by diluting a 446 μL aliquot of the *E. coli* DNA stock solution in a 10.0 mL volumetric flask. A concentration of 50.0 ng/μL ss-DNA used for the comparative study with the *E. coli* DNA was prepared by dissolving 47 μL of the 8 μM ss-DNA stock solution in a 10.0 mL volumetric flask to give an A_{260} of 0.101. Also, for the ct-DNA used in the *E. coli* comparative experiments, a stock solution of concentration 93.5 ng/μL with an A_{260} of 0.188 was prepared by first dissolving 0.0008 g of ct-DNA fiber in a 10.0 ml volumetric flask and leaving it overnight at -20 ˚C. The stock solution was then allowed to thaw to room temperature, and then a 50 ng/μL ct-DNA solution with an A_{260} was prepared by diluting 5348 μL of the 93.5 ng/μL stock solution in a 10.0 mL volumetric flask. All absorbance and concentration measurements were carried out at room temperature using the P360 nanophotometer with nanopure water used as blank and a 1

mm path length. Samples were vortexed, pipetted into 5 mL cuvettes, irradiated and subjected to the same procedures as those used in the ct-DNA and ss-DNA comparative experiments as explained in Chapter 2.

3.2.5 Fluorescence measurements

For the comparative experiments between the ct-DNA and ss-DNA, irradiated DNA solutions were hybridized with EG® after various amounts of irradiation time and subjected to the same procedures as detailed in Chapter 2. For both ct-DNA and ss-DNA, 84 μL of 0.0605 μM irradiated DNA aliquot was pipetted into each of two 1 mL Eppendorf tubes. Two replicate samples for each time point were obtained in this way. To each Eppendorf tube containing 84 μL of the DNA sample aliquot, 32.0 μL of 26.6 μM EG® and 60 μL of buffer (100 mM Tris, 100 mM NaCl, 1 mM EDTA, pH ~ 7.4) solution and 424 μL of nanopure were added. This gave a final DNA concentration of 0.00847 μM and a final buffer concentration of 10 mM Tris, 10 mM NaCl, 1 mM EDTA, and pH ~ 7.4. A 200 μL aliquot of this 0.00847 μM mixture for each replicate was then pipetted into a 96 well-plate (Corning Special Optics, NY, USA). The 96-well plates were incubated at 37 ˚C for 20 min in an oven in the dark before the fluorescence measurement. Fluorescence intensity measurements were then performed by using the SpectraMax (Molecular Devices, San Jose, CA, USA) i3x plate reader with the excitation and emission wavelengths set at 485 and 535 nm, respectively.

In the comparative experiments of the *E. coli* DNA with either ss-DNA or ct-DNA, irradiated DNA solutions were hybridized with EG® after various amounts of irradiation time and subjected to the same procedures as detailed in Chapter 2. For the *E. coli* DNA, ct-DNA, and ss-DNA, 138 μL of this aliquot was pipetted into each of two 1 mL Eppendorf tubes. Two replicate samples for each time point were obtained in this way. To each Eppendorf tube containing 138 μL of the DNA sample aliquot, 32.0 μL of 26.6 μM EG® and 60 μL of buffer (100 mM Tris, 100 mM NaCl, 1 mM EDTA, pH ~ 7.4) solution and 370 μL of nanopure water were added. This gave a final DNA concentration of 0.00847 μM and a final buffer concentration of 10 mM Tris, 10 mM NaCl, 1 mM EDTA, pH ~ 7.4. A 200 μL aliquot of this 0.00847 μM mixture for each replicate was then pipetted into a 96 well-plate. The 96-well plates were incubated at 37 ˚C for 20 min in an oven in the dark before the fluorescence measurement.

Fluorescence intensity measurements were then performed by using the SpectraMax i3x plate reader with the excitation and emission wavelengths set at 485 and 535 nm, respectively. For each comparative run, the absorbances and concentrations of the irradiated DNA solutions were kept as similar as possible.

3.3 Results and discussion.

In this study, we attempt to show the detection and comparison of UVC-induced DNA damage in long nucleotide sequences of ct-DNA, ss-DNA, and *E. coli* DNA samples consisting of thousands of base pairs using EG® as a probe. All samples being compared were exposed simultaneously to UVC radiation in a bid to achieve reproducibility and a direct comparison to their relative damage susceptibilities. UVC-induced DNA damage will be discussed as a function of the decrease in fluorescence intensity of EG® with increasing irradiation time. The extent or susceptibility to UVC induced damage of the various DNA samples will be discussed as a function of their AT% compositions. We also attempt to explain the potential reasons for the differences in damage time constants obtained, and the limitation of this assay towards detecting genomic UV-induced DNA damage, while also touching on its inherent advantages.

3.3.1 Simultaneous irradiation of *E. coli* DNA, ct-DNA, and ss-DNA with UVC light

In this study, samples of ct-DNA, ss-DNA and *E. coli* DNA were irradiated with UVC light for a maximum exposure time of 250 min under anoxic conditions. For the ss-DNA and ct-DNA experiments, samples were irradiated together simultaneously. For the comparison experiments involving the *E. coli* DNA, both the ss- and E. coli DNA samples and the ct- and E. coli DNA samples were irradiated together simultaneously as pairs. DNA control samples (unirradiated DNA samples) were prepared and treated under all the same conditions as the irradiated DNA samples, except that they were not exposed to UVC light. UVC-induced DNA damage was measured as a function of the exponential decrease in the fluorescence intensity of the EG® with increasing irradiation time. The intrinsically low fluorescence of free EG® and its increase in fluorescence upon intercalation with undamaged dsDNA, which plays an important role in its suitability for this study as a detection assay, has been explained in detail in the previous Chapter.

Figure 3.1 shows the kinetic plots of simultaneous UVC-irradiated ct-DNA and ss-DNA over three experimental trials. The lines are single exponential fits to the decrease in fluorescence intensity of EG® expected upon introduction of UVC-induced DNA damage into these two DNA samples (Ch. 2). Damage time constants of 87 ± 9 min, 120 ± 20 min, and 95 ± 20 min were obtained for trials 1, 2, and 3, respectively, of ct-DNA, while 94 ± 1 min, 124 ± 37 min and 117 ± 20 min were observed for trials 1, 2, and 3, respectively, of ss-DNA.

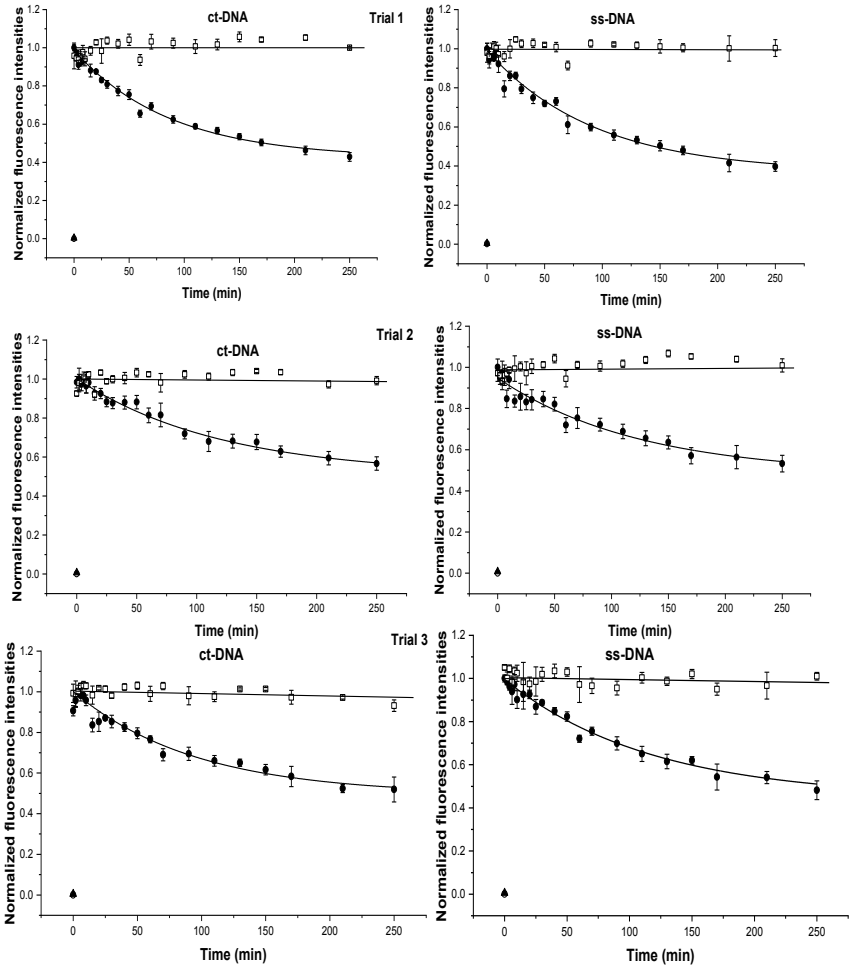

Figure 3.1. Normalized EG® fluorescence intensity as a function of UVC irradiation time for ct-DNA and ss-DNA in Trials 1, 2, and 3. EG® fluorescence detection of UVC-irradiated ct-DNA, (filled circles) and an unirradiated control (open squares) were obtained for the three experimental trials by exciting a hybridization mixture containing either 0.0085 μM ct-DNA or ss-DNA, and 5 μM EG® in Tris buffer (10 mM Tris, 1 mM EDTA, 10 mM NaCl, pH~7.4) at 485

nm and recording emission at 535 nm. The solid lines through the points are single exponential fits to the equation, $I_F = I_0 + Ae^{t/T}$, where I_F is the fluorescence intensity at time t, I_0 is the fluorescence intensity at t=0, A is the pre-exponential factor and T is the time constant. For the three ct-DNA trials, T = 87 ± 9 min, 120 ± 20 min, and 95 ± 20 min, respectively, and for the three ss-DNA trials, T = 94 ± 1 min, 124 ± 37 min, and 117 ± 20 min, respectively. For the three trials of ct-DNA, I_0= 0.4229 ± 0.02504, 0.5085 ± 0.03931 and 0.4938 ± 0.05033, respectively, and for the three trials of ss-DNA, I_0= 0.3680, 0.4796 ± 0.07219 and 0.4459 ± 0.05108, respectively. For the three ct-DNA trials, A= 0.5818, 0.4761, and 0.4572 respectively, and for the three ss-DNA trials, A= 0.6434, 0.4673, 0.5688, respectively. The solid lines through the control points are linear fits. Also shown are the fluorescence signals for EG® alone (filled triangles) and DNA alone (open circles). Irradiated DNA concentrations for ct-DNA are 0.00603 μM (1) and 0.0605 μM (2 and 3), and 0.0603 μM (1), 0.0604 μM (2) and 0.0605 μM (3) for the irradiated ss-DNA concentrations**.**

The results show that over these three experimental trials, ss-DNA had a higher damage time constant than ct-DNA. Also, it is observed from the plots that appreciable damage occurs until about the 170 min time point where it levels off. The supposed reasons for this have been extensively discussed in Chapter 2. The average damage time constant obtained for ct-DNA and ss-DNA over the three experimental trials are 101 ± 24 min and 112 ± 25 min respectively, and the reason for the differences in the damage time constants as observed for these individual samples has been discussed in Chapter 2.

Table 3.1 shows the concentrations, absorbances, and damage time constants obtained over three experimental trials for ct-DNA and ss-DNA. Trial 2 gave the most error for ss-DNA, while the errors for trials 2 and 3 were same for the ct-DNA. Trial 1 for both samples gave the least error. The concentrations and absorbances of the individual irradiated DNA samples were quite similar and the observed damage time constants were not the same within experimental error. One of the reasons why the damage time constants for the same sample differ irrespective of their similar concentrations could be because these individual experiments were done at different times and hence one or two experimental conditions might have been altered and this in

turn affects the damage time constants obtained per experiment. The explanation for the varying errors as observed in this table have been discussed extensively in Chapter 2.

Table 3.1 Damage time constants for ct-DNA and ss-DNA

Trials	DNA	Concentration (μM)	Absorbance	Damage time constants (min)
1	ct	0.060	1.591	87 ± 9
	ss	0.060	1.591	94 ± 1
2	ct	0.061	1.592	120 ± 20
	ss	0.060	1.591	124 ± 37
3	ct	0.061	1.592	95 ± 20
	ss	0.061	1.592	117 ± 20

In this table, the UVC-induced damage time constants in minutes at various concentrations in μM and resulting absorbances of ct-DNA and ss-DNA are shown. Results shown are means that have been averaged over three trials and the errors shown are one standard deviation.

Figure 3.2 shows a plot of the average damage time constants as a function of AT% composition obtained for ct-DNA and ss-DNA over three experimental trials. Ct-DNA with an AT% composition of 58.1 had a lower damage time constant (meaning that it damaged faster under the UVC irradiation conditions) than ss-DNA which has an AT% composition of 56.9 as expected. These results are indeed consistent with earlier studies and the UVC-induced susceptibilities of these two samples also followed the same trend with the results presented in Chapter 2 of this text. The expected susceptibilities of these DNA samples to UVC-induced damage as a function of their AT% composition has been discussed in detail in Chapter 2. The average damage time constants obtained for ct-DNA and ss-DNA were 101 ± 24 min and 112 ± 25 min respectively and are similar within experimental error. These average damage time constants were obtained from the three individual trials of both samples. The errors in these average damage time constants were obtained by the square root of the sum of the squares of the

standard deviations from the values of the individual damage time constants and average of the of the standard deviations of the individual damage time constants. In this way, the error propagation was ensured while calculating the average damage time constants.

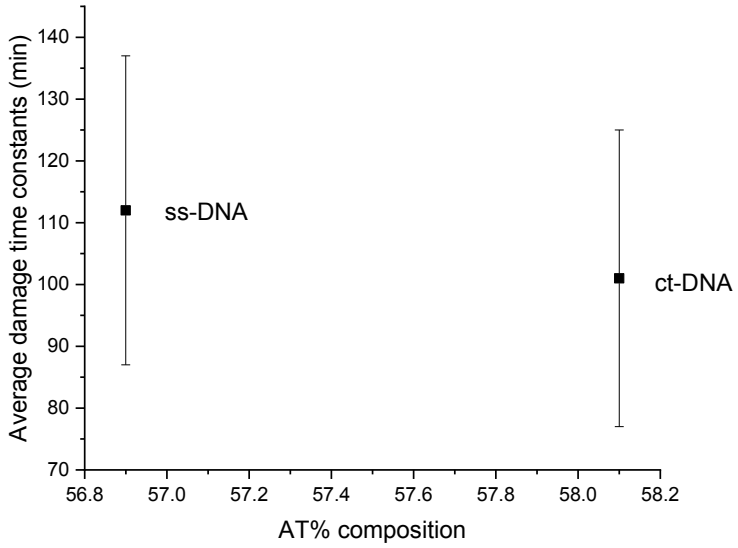

Figure 3.2. A plot of the average time constant for ct-DNA and ss-DNA as a function of their AT% composition obtained over three experimental trials. The average time constants obtained are 101 ± 24 min and 112 ± 25 min for ct-DNA and ss-DNA, respectively.

The standard deviations obtained for these average damage time constants were still fairly high when compared to the results obtained in Chapter 2, which is an indication of the error propagation from the individual damage time errors obtained from these experimental trials. Although the individual damage time constant errors appear to be slightly better than those obtained in Chapter 2 which suggests that human error may play a significant role in the uncertainties i.e., the errors improved with practice.

3.3.2 Comparison of UVC-induced DNA damage in *E. coli* DNA and ss-DNA

In this study, ss-DNA and *E. coli* (DH5α) DNA were prepared and irradiated as discussed in the experimental section. The *E. coli* DNA was approximated to 2000 bp to have the same base pair concentration for all samples. Another reason for the approximation is that at elevated base pair concentrations, a higher concentration of EG® is needed which will not be feasible as earlier

studies[15] suggest that at higher concentrations, EG® has the ability to form aggregates which will lead to unwanted loss in precision and sensitivity of the method. The approximation was calculated as per Chapter 2.

Figure 3.3 shows the fluorescence decay curves obtained from three experimental trials of simultaneous exposures of 50 ng/μL concentrations of both *E. coli* DNA and ss-DNA to UVC radiation for 250 min at room temperature. The damage time constants obtained for *E. coli* DNA were 68 ± 13 min, 65 ± 4 min, and 75 ± 13 min for trials 1, 2, and 3, respectively, and the damage time constants obtained for ss-DNA were 63 ± 5, 58 ± 4, and 68 ± 3 min for trials 1, 2, and 3, respectively. *E. coli* DNA over the three experimental trials showed a higher damage time constant than its ss-DNA counterpart. This is expected, because *E. coli* DNA has a lower AT% composition of 49.6 as compared to ss-DNA with an AT% composition of 56.9. The damage susceptibilities as a function of AT% composition for *E. coli* DNA, ss-DNA and ct-DNA will be discussed in the later part of this Chapter.

As seen in Figure 3.3 and consistently throughout this research work, damage is observed with increased UVC irradiation time as a function of the continual exponential decrease in the fluorescence intensity of EG® up until the 170 min mark where it begins to level off. The plausible reasons for this have been explained in Chapter 2. It is also important to mention that the free EG® in solution as seen from the plots had a zero-background fluorescence as with the unirradiated DNA, indicating its sensitivity as a prospective tool in detecting UVC-induced damage in long nucleotide sequences. The average damage time constant calculated from the individual damage time constants obtained from the three runs of the *E. coli* and ss-DNA as shown in plot 3.3 are 105 ± 29 min and 66 ± 12 min. These average damage time constants and their relationship with the different AT% compositions of these two samples are discussed in the appropriate section of this Chapter. The errors in the data points as seen in Figure 3.4 are improved when compared to the earlier results obtained in this Chapter and in the previous Chapter. This is because the errors improved with increased practice and hence agrees with earlier explanations that the errors in the data points are mostly due to human errors. Also, the control points in trials 1 and 2 appear to stop at the 110 min time point. This is due to insufficient control samples during the experiments. However, the plot for trial 3 shows more control points than these two. The curve for the *E. coli* DNA in trial 1 and 3 appears to be more linear which

explains the reason for the higher errors seen in the timepoints for these trails as the curve for trial 2 will fit better to the single exponential fit.

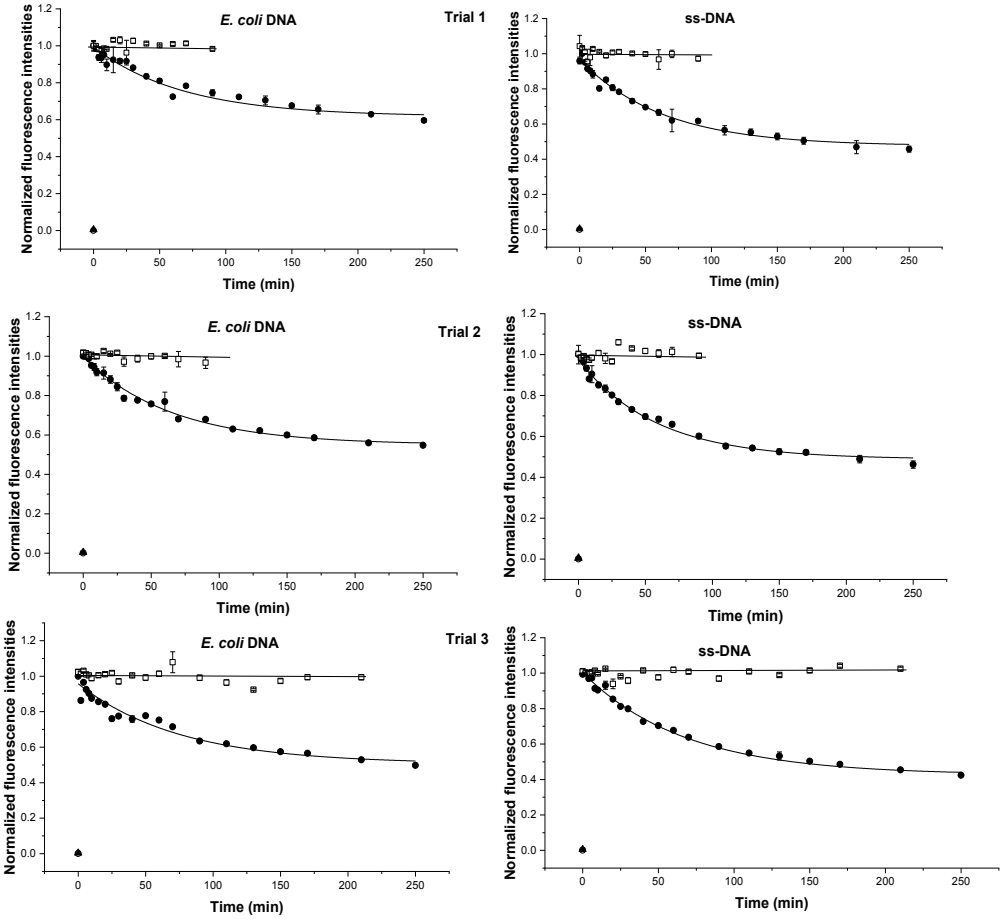

Figure 3.3. Normalized EG® fluorescence intensity as a function of UVC irradiation time for *E. coli*-DNA and ss-DNA in Trials 1, 2, and 3. EG® fluorescence detection of UVC-irradiated ss-DNA and *E. coli* DNA, (filled circles) and an unirradiated control (open squares) were obtained for the three experimental trials by exciting a hybridization mixture containing 0.0085 µM *E. coli* DNA and ss-DNA and 5 µM EG® in Tris buffer (10 mM Tris, 1 mM EDTA, 10 mM NaCl, pH~ 7.4) at 485 nm and recording emission at 535 nm. The solid lines through the points are single exponential fits to the equation, $I_F = I_0 + Ae^{t/T}$, where I_F is the fluorescence intensity at time t, I_0 is the fluorescence intensity at t=0, A is the pre-exponential factor and T is the time constant. For the three *E. coli*-DNA trials, T = 68 ± 13 min, 65 ± 4 min, and 75 ± 13 min respectively, and for the three trials of ss-DNA, T= 63 ± 5 min, 58 ± 4 min, 68 ± 3 min. For the

three trials of *E. coli*-DNA, I_0= 0.6175 ± 0.02733, 0.5498 ± 0.00857 and 0.5061 ± 0.02731, and for the three trials of ss-DNA, I_0= 0.4750 ± 0.02080, 0.4880 ± 0.01469 and 0.4261 ± 0.01038 respectively. For the three trials of *E. coli*-DNA, A= 0.3834, 0.4564, and 0.4290, and for the trials of ss-DNA, A= 0.5053, 0.5146, 0.5836. The solid lines through the control points are linear fits. Also shown are the fluorescence signals for EG® alone (filled triangles) and DNA alone (open circles). Irradiated DNA concentrations for *E. coli*-DNA and ss-DNA were 50 ng/μL for the three trials**.** Control points in trials 1 and 2 ended around the 110 min timepoint due to insufficient sample.

Table 3.2 Damage time constants for *E. coli* DNA and ss-DNA

Trials	DNA	Concentration (ng/μL)	Absorbance	Damage time constants (min)
1	*E. coli*	50.0	0.100	68 ± 13
	ss	50.0	0.100	63 ± 5
2	*E. coli*	50.0	0.100	65 ± 4
	ss	50.0	0.100	58 ± 4
3	*E. coli*	50.0	0.100	75 ± 13
	ss	50.0	0.100	68 ± 3

In this table, the UVC-induced damage time constants in minutes at various concentrations in μM and resulting absorbances of *E. coli* -DNA and ss-DNA are shown. Results shown are means that have been averaged over three trials and the errors shown are one standard deviation.

Table 3.2 represents the concentrations, absorbances, and the damage time constants obtained for *E. coli* DNA and ss-DNA over three experimental trials. As seen from the results, E. *coli* DNA had a higher damage time constant over the three experimental runs carried out. For reproducibility and precision, the concentrations and absorbance values were carefully measured

to be similar. The values of the damage time constants obtained were all similar within experimental error and were consistent through all trials, unlike those obtained in Chapter 2.

Figure 3.4 represents the correlation between the averaged UVC-induced DNA damage time constants for *E. coli* DNA and ss-DNA, and their AT% composition. The errors as calculated from the mean of three individual trials of each sample were different for the two samples. The *E. coli* DNA and the ss-DNA show similar average damage time constants within experimental errors, although *E. coli* DNA has a lower AT% composition.

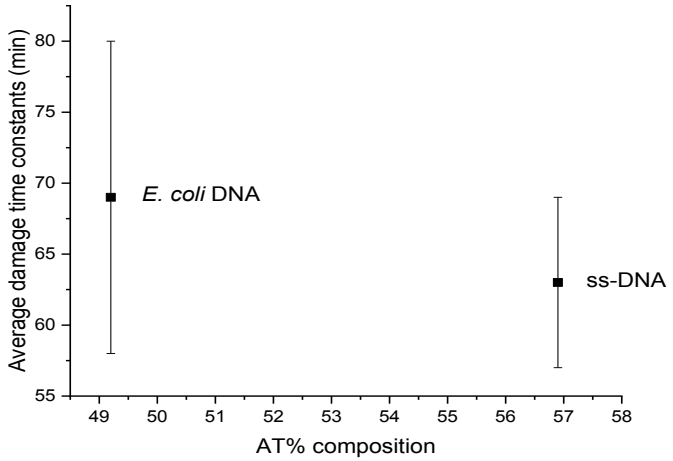

Figure 3.4. A plot of the average time constant for *E. coli* DNA and ss-DNA as a function of their AT% composition obtained over three experimental trials. The average time constants obtained are 69 ± 11 min and 63 ± 6 min for *E. coli* DNA and ss-DNA, respectively.

The large errors in the average damage time constant as seen in Figure 3.4 reflects the large errors in the individual damage time constants of the two samples over the three experimental trials.

3.3.3 Comparison of UVC-induced DNA damage in *E. coli* DNA and ct-DNA

In this section, both the *E. coli* DNA and ct-DNA were prepared as stated in the experimental section of this Chapter and were exposed simultaneously to UVC irradiation for a maximum exposure time of 250 min following the experimental procedure in Chapter two. The absorbance and concentration measurements were obtained in the same way as in the comparison experiment

of *E. coli* DNA and ss-DNA as stated in the penultimate section, with nanopure water used as a blank for the absorbance measurements.

Figure 3.5 shows the kinetic plots obtained for *E. coli* DNA and ct-DNA by simultaneously exposing each sample in a cuvette to UVC radiation. The results over the three experimental trials consistently showed that *E. coli* DNA with a lower AT% composition was damaged slower than its ct-DNA counterpart, as expected. Also, the larger AT% composition of ct-DNA means it has more photo-labile sites that are easily susceptible to UVC-induced DNA damage and hence its lower damage time constant (meaning it damages more quickly) as seen in the three experimental trials and vice versa for the *E. coli* DNA. The damage constant times obtained for the three *E. coli* DNA trials were 105 ± 33 min, 89 ± 4 min, and 120 ± 35 min respectively, while for the three ct-DNA trials, the damage time constants obtained were 68 ± 7 min, 74 ± 8 min, 56 ± 6 min respectively. The differences in the damage time constants obtained for these DNA samples as a function of their AT% compositions with increased irradiation time are indeed consistent with earlier studies which has shown that a higher AT% content in a nucleotide sequence leads to more susceptibility to UV-induced damage[16-18]. The errors were observed to be much higher for the damage time constants obtained for the *E. coli* DNA as compared to that of the ct-DNA. The supposed reasons for these errors have been discussed in Chapter 2.

The plots also show an exponential decrease in the fluorescence intensities of the two samples up to the 170 min time point where they level off for potential reasons which have been extensively discussed in Chapter 2. Both the unirradiated DNA and EG® showed no background fluorescence in all the plots, a good indication that EG® is a sensitive and potential tool for the detection of UVC-induced DNA damage in long nucleotide sequences, and that the observed decrease in fluorescence intensity as seen in these plots is due to UVC-induced DNA damage.

Although the aim of this experiments was not to determine the total time taken for the entire photolabile sites in the DNA samples used in this study to be fully damaged, it nevertheless poses both an interesting and exciting area of research to explore the time it will take all the photolabile sites in DNA to damage as a function of increased UV irradiation using EG® as probe.

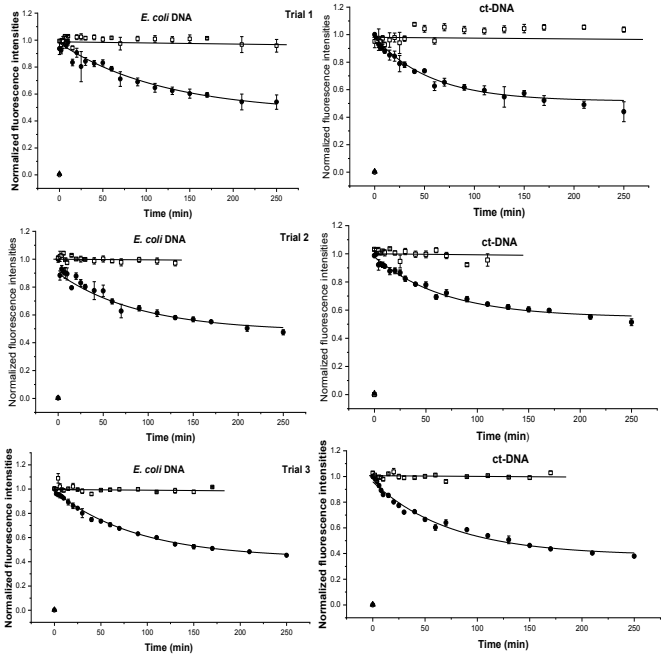

Figure 3.5. Normalized EG® fluorescence intensity as a function of UVC irradiation time for ct-DNA and *E. coli*-DNA in Trials 1, 2 and 3. EG® fluorescence detection of UVC-irradiated ct-DNA and *E. coli* DNA, (filled circles) and an unirradiated control (open squares) were obtained for the three experimental trials by exciting a hybridization mixture containing 0.0085 µM ct-DNA and *E. coli* DNA and 5 µM EG® in Tris buffer (10 mM Tris, 1 mM EDTA, 10 mM NaCl, pH~ 7.4) at 485 nm and recording emission at 535 nm. The solid lines through the points are single exponential fits to the equation, $I_F = I_0 + Ae^{t/T}$, where I_F is the fluorescence intensity at time t, I_0 is the fluorescence intensity at t=0, A is the pre-exponential factor and T is the time constant. For the three *E. coli*-DNA trials, T = 105 ± 33 min, 89 ± 4 min, and 120 ± 35 min respectively, and for the three trials of ct-DNA, T= 68 ± 7 min, 74 ± 8 min, 56 ± 6 min. For the three trials of *E. coli* DNA, I_0= 0.4610 ± 0.05522, 0.4292 ± 0.01014 and 0.4616 ± 0.07877, and for the three trials of ct-DNA, I_0= 0.5480 ± 0.01672, 0.3846 ± 0.02498 and 0.5164 ± 0.02422 respectively. For the three trials of *E. coli* DNA, A= 0.4797, 0.5628, and 0.4052. For the three

trials of ct-DNA, A= 0.4600, 0.6034, 0.5238. The solid lines through the control points are linear fits. Also shown are the fluorescence signals for EG® alone (filled triangles) and DNA alone (open circles). Irradiated DNA concentrations for *E. coli*-DNA and ss-DNA was 50 ng/μL for the three trials**.** Control points in trials 1 and 2 ended around the 110 and 170 min timepoints respectively due to insufficient sample.

Table 3.3 Damage time constants for *E. coli* DNA and ct-DNA

Trials	DNA	Concentration (ng/μL)	Absorbance	Damage time constants (min)
1	*E. coli*	50.0	0.100	105 ± 33
	ct	50.0	0.100	68 ± 7
2	*E. coli*	50.0	0.100	89 ± 4
	ct	50.0	0.100	74 ± 8
3	*E. coli*	50.0	0.100	120 ± 35
	ct	50.0	0.100	56 ± 6

In this table, the UVC-induced damage time constants in minutes at various concentrations in μM and resulting absorbances of *E. coli* -DNA and ss-DNA are shown. Results shown are means that have been averaged over three trials and the errors shown are one standard deviation.

Table 3.3 shows the damage time constants obtained for *E. coli* and ct-DNA over three experimental trials. The average time constants calculated from the individual damage time constants obtained over the three experimental trials are 105 ± 29 and 66 ± 12 for *E. coli* and ct-DNA respectively. As expected, *E. coli* DNA with a lower AT% composition of 49.2 has a higher damage time constant than the ct-DNA of AT% composition of 58.1. This therefore will suggest that the damage time constant obtained for a DNA sample is a function of its AT% composition.

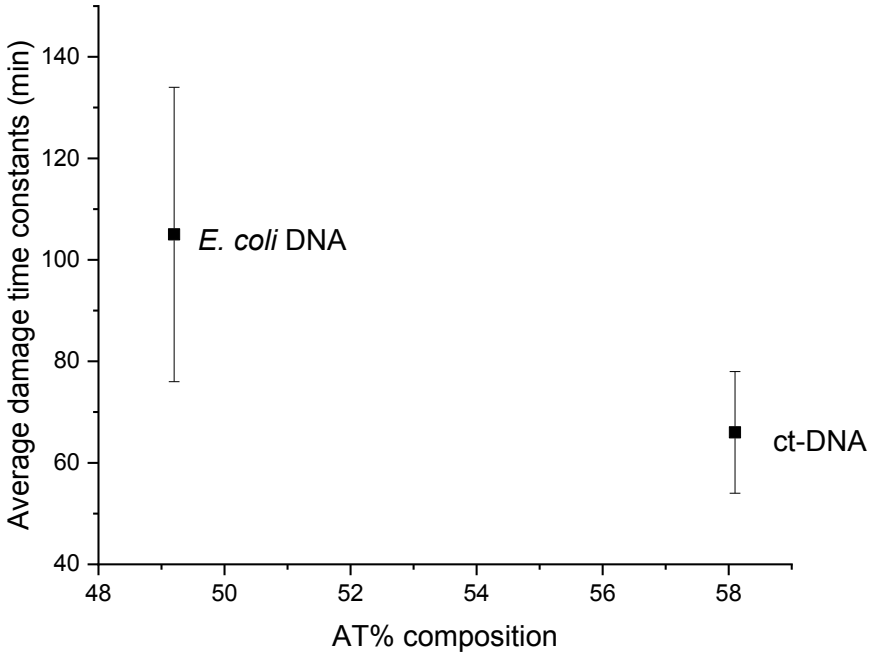

Figure 3.6. A plot of the average time constant for *E. coli* DNA and ct-DNA as a function of their AT% composition obtained over three experimental trials. The average time constants obtained are 105 ± 29 min and 66 ± 12 min for *E. coli* DNA and ct-DNA, respectively.

Figure 3.6 represents the correlation between the averaged UVC-induced DNA damage time constants for *E. coli* DNA and ct-DNA, and their AT% composition. The errors as calculated from the mean of three individual trials of each sample were higher for *E. coli* DNA than ct-DNA. The *E. coli* DNA, as expected and consistent with other results obtained, still shows a higher damage time constant (meaning it damages more slowly) than the ct-DNA, because the *E. coli* DNA has a lower AT% composition.

The consistency in the observed differences in the damage time constants obtained for the *E. coli* DNA, ct-DNA and ss-DNA confirms that the AT% composition is a determinant factor in the varying susceptibilities of DNA samples to UVC-induced DNA damage, since these samples show differences in their rate of damage with increased irradiation time when simultaneously exposed to UVC radiation at room temperature under similar conditions. With a zero-background fluorescence, the EG® probe boasts an inherent sensitivity which takes care of any

uncertainties that might arise due to inadequate quenching of the fluorophore by the quencher, a shortfall seen in other fluorescence-based techniques such as MB and the smart probes[7]. Background fluorescence can lead to insensitive and inaccurate fluorescence mediated results, as any supposed small-scale UV-induced DNA damage that might occur during the initial stages of irradiation might be lost as background fluorescence. This would have been an added demerit to this method as nucleic damage detection using EG® as probe is a negative detection technique which measures differences in fluorescence intensity values of large magnitudes with increased irradiation time.

3.4. Conclusion

The results obtained from the simultaneous irradiation of the DNA samples used in this study showed that EG® can be used as a probe to detect UV-induced DNA damage in long nucleotide sequences, with a potential of detecting nucleic acid damage up to genomic levels as can be seen from the change in fluorescence intensities as a function of increased irradiation time. Also, the rate of damage of the DNA samples which is a function of the damage time constants obtained from the fluorescence kinetic plots showed good correlation with their AT% compositions, with *E. coli* having an AT% composition of 49.2 showing the largest average damage time constant across the whole experimental trials, while ss-DNA having an AT% composition of 56.9 showed a higher average damage time constant than ct-DNA with an AT% composition of 58.1, although in the simultaneous irradiation of ct-DNA and ss-DNA, their average damage time constants appeared similar within experimental error and same goes for the simultaneous irradiation of *E. coli* DNA and ss-DNA. This therefore suggests that the AT% composition of a DNA nucleotide sequence is a major determinant factor in the damage susceptibility of the sequence, a trend that correlates positively with earlier UV-induced DNA damage studies. Finally, EG® provides a simple, sequence-independent, and cost-effective option of detecting UV-induced DNA damage.

Reference list

(1) Kligman, L. H. Photoaging. Manifestations, Prevention, and Treatment. *Dermatol. Clin.* **1986**, *4* (3), 518–528.

(2) D'Orazio, J.; Jarrett, S.; Amaro-Ortiz, A.; Scott, T. UV Radiation and the Skin. *Int. J. Mol. Sci.* **2013**, *14* (6), 12222–12248. https://doi.org/10.3390/ijms140612222.

(3) Kumari, S.; Rastogi, R.; Singh, K.; Singh, S.; Sinha, R. DNA Damage: Detection Strategies. *Excli J* **2008**, *7*, 44–62.

(4) El-Yazbi, A. F.; Loppnow, G. R. Detecting UV-Induced Nucleic-Acid Damage. *TrAC Trends Anal. Chem.* **2014**, *61*, 83–91.

(5) El-Yazbi, A. F.; Loppnow, G. R. 2-Aminopurine Hairpin Probes for the Detection of Ultraviolet-Induced DNA Damage. *Anal. Chim. Acta* **2012**, *726*, 44–49. https://doi.org/10.1016/j.aca.2012.03.021.

(6) El-Yazbi, A. F.; Loppnow, G. R. Chimeric RNA–DNA Molecular Beacons for Quantification of Nucleic Acids, Single Nucleotide Polymophisms, and Nucleic Acid Damage. *Anal. Chem.* **2013**, *85* (9), 4321–4327. https://doi.org/10.1021/ac301669y.

(7) Nair, S. G.; Loppnow, G. R. Multiplexed, UVC-Induced, Sequence-Dependent DNA Damage Detection. *Photochem. Photobiol.* **2013**, *89* (4), 884–890. https://doi.org/10.1111/php.12066.

(8) El-Yazbi, A.; Loppnow, G. R. Locked Nucleic Acid Hairpin Detection of UV-Induced DNA Damage. *Can. J. Chem.* **2011**, *89* (3), 402–408. https://doi.org/10.1139/V10-165.

(9) Oladepo, S. A.; Loppnow, G. R. Self-Quenching Smart Probes as a Platform for the Detection of Sequence-Specific UV-Induced DNA Photodamage. *Anal. Bioanal. Chem.* **2010**, *397* (7), 2949–2957. https://doi.org/10.1007/s00216-010-3896-0.

(10) El-Yazbi, A. F.; Loppnow, G. R. A Selective, Inexpensive Probe for UV-Induced Damage in Nucleic Acids. *Can. J. Chem.* **2012**, *91* (5), 320–325. https://doi.org/10.1139/cjc-2012-0417.

(11) El-Yazbi, A. F.; Loppnow, G. R. Terbium Fluorescence as a Sensitive, Inexpensive Probe for UV-Induced Damage in Nucleic Acids. *Anal. Chim. Acta* **2013**, *786*, 116–123. https://doi.org/10.1016/j.aca.2013.04.068.

(12) El-Yazbi, A. F.; Wong, A.; Loppnow, G. R. A Luminescent Probe of Mismatched DNA Hybridization: Location and Number of Mismatches. *Anal. Chim. Acta* **2017**, *994*, 92–99. https://doi.org/10.1016/j.aca.2017.09.036.

(13) Kumari, S.; Rastogi, R.; Singh, K.; Singh, S.; Sinha, R. DNA Damage: Detection Strategies. *Excli J* **2008**, *7*, 44–62.

(14) Figueroa-González, G.; Pérez-Plasencia, C. Strategies for the Evaluation of DNA Damage and Repair Mechanisms in Cancer. *Oncol. Lett.* **2017**, *13* (6), 3982–3988. https://doi.org/10.3892/ol.2017.6002.

(15) Shoute, L. C. T.; Loppnow, G. R. Characterization of the Binding Interactions between EvaGreen Dye and DsDNA. *Phys. Chem. Chem. Phys.* **2018**, *20* (7), 4772–4780. https://doi.org/10.1039/C7CP06058K.

(16) Nair, S. G.; Loppnow, G. R. Comparison of K-Ras and N-Ras Mutagenic Hot Spots for UVC Damage. *ACS Omega* **2019**, *4* (2), 3469–3475. https://doi.org/10.1021/acsomega.8b03017.

(17) Horspool, M. W.; Song, P.-S. *CRC Handbook of Organic Photochemistry and Photobiology*, 1st ed.; Horspool, W., Song, P.-S., Eds.; CRC-Press: New york, 1995.

(18) Rastogi, R. P.; Richa; Kumar, A.; Tyagi, M. B.; Sinha, R. P. Molecular Mechanisms of Ultraviolet Radiation-Induced DNA Damage and Repair. *J. Nucleic Acids* **2010**, *2010*, 592980. https://doi.org/10.4061/2010/592980.

Chapter Four

Thesis conclusion and future work

4.1 Conclusions

Our study shows that EG® has a zero-background fluorescence, thus the increase in fluorescence intensity of EG® upon interaction with dsDNA is a result of the intercalation of EG® with the stacked base pairs, consistent with earlier studies[1]. Also, the exponential decrease in the fluorescence intensities with increasing UVC irradiation time as seen in the kinetic plots shows the ability of EG® to detect UVC-induced DNA damage in long nucleotide sequences. Finally, our results consistently showed different UVC-induced damage time constants for the three different DNA samples used in this thesis, and which correlate well with their different AT% compositions. This result is also consistent with findings from earlier studies[2]. The major conclusion of this work is that EG® is a useful detection assay for DNA damage in DNA from very small oligomeric strands to genomic DNA.

As discussed in Ch. 1, other DNA damage detection techniques exist, including hair pin probes (molecular beacon probes (MB) and its analogues, smart probes (SP), and 2-amino purine (2AP) probes); MS-based methods such as LC–ESI–MS and GC-MS; methods that employ electrophoresis (halo and comet assays); immunology-based methods such as IHC and ELISA; PCR and qPCR methods; and other fluorescent techniques such as Tb^{3+}. EG® is in many ways a cheaper technique than hair pin probes and MS-based techniques, while retaining many of the same largely generalizable detection properties of electrophoretic and MS-based techniques. In addition, EG® doesn't suffer from the prospect of introducing more lesions during sample preparation unlike MS-based techniques, and also is not limited by background fluorescence which is a demerit when considering hair pin probes such as smart probes and MB analogues for DNA damage detection. It is also important to mention that because EG® is not sequence dependent, it offers a wider application range for detecting nucleic acid damage, although it can only be used to detect overall damage and is not sensitive to particular damage types. This technique therefore adds to the growing list of options available for the detection of DNA damage and in so doing overcomes inherent challenges posed by other DNA damage detection strategies as outlined above. It also opens an area of research with so much potential to explore

and which other scientists will find interesting as will be duly mentioned in the later paragraphs in this Chapter.

Although DNA damage is occurring constantly in our cells, occasionally DNA damage can lead to cancer. Therefore, developing techniques to adequately and easily detect DNA damage may improve the ability to detect and treat cancers early. For skin cancer in particular, after physical examinations have been carried out on a potential patient, there are currently two known tests used in diagnosing skin cancers which are broadly categorized as biopsy and imaging tests. Although there are several contemporary biopsy test methods which include excisional, punch, and shave biopsies, a common denominator with all the three types involves getting a tissue sample from the patient in order to obtain a detailed analysis of the suspected cancerous area of the body[3]. This is especially true in the case of the excisional biopsy method, which involves a lot of pain during the tissue extraction[3]. Imaging tests can be done by computed tomography (CT), X-ray or magnetic resonance imaging (MRI) scans, which are non-invasive and painless[3]. Although these scan tests can provide pictorial images of the affected areas to varying degrees of resolutions, invasive biopsy tests are still required. These imaging and biopsy methods therefore show a trade-off between convenience and the detailed analysis of a developing or serious cancerous tumor, but at the same time can be used in tandem to better understand the stage at which a cancerous tumor is at, and further arrive at a better analysis inference or conclusion. It also means that to better understand skin cancer tumors, more information is needed in the area of DNA damage. This information can be useful to know the mechanisms of DNA damage or what mechanism(s) may lead to the DNA becoming severely damaged enough to trigger cancer.

Furthermore, early diagnosis can help in providing information that can be used to advise the potential skin cancer patient as to when it becomes very necessary to avoid particular types of DNA insults that may lead to future damage or cancer. With that being said, the use of EG® can become a potential tool in the prognosis of skin cancer. This assay can possibly be used to detect UV-induced damage in human patients which can be made possible through fragmenting the genomic DNA up to a length within the measurable scale of EG®. This therefore offers a very cheap, mild and easy method to detect UV-induced damage in skin cancer patients without

complications. Since EG® is non-toxic and is not harmful, it therefore offers an environmentally friendly method at this point in time when the world is seriously being affected by the problems posed by climate change, and also it means it is safe to handle and does not pose a health threat to the handler.

4.2 FUTURE WORK

As with every method, there is always room for improvement and the potential to make it even better in order to overcome any inherent demerits associated with it. This therefore creates the need for further research studies. For the use of EG® as a potential probe to detect UV-induced DNA damage, further future work needs to be done which will be briefly discussed in the next paragraphs. In the grand scheme of things, the importance of research and science is appreciated for its ability to influence and add much needed quality to life. This requirement therefore means that it is important to explore the possibility of being able to adapt this technique to real life situations.

Further research needs to be carried out to determine at exactly what base pair length the use of EG® become limited. This will become helpful in knowing in a way the applicability limit of this assay as regards base pair length, and how it can be further adapted and used to determine nucleic acid damage up to genomic level. A good experimental set up for this type of analysis can involve any genomic DNA, for example extracted DNA from cultured bacteria cells.

Another possible future research project that can be done to further improve the relevance of this assay is to use it in establishing a library for the different damage kinetics/patterns of different DNA samples of different base pair compositions. Results from such experiments can be consulted at any time for either research or diagnostic purposes. Although this will probably involve a huge amount of work which will span many years, the data obtained from this sort of experiments will go a long way in providing useful mechanistic and diagnostic information for UVC-induced (indeed, any type of) DNA damage which can be consulted. Any DNA sample should be suitable for this method as the EG® detection method is sequence independent and can be potentially used to detect overall damage in any DNA sequence. Comparing the kinetic

fluorescence plots obtained from these various samples will show any differences in UVC-induced damaged profiles that might be occurring as a function of increased irradiation time

Although the purpose of this work was not to discover the total time taken for the DNA samples to fully damage on exposure to UV light, it will be interesting to adapt this method to determining the average time it takes for all the photo-labile sites of various DNA samples to damage when exposed to UV radiation. As discussed earlier, the average time it takes a DNA sample to fully damage will be very useful in both prognosis and diagnosis of skin cancer. The supposed experimental set up for this will involve an MS-based technique such as MALDI-TOF-MS to find out the time at which all the photolabile sites in the DNA are fully damaged.

Finally, studies to show if this assay can be applied to directly determine UV-induced damage in cells serves up an interesting research area, although it may be a challenge to navigate the EG® past the cell walls. One way this can be done is by irradiating cells for a period of time, extract DNA from the irradiated cells and use EG® to detect the overall UV-induced damage. Then a second experiment could be done which will involve irradiating the cells and using EG® to directly probe the UV-induced cellular DNA damage. In this case, the UV-induced DNA damage will have to be detected *in situ*. The reason is because the irradiated cells will need to be digested in order to get rid of the cell walls to enable the navigation of EG® into the cells, and hence possible detection of the potential UV-induced damage. The digestion of the cell walls can be done using ribozyme and EDTA if bacterial cells are being used. This will constitute a major breakthrough in directly detecting cellular nucleic acid damage *in situ*. Successful direct detection of DNA damage in cells using EG® could have the advantage of limiting the need for invasive biopsies to only the most critical situations.

Reference list.

(1) Shoute, L. C. T.; Loppnow, G. R. Characterization of the Binding Interactions between EvaGreen Dye and DsDNA. *Phys. Chem. Chem. Phys.* **2018**, *20* (7), 4772–4780. https://doi.org/10.1039/c7cp06058k.

(2) Nair, S. G.; Loppnow, G. R. Multiplexed, UVC-Induced, Sequence-Dependent DNA Damage Detection. *Photochem. Photobiol.* **2013**, *89* (4), 884–890. https://doi.org/10.1111/php.12066.

(3) Markman, M. Diagnosing skin cancer https://www.cancercenter.com/cancer-types/skin cancer/diagnosis-and-detection (accessed Dec 10, 2020).

Bibliography

(1) Vranken, D. Van; Weiss, G. *Introduction to Bioorganic Chemistry and Chemical Biology*; Scholl, S., Ed.; Garland Science, Taylor & Francis Group, LLC: New York, 2013; Vol. 36.

(2) Alberts, B.; Johnson, A.; Lewis, J.; Raff, M.; Roberts, K.; Peter Walter. *Molecular Biology of the Cell*, 4th ed.; Garland Science: New York, 2002.

(3) Berg, J. M.; Tymoczko, J. L.; Stryer, L. *Biochemistry*, 5th Revise.; W H Freeman & Co (Sd): New York, 2002.

(4) Brown, T. A. *Genomes*, 2nd ed.; Wiley-Liss: Oxford, 2002.

(5) Aylon, Y.; Kupiec, M. DSB Repair: The Yeast Paradigm. *DNA Repair (Amst).* **2004**, *3* (8–9), 797–815. https://doi.org/10.1016/j.dnarep.2004.04.013.

(6) Li, X.; Heyer, W. D. Homologous Recombination in DNA Repair and DNA Damage Tolerance. *Cell Res.* **2008**, *18* (1), 99–113. https://doi.org/10.1038/cr.2008.1.

(7) Barzel, A.; Kupiec, M. Finding a Match: How Do Homologous Sequences Get Together for Recombination? *Nat. Rev. Genet.* **2008**, *9* (1), 27–37. https://doi.org/10.1038/nrg2224.

(8) Corrêa, M. D. P. Amounts Observed in Brazil and South America *. **2015**, *90* (3), 297–310.

(9) Becker, M. M.; Wang, Z. Origin of Ultraviolet Damage in DNA. *J. Mol. Biol.* **1989**, *210* (3), 429–438. https://doi.org/10.1016/0022-2836(89)90120-4.

(10) Young, A. R. Acute Effects of UVR on Human Eyes and Skin. *Prog. Biophys. Mol. Biol.* **2006**, *92* (1), 80–85. https://doi.org/10.1016/j.pbiomolbio.2006.02.005.

(11) Chang, N. Bin; Feng, R.; Gao, Z.; Gao, W. Skin Cancer Incidence Is Highly Associated with Ultraviolet-B Radiation History. *Int. J. Hyg. Environ. Health* **2010**, *213* (5), 359–368. https://doi.org/10.1016/j.ijheh.2010.06.006.

(12) D'Orazio, J.; Jarrett, S.; Amaro-Ortiz, A.; Scott, T. UV Radiation and the Skin. *Int. J. Mol. Sci.* **2013**, *14* (6), 12222–12248. https://doi.org/10.3390/ijms140612222.

(13) Madan, V.; Lear, J. T.; Szeimies, R.-M. Non-Melanoma Skin Cancer. *Lancet (London, England)* **2010**, *375* (9715), 673–685. https://doi.org/10.1016/S0140-6736(09)61196-X.

(14) Alscher, R. G.; Donahue, J. L.; Cramer, C. L. Reactive Oxygen Species and Antioxidants: Relationships in Green Cells. *Physiol. Plant.* **1997**, *100* (2), 224–233. https://doi.org/10.1034/j.1399-3054.1997.1000203.x.

(15) Toyokuni, S. Oxidative Stress as an Iceberg in Carcinogenesis and Cancer Biology. *Arch. Biochem. Biophys.* **2016**, *595*, 46–49. https://doi.org/10.1016/j.abb.2015.11.025.

(16) Cooke, M. S.; Evans, M. D.; Dizdaroglu, M.; Lunec, J. Oxidative DNA Damage: Mechanisms, Mutation, and Disease. *FASEB J.* **2003**, *17* (10), 1195–1214. https://doi.org/10.1096/fj.02-0752rev.

(17) Rastogi, R. P.; Richa; Kumar, A.; Tyagi, M. B.; Sinha, R. P. Molecular Mechanisms of Ultraviolet Radiation-Induced DNA Damage and Repair. *J. Nucleic Acids* **2010**, *2010*, 592980. https://doi.org/10.4061/2010/592980.

(18) Hidaka, H.; Horikoshi, S.; Serpone, N.; Knowland, J. In Vitro Photochemical Damage to DNA, RNA and Their Bases by an Inorganic Sunscreen Agent on Exposure to UVA and UVB Radiation. *J. Photochem. Photobiol. A Chem.* **1997**, *111* (1–3), 205–213. https://doi.org/10.1016/S1010-6030(97)00229-3.

(19) Kligman, L. H. Photoaging. Manifestations, Prevention, and Treatment. *Dermatol. Clin.* **1986**, *4* (3), 517–528.

(20) Kligman, L. H.; Akin, F. J.; Kligman, A. M. The Contributions of UVA and UVB to Connective Tissue Damage in Hairless Mice. *J. Invest. Dermatol.* **1985**, *84* (4), 272–276. https://doi.org/10.1111/1523-1747.ep12265353.

(21) Kvam, E.; Tyrrell, R. M. Induction of Oxidative DNA Base Damage in Human Skin Cells by UV and near Visible Radiation. *Carcinogenesis* **1997**, *18* (12), 2379–2384. https://doi.org/10.1093/carcin/18.12.2379.

(22) Tyrrell, R. M. induction of Pyrimidine dimers in Bacterial DNA by 365 nm Radiation. *Photochem. Photobiol.* **1973**, *17* (1), 69–73. https://doi.org/10.1111/j.1751-1097.1973.tb06334.x.

(23) Perdiz, D.; Grof, P.; Mezzina, M.; Nikaido, O.; Moustacchi, E.; Sage, E. Distribution and Repair of Bipyrimidine Photoproducts in Solar UV-Irradiated Mammalian Cells. Possible Role of Dewar Photoproducts in Solar Mutagenesis. *J. Biol. Chem.* **2000**, *275* (35), 26732–26742. https://doi.org/10.1074/jbc.M001450200.

(24) Douki, T.; Reynaud-Angelin, A.; Cadet, J.; Sage, E. Bipyrimidine Photoproducts Rather than Oxidative Lesions Are the Main Type of DNA Damage Involved in the Genotoxic Effect of Solar UVA Radiation. *Biochemistry* **2003**, *42* (30), 9221–9226. https://doi.org/10.1021/bi034593c.

(25) Courdavault, S.; Baudouin, C.; Charveron, M.; Favier, A.; Cadet, J.; Douki, T. Larger Yield of Cyclobutane Dimers than 8-Oxo-7,8-Dihydroguanine in the DNA of UVA-Irradiated Human Skin Cells. *Mutat. Res. - Fundam. Mol. Mech. Mutagen.* **2004**, *556* (1–2), 135–142. https://doi.org/10.1016/j.mrfmmm.2004.07.011.

(26) El Ghissassi, F.; Baan, R.; Straif, K.; Grosse, Y.; Secretan, B.; Bouvard, V.; Benbrahim-Tallaa, L.; Guha, N.; Freeman, C.; Galichet, L.; Cogliano, V. A Review of Human Carcinogens--Part D: Radiation. *Lancet Oncol.* **2009**, *10* (8), 751–752. https://doi.org/10.1016/s1470-2045(09)70213-x.

(27) Ikehata, H.; Kawai, K.; Komura, J. I.; Sakatsume, K.; Wang, L.; Imai, M.; Higashi, S.; Nikaido, O.; Yamamoto, K.; Hieda, K.; Watanabe, M.; Kasai, H.; Ono, T. UVA1 Genotoxicity Is Mediated Not by Oxidative Damage but by Cyclobutane Pyrimidine Dimers in Normal Mouse Skin. *J. Invest. Dermatol.* **2008**, *128* (9), 2289–2296. https://doi.org/10.1038/jid.2008.61.

(28) Agar, N. S.; Halliday, G. M.; Barnetson, R. S.; Ananthaswamy, H. N.; Wheeler, M.; Jones, A. M. The Basal Layer in Human Squamous Tumors Harbors More UVA than UVB Fingerprint Mutations: A Role for UVA in Human Skin Carcinogenesis. *Proc. Natl. Acad. Sci. U. S. A.* **2004**, *101* (14), 4954 LP – 4959. https://doi.org/10.1073/pnas.0401141101.

(29) Urbach, F. Potential Effects of Altered Solar Ultraviolet Radiation on Human Skin Cancer. *Photochem. Photobiol.* **1989**, *50* (4), 507–513. https://doi.org/10.1111/j.1751-1097.1989.tb05556.x.

(30) Peak, M. J.; Peak, J. G.; Moehring, M. P.; Webb, R. B. Ultraviolet Action Spectra for DNA Dimer Induction, Lethality, and Mutagenesis in Escherichia Coli with Emphasis on the UVB Region. *Photochem. Photobiol.* **1984**, *40* (5), 613–620. https://doi.org/10.1111/j.1751-1097.1984.tb05349.x.

(31) Dylan Trotsek. *Sunscreen Photobiology.Molecular, Cellular and Physiological Aspects*; 2017; Vol. 110.

(32) Murphy, G. M. Sunblocks: Mechanisms of Action. **1999**, 34–36.

(33) Scott, L. C. Survival and Sex Ratios of the Intertidal Copepod, Tigriopus Californicus, Following Ultraviolet-B (290–320 Nm) Radiation Exposure. *Mar. Biol.* **1995**, *123* (4), 799–804. https://doi.org/10.1007/BF00349123.

(34) Peak, M. J.; Peak, J. G. Single-Strand Breaks Induced in Bacillus Subtilis DNA by Ultraviolet Light: Action Spectrum and Properties. *Photochem. Photobiol.* **1982**, *35* (5), 675–680. https://doi.org/10.1111/j.1751-1097.1982.tb02628.x.

(35) Sinha, R. P.; Dautz, M.; Häder, D. P. A Simple and Efficient Method for the Quantitative Analysis of Thymine Dimers in Cyanobacteria, Phytoplankton and Macroalgae. *Acta Protozool.* **2001**, *40* (3), 187–195.

(36) Buma, A. G. J.; De Boer, M. K.; Boelen, P. Depth Distributions of DNA Damage in Antarctic MarinE Phyto- and Bacterioplankton Exposed TO SUMMERTIME UV Radiation. *J. Phycol.* **2001**, *37* (2), 200–208. https://doi.org/10.1046/j.1529-8817.2001.037002200.x.

(37) Pakker, H.; Beekman, C.; Breeman, A. Efficient Photoreactivation of UVBR-Induced DNA Damage in the Sublittoral Macroalga Rhodymenia Pseudopalmata (Rhodophyta). *Eur. J. Phycol.* **2000**, *35* (2), 109–114. https://doi.org/10.1080/09670260010001735691.

(38) Quaite, F. E.; Sutherland, B. M.; Sutherland, J. C. Running Title: Gel Electrophoresis Assay for Pyrimidine Dimers in Plant DNA Key Words: Ozone Depletion, Ultraviolet Radiation, DNA, Pyrimidine Dimer, Gel Electrophoresis.

(39) Stein, B.; Rahmsdorf, H. J.; Steffen, A.; Litfin, M.; Herrlich, P. UV-Induced DNA Damage Is an Intermediate Step in UV-Induced Expression of Human Immunodeficiency Virus Type 1, Collagenase, c-Fos, and Metallothionein. *Mol. Cell. Biol.* **1989**, *9* (11), 5169–5181. https://doi.org/10.1128/mcb.9.11.5169.

(40) Lima-Bessa, K. M. de; Armelini, M. G.; Chiganças, V.; Jacysyn, J. F.; Amarante-Mendes, G. P.; Sarasin, A.; Menck, C. F. M. CPDs and 6-4PPs Play Different Roles in UV-Induced Cell Death in Normal and NER-Deficient Human Cells. *DNA Repair (Amst).* **2008**, *7* (2), 303–312. https://doi.org/10.1016/j.dnarep.2007.11.003.

(41) Sinha, R. P.; Häder, D.-P. UV-Induced DNA Damage and Repair: A Review. *Photochem. Photobiol. Sci.* **2002**, *1* (4), 225–236. https://doi.org/10.1039/B201230H.

(42) Taylor, J.-S.; Lu, H.-F.; Kotyk, J. J. Quantitative Conversion of the (6–4) photoproduct of TpdC to its Dewar Valence Isomer Upon Exposure to Simulated Sunlight. *Photochem. Photobiol.* **1990**, *51* (2), 161–167. https://doi.org/10.1111/j.1751-1097.1990.tb01698.x.

(43) Slieman, T. A.; Nicholson, W. L. Artificial and Solar UV Radiation Induces Strand Breaks and Cyclobutane Pyrimidine Dimers in <Em>Bacillus Subtilis</Em>

Spore DNA. *Appl. Environ. Microbiol.* **2000**, *66* (1), 199 LP – 205. https://doi.org/10.1128/AEM.66.1.199-205.2000.

(44) Nikandrova, Y.; Baumstark-Khan, C.; Horneck, G. Repair-Induced DNA Strand Breaks in UV-Irradiated Mammalian Cells. In *Fundamentals for the Assessment of Risks from Environmental Radiation*; Baumstark-Khan, C., Kozubek, S., Horneck, G., Eds.; Springer Netherlands: Dordrecht, 1999; pp 155–160. https://doi.org/10.1007/978-94-011-4585-5_20.

(45) Limoli, C. L.; Giedzinski, E.; Bonner, W. M.; Cleaver, J. E. UV-Induced Replication Arrest in the Xeroderma Pigmentosum Variant Leads to DNA Double-Strand Breaks, γ-H2AX Formation, and Mre11 Relocalization. *Proc. Natl. Acad. Sci.* **2002**, *99* (1), 233 LP – 238. https://doi.org/10.1073/pnas.231611798.

(46) Batista, L. F. Z.; Kaina, B.; Meneghini, R.; Menck, C. F. M. How DNA Lesions Are Turned into Powerful Killing Structures: Insights from UV-Induced Apoptosis. *Mutat. Res. - Rev. Mutat. Res.* **2009**, *681* (2–3), 197–208. https://doi.org/10.1016/j.mrrev.2008.09.001.

(47) Ichihashi, M. ; Ueda, M. ; Budiyanto, A. ; Bito, T. ; Oka, M. ; Fukunaga, M. ; Tsuru, K. ; Horikawa, T. UV-Induced Skin Damage. *Toxicology* **2003**, *189* (1–2), 21–39. https://doi.org/10.1016/s0300-483x(03)00150-1.

(48) Pescheck, F.; Lohbeck, K. T.; Roleda, M. Y.; Bilger, W. UVB-Induced DNA and Photosystem II Damage in Two Intertidal Green Macroalgae: Distinct Survival Strategies in UV-Screening and Non-Screening Chlorophyta. *J. Photochem. Photobiol. B Biol.* **2014**, *132*, 85–93. https://doi.org/https://doi.org/10.1016/j.jphotobiol.2014.02.006.

(49) Bérubé, R.; Drigeard Desgarnier, M.-C.; Douki, T.; Lechasseur, A.; Rochette, P. Persistence and Tolerance of DNA Damage Induced by Chronic UVB Irradiation of the Human Genome. *J. Invest. Dermatol.* **2017**, *138*. https://doi.org/10.1016/j.jid.2017.08.044.

(50) Ali, D.; Ray, R. S.; Hans, R. K. UVA-Induced Cyototoxicity and DNA Damaging Potential of Benz (e) Acephenanthrylene. *Toxicol. Lett.* **2010**, *199* (2), 193–200. https://doi.org/https://doi.org/10.1016/j.toxlet.2010.08.023.

(51) Loppnow, G. R.; Billinghurst, B. E.; Oladepo, S. A. *In Radiation Induced Molecular Phenomena in Nucleic Acids – A Comprehensive Theoretical and Experimental Analysis*

Series: Challenges and Advances in Computational Chemistry and Physics; Shukla, M. K. L., Ed.; Springer: Netherland, 2008.

(52) Horspool, M. W.; Song, P.-S. *CRC Handbook of Organic Photochemistry and Photobiology*, 1st ed.; Horspool, W., Song, P.-S., Eds.; CRC-Press: New york, 1995.

(53) Kundu, L. M.; Loppnow, G. R. Direct Detection of 8-Oxo-Deoxyguanosine Using UV Resonance Raman Spectroscopy†. *Photochem. Photobiol.* **2007**, *83* (3), 600–602. https://doi.org/doi:10.1562/2006-04-15-RA-876.

(54) Faichuk, M.; Mah, A.; Loppnow, G. R. Photochemistry of 5Fluorouracil Dideoxyribonucleoside Monophosphate. *Photochem. Photobiol.* **2007**, *83*.

(55) Horspool, L. Francesco, W. *CRC Handbook of Organic Photochemistry and Photobiology*; CRC Press: USA, 2003.

(56) Ravanat, J. L.; Douki, T.; Cadet, J. Direct and Indirect Effects of UV Radiation on DNA and Its Components. *J. Photochem. Photobiol. B.* **2001**, *63* (1–3), 88–102. https://doi.org/10.1016/s1011-1344(01)00206-8.

(57) Li, J.; Liu, Z.; Tan, C.; Guo, X.; Wang, L.; Sancar, A.; Zhong, D. Dynamics and Mechanism of Repair of Ultraviolet-Induced (6–4) Photoproduct by Photolyase. *Nature* **2010**, *466* (7308), 887–890. https://doi.org/10.1038/nature09192.

(58) Bose, S. N.; Davies, R. J.; Sethi, S. K.; McCloskey, J. A. Formation of an Adenine-Thymine Photoadduct in the Deoxydinucleoside Monophosphate d(TpA) and in DNA. *Science (80-.).* **1983**, *220* (4598), 723 LP – 725. https://doi.org/10.1126/science.6836308.

(59) Bose, S. N.; Kumar, S.; Davies, R. J.; Sethi, S. K.; McCloskey, J. A. The Photochemistry of d(T-A) in Aqueous Solution and in Ice. *Nucleic Acids Res.* **1984**, *12* (20), 7929–7947. https://doi.org/10.1093/nar/12.20.7929.

(60) Koning, T. M. G.; Davies, R. J. H.; Kaptein, R. The Solution Structure of the Intramolecular Photoproduct of d(TpA) Derived with the Use of NMR and a Combination of Distance Geometry and Molecular Dynamics. *Nucleic Acids Res.* **1990**, *18* (2), 277–284. https://doi.org/10.1093/nar/18.2.277.

(61) Pörschke, D. A Specific Photoreaction in Polydeoxyadenylic Acid. *Proc. Natl. Acad. Sci. U. S. A.* **1973**, *70* (9), 2683–2686. https://doi.org/10.1073/pnas.70.9.2683.

(62) Figueroa-González, G.; Pérez-Plasencia, C. Strategies for the Evaluation of DNA Damage and Repair Mechanisms in Cancer. *Oncol. Lett.* **2017**, *13* (6), 3982–3988. https://doi.org/10.3892/ol.2017.6002.

(63) Grimaldi, K. A.; McGurk, C. J.; McHugh, P. J.; Hartley, J. A. PCR-Based Methods for Detecting DNA Damage and Its Repair at the Sub-Gene and Single Nucleotide Levels in Cells. *Mol. Biotechnol.* **2002**, *20* (2), 181–196. https://doi.org/10.1385/MB:20:2:181.

(64) Santos, J. H.; Meyer, J. N.; Mandavilli, B. S.; Van Houten, B. Quantitative PCR-Based Measurement of Nuclear and Mitochondrial DNA Damage and Repair in Mammalian Cells. *Methods Mol. Biol.* **2006**, *314*, 183–199. https://doi.org/10.1385/1-59259-973-7:183.

(65) Senoo, T.; Yamanaka, M.; Nakamura, A.; Terashita, T.; Kawano, S.; Ikeda, S. Quantitative PCR for Detection of DNA Damage in Mitochondrial DNA of the Fission Yeast Schizosaccharomyces Pombe. *J. Microbiol. Methods* **2016**, *127*, 77–81. https://doi.org/10.1016/j.mimet.2016.05.023.

(66) De Boer, J. G.; Glickman, B. W. Mutations Recovered in the Chinese Hamster Aprt Gene after Exposure to Carboplatin: A Comparison with Cisplatin. *Carcinogenesis* **1992**, *13* (1), 15–17. https://doi.org/10.1093/carcin/13.1.15.

(67) Pfeifer, G. P.; Tornaletti, S. Footprinting with UV Irradiation and LMPCR. *Methods* **1997**, *11* (2), 189–196. https://doi.org/10.1006/meth.1996.0405.

(68) Strauss, E. C.; Orkin, S. H. Guanine-Adenine Ligation-Mediated PCR in Vivo Footprinting. *Methods* **1997**, *11* (2), 164–170. https://doi.org/10.1006/meth.1996.0402.

(69) Gowda, G. A. N.; Djukovic, D. Overview of Mass Spectrometry-Based Metabolomics: Opportunities and Challenges. *Methods Mol. Biol.* **2014**, *1198*, 3–12. https://doi.org/10.1007/978-1-4939-1258-2_1.

(70) Sato, K.; Greenberg, M. M. Selective Detection of 2-Deoxyribonolactone in DNA. *J. Am. Chem. Soc.* **2005**, *127* (9), 2806–2807. https://doi.org/10.1021/ja0426185.

(71) Dizdaroglu, M.; Coskun, E.; Jaruga, P. Measurement of Oxidatively Induced DNA Damage and Its Repair, by Mass Spectrometric Techniques. *Free Radic. Res.* **2015**, *49* (5), 525–548. https://doi.org/10.3109/10715762.2015.1014814.

(72) Gajewski, E.; Dizdaroglu, M. Hydroxyl Radical Induced Cross-Linking of Cytosine and Tyrosine in Nucleohistone. *Biochemistry* **1990**, *29* (4), 977–980. https://doi.org/10.1021/bi00456a020.

(73) Koivisto, P.; Peltonen, K. Analytical Methods in DNA and Protein Adduct Analysis. *Anal. Bioanal. Chem.* **2010**, *398* (6), 2563–2572. https://doi.org/10.1007/s00216-010-4217-3.

(74) Dizdaroglu, M.; Gajewski, E. Structure and Mechanism of Hydroxyl Radical-Induced Formation of a DNA-Protein Cross-Link Involving Thymine and Lysine in Nucleohistone. *Cancer Res.* **1989**, *49* (13), 3463–3467.

(75) Kumari, S.; Rastogi, R.; Singh, K.; Singh, S.; Sinha, R. DNA Damage: Detection Strategies. *Excli J* **2008**, *7*, 44–62.

(76) El-Yazbi, A. F.; Loppnow, G. R. Detecting UV-Induced Nucleic-Acid Damage. *TrAC Trends Anal. Chem.* **2014**, *61*, 83–91. https://doi.org/https://doi.org/10.1016/j.trac.2014.05.010.

(77) Douki, T.; Cadet, J. Individual Determination of the Yield of the Main UV-Induced Dimeric Pyrimidine Photoproducts in DNA Suggests a High Mutagenicity of CC Photolesions. *Biochemistry* **2001**, *40* (8), 2495–2501. https://doi.org/10.1021/bi0022543.

(78) Cadet, J.; Douki, T.; Frelon, S.; Sauvaigo, S.; Pouget, J.-P.; Ravanat, J.-L. Assessment of Oxidative Base Damage to Isolated and Cellular DNA by HPLC-MS/MS Measurement. *Free Radic. Biol. Med.* **2002**, *33* (4), 441–449. https://doi.org/10.1016/s0891-5849(02)00820-1.

(79) Singh, R.; Farmer, P. B. Liquid Chromatography-Electrospray Ionization-Mass Spectrometry: The Future of DNA Adduct Detection. *Carcinogenesis* **2006**, *27* (2), 178–196. https://doi.org/10.1093/carcin/bgi260.

(80) Bespalov, V. A.; Conconi, A.; Zhang, X.; Fahy, D.; Smerdon, M. J. Improved Method for Measuring the Ensemble Average of Strand Breaks in Genomic DNA. *Environ. Mol. Mutagen.* **2001**, *38* (2- 3), 166–174. https://doi.org/10.1002/em.1068.

(81) Santella, R. M. Immunological Methods for Detection of Carcinogen-DNA Damage in Humans. *Cancer Epidemiol. biomarkers Prev. a Publ. Am. Assoc. Cancer Res. cosponsored by Am. Soc. Prev. Oncol.* **1999**, *8* (9), 733–739.

(82) Waller, H.; Friess, E.; Kiefer, J. On the Immunological Detection of X-Ray Induced DNA Damage. *Radiat. Environ. Biophys.* **1981**, *19* (4), 259–264. https://doi.org/10.1007/BF01324091.

(83) L. Mitchell, D.; Clarkson, J. M. Use of Synthetic Polynucleotides to Characterise an Antiserum Made Against Uv- Irradiated Dna. *Photochem. Photobiol.* **1984**, *40* (6), 743–748. https://doi.org/10.1111/j.1751-1097.1984.tb04646.x.

(84) J. Cadet, P. V. *The Photochemistry of Nucleic Acids*; Morrison, H., Ed.; John Wiley & Sons, Ltd: New York, 1990.

(85) Cuquerella, M. C.; Lhiaubet-Vallet, V.; Cadet, J.; Miranda, M. A. Benzophenone Photosensitized DNA Damage. *Acc. Chem. Res.* **2012**, *45* (9), 1558–1570. https://doi.org/10.1021/ar300054e.

(86) Mizuno, T.; Matsunaga, T.; Ihara, M.; Nikaido, O. Establishment of a Monoclonal Antibody Recognizing Cyclobutane-Type Thymine Dimers in DNA: A Comparative Study with 64M-1 Antibody Specific for (6-4) Photoproducts. *Mutat. Res. Repair* **1991**, *254* (2), 175–184. https://doi.org/https://doi.org/10.1016/0921-8777(91)90009-E.

(87) Yatabe, Y. ALK FISH and IHC: You Cannot Have One without the Other. *Journal of thoracic oncology: official publication of the International Association for the Study of Lung Cancer*. United States April 2015, pp 548–550. https://doi.org/10.1097/JTO.0000000000000461.

(88) Peccia, J.; Hernandez, M. Rapid Immunoassays for Detection of UV-Induced Cyclobutane Pyrimidine Dimers in Whole Bacterial Cells. *Appl. Environ. Microbiol.* **2002**, *68* (5), 2542 LP – 2549. https://doi.org/10.1128/AEM.68.5.2542-2549.2002.

(89) Sokol, D. L.; Zhang, X.; Lu, P.; Gewirtz, A. M. Real Time Detection of DNA.RNA Hybridization in Living Cells. *Proc. Natl. Acad. Sci. U. S. A.* **1998**, *95* (20), 11538–11543. https://doi.org/10.1073/pnas.95.20.11538.

(90) Bonnet, G.; Tyagi, S.; Libchaber, A.; Kramer, F. R. Thermodynamic Basis of the Enhanced Specificity of Structured DNA Probes. *Proc. Natl. Acad. Sci.* **1999**, *96* (11), 6171 LP – 6176. https://doi.org/10.1073/pnas.96.11.6171.

(91) Leone, G.; van Schijndel, H.; van Gemen, B.; Kramer, F. R.; Schoen, C. D. Molecular Beacon Probes Combined with Amplification by NASBA Enable Homogeneous, Real-

Time Detection of RNA. *Nucleic Acids Res.* **1998**, *26* (9), 2150–2155. https://doi.org/10.1093/nar/26.9.2150.

(92) Beacons of Light. *Nat. Biotechnol.* **2006**, *24* (3), 303–304. https://doi.org/10.1038/nbt0306-303b.

(93) Yarasi, S.; McConachie, C.; Loppnow, G. R. Molecular Beacon Probes of Photodamage in Thymine and Uracil Oligonucleotides¶. *Photochem. Photobiol.* **2005**, *81* (2), 467–473. https://doi.org/10.1111/j.1751-1097.2005.tb00209.x.

(94) Nair, S. G.; Loppnow, G. R. Multiplexed, UVC-Induced, Sequence-Dependent DNA Damage Detection. *Photochem. Photobiol.* **2013**, *89* (4), 884–890. https://doi.org/10.1111/php.12066.

(95) Stöhr, K.; Häfner, B.; Nolte, O.; Wolfrum, J.; Sauer, M.; Herten, D.-P. Species-Specific Identification of Mycobacterial 16S RRNA PCR Amplicons Using Smart Probes. *Anal. Chem.* **2005**, *77* (22), 7195–7203. https://doi.org/10.1021/ac051447z.

(96) Knemeyer, J.-P.; Marmé, N.; Sauer, M. Probes for Detection of Specific DNA Sequences at the Single-Molecule Level. *Anal. Chem.* **2000**, *72* (16), 3717–3724. https://doi.org/10.1021/ac000024o.

(97) Heinlein, T.; Knemeyer, J.-P.; Piestert, O.; Sauer, M. Photoinduced Electron Transfer between Fluorescent Dyes and Guanosine Residues in DNA-Hairpins. *J. Phys. Chem. B* **2003**, *107* (31), 7957–7964. https://doi.org/10.1021/jp0348068.

(98) Misra, A.; Shahid, M. Immobilization of Self-Quenched DNA Hairpin Probe with a Heterobifunctional Reagent on a Glass Surface for Sensitive Detection of Oligonucleotides. *Bioorg. Med. Chem.* **2009**, *17* (16), 5826–5833. https://doi.org/10.1016/j.bmc.2009.07.015.

(99) El-Yazbi, A. F.; Loppnow, G. R. Chimeric RNA–DNA Molecular Beacons for Quantification of Nucleic Acids, Single Nucleotide Polymophisms, and Nucleic Acid Damage. *Anal. Chem.* **2013**, *85* (9), 4321–4327. https://doi.org/10.1021/ac301669y.

(100) Misra, A.; Kumar, P.; Gupta, K. C. Synthesis of Hairpin Probe Using Deoxyguanosine as a Quencher: Fluorescence and Hybridization Studies. *Anal. Biochem.* **2007**, *364* (1), 86–88. https://doi.org/10.1016/j.ab.2007.02.003.

(101) Kim, Y.; Yang, C. J.; Tan, W. Superior Structure Stability and Selectivity of Hairpin Nucleic Acid Probes with an L-DNA Stem. *Nucleic Acids Res.* **2007**, *35* (21), 7279–7287. https://doi.org/10.1093/nar/gkm771.

(102) Oladepo, S. A.; Loppnow, G. R. Self-Quenching Smart Probes as a Platform for the Detection of Sequence-Specific UV-Induced DNA Photodamage. *Anal. Bioanal. Chem.* **2010**, *397* (7), 2949–2957. https://doi.org/10.1007/s00216-010-3896-0.

(103) El-Yazbi, A. F.; Loppnow, G. R. 2-Aminopurine Hairpin Probes for the Detection of Ultraviolet-Induced DNA Damage. *Anal. Chim. Acta* **2012**, *726*, 44–49. https://doi.org/10.1016/j.aca.2012.03.021.

(104) Mao, F.; Leung, W.-Y.; Xin, X. Characterization of EvaGreen and the Implication of Its Physicochemical Properties for QPCR Applications. *BMC Biotechnol.* **2007**, *7*, 76. https://doi.org/10.1186/1472-6750-7-76.

(105) Ihrig, J.; Lill, R.; Mühlenhoff, U. Application of the DNA-Specific Dye EvaGreen for the Routine Quantification of DNA in Microplates. *Anal. Biochem.* **2007**, *359*, 265–267. https://doi.org/10.1016/j.ab.2006.07.043.

(106) González-Giraldo, Y.; Rodríguez-Dueñas, M.; Forero, D. A. Development of Novel High-Resolution Melting-Based Assays for Genotyping Two Alu Insertion Polymorphisms (FXIIIB and PV92). *Mol. Biotechnol.* **2016**, *58* (3), 197–201. https://doi.org/10.1007/s12033-016-9915-4.

(107) Wang, W.; Chen, K.; Xu, W. DNA Quantification Using EvaGreen and a Real-Time PCR Instrument. *Anal. Biochem.* **2006**, *356*, 303–305. https://doi.org/10.1016/j.ab.2006.05.027.

(108) Eischeid, A. C. SYTO Dyes and EvaGreen Outperform SYBR Green in Real-Time PCR. *BMC Res. Notes* **2011**, *4* (1), 263. https://doi.org/10.1186/1756-0500-4-263.

(109) Shoute, L. C. T.; Loppnow, G. R. Characterization of the Binding Interactions between EvaGreen Dye and DsDNA. *Phys. Chem. Chem. Phys.* **2018**, *20* (7), 4772–4780. https://doi.org/10.1039/C7CP06058K.

(110) El-Yazbi, A.; Loppnow, G. Probing DNA Damage Induced by Common Antiviral Agents Using Multiple Analytical Techniques. *J. Pharm. Biomed. Anal.* **2018**, *157*. https://doi.org/10.1016/j.jpba.2018.05.019.

(111) Nair, S. G.; Loppnow, G. R. Comparison of K-Ras and N-Ras Mutagenic Hot Spots for UVC Damage. *ACS Omega* **2019**, *4* (2), 3469–3475.

(112) Shimada, H.; Nagano, M.; Funakoshi, T.; Kojima, S. Pulmonary Toxicity of Systemic Terbium Chloride in Mice. *J. Toxicol. Environ. Health* **1996**, *48* (1), 81–92. https://doi.org/10.1080/009841096161483.

(113) Fu, P. K.-L.; Turro, C. Energy Transfer from Nucleic Acids to Tb (III): Selective Emission Enhancement by Single DNA Mismatches. *J. Am. Chem. Soc.* **1999**, *121* (1), 1–7. https://doi.org/10.1021/ja9826082.

(114) El-Yazbi, A. F.; Loppnow, G. R. Terbium Fluorescence as a Sensitive, Inexpensive Probe for UV-Induced Damage in Nucleic Acids. *Anal. Chim. Acta* **2013**, *786*, 116–123. https://doi.org/10.1016/j.aca.2013.04.068.

(115) El-Yazbi, A. F.; Wong, A.; Loppnow, G. R. A Luminescent Probe of Mismatched DNA Hybridization: Location and Number of Mismatches. *Anal. Chim. Acta* **2017**, *994*, 92–99. https://doi.org/10.1016/j.aca.2017.09.036.

(116) Nguyen, B. T.; Kang, M.-J. Application of Capillary Electrophoresis with Laser-Induced Fluorescence to Immunoassays and Enzyme Assays. *Molecules* **2019**, *24* (10). https://doi.org/10.3390/molecules24101977.

(117) Goulko, A. A. Development and Application of a Capillary Electrophoresis Immunoassay for DNA Lesions Induced by Ultraviolet Light; 2011.

(118) Le, X. C.; Xing, J. Z.; Lee, J.; Leadon, S. A.; Weinfeld, M. Inducible Repair of Thymine Glycol Detected by an Ultrasensitive Assay for DNA Damage. *Science* **1998**, *280* (5366), 1066–1069. https://doi.org/10.1126/science.280.5366.1066.

(119) Yarosh, D. B.; Boumakis, S.; Brown, A. B.; Canning, M. T.; Galvin, J. W.; Both, D. M.; Kraus, E.; O'Connor, A.; Brown, D. A. Measurement of UVB-Induced DNA Damage and Its Consequences in Models of Immunosuppression. *Methods* **2002**, *28* (1), 55–62. https://doi.org/10.1016/s1046-2023(02)00209-8.

(120) Sauvaigo, S.; Serres, C.; Signorini, N.; Emonet, N.; Richard, M.-J.; Cadet, J. Use of the Single-Cell Gel Electrophoresis Assay for the Immunofluorescent Detection of Specific DNA Damage. *Anal. Biochem.* **1998**, *259* (1), 1–7. https://doi.org/https://doi.org/10.1006/abio.1998.2628.

(121) Shaposhnikov, S.; Thomsen, P. D.; Collins, A. R. Combining Fluorescent in Situ Hybridization with the Comet Assay for Targeted Examination of DNA Damage and Repair. *Methods Mol. Biol.* **2011**, *682*, 115–132. https://doi.org/10.1007/978-1-60327-409-8_10.

(122) Shaposhnikov, S.; Frengen, E.; Collins, A. R. Increasing the Resolution of the Comet Assay Using Fluorescent in Situ Hybridization—a Review. *Mutagenesis* **2009**, *24* (5), 383–389. https://doi.org/10.1093/mutage/gep021.

(123) Rastogi, R. P.; Richa; Kumar, A.; Tyagi, M. B.; Sinha, R. P. Molecular Mechanisms of Ultraviolet Radiation-Induced DNA Damage and Repair. *J. Nucleic Acids* **2010**, *2010*.

(124) Douki, T. The Variety of UV-Induced Pyrimidine Dimeric Photoproducts in DNA as Shown by Chromatographic Quantification Methods. *Photochem. Photobiol. Sci.* **2013**, *12* (8), 1286–1302.

(125) Horspool, M. W.; Song, P.-S. *CRC Handbook of Organic Photochemistry and Photobiology*, 1st ed.; Horspool, W., Song, P.-S., Eds.; CRC-Press: New York, 1995. 1297-1304

(126) Schreier, W. J.; Gilch, P.; Zinth, W. Early Events of DNA Photodamage. *Annu. Rev. Phys. Chem.* **2015**, *66* (1), 497–519.

(127) Law, Y. K.; Forties, R. A.; Liu, X.; Poirier, M. G.; Kohler, B. Sequence-Dependent Thymine Dimer Formation and Photoreversal Rates in Double-Stranded DNA. *Photochem. Photobiol. Sci.* **2013**, *12* (8), 1431–1439.

(128) Cadet, J.; Mouret, S.; Ravanat, J. L.; Douki, T. Photoinduced Damage to Cellular DNA: Direct and Photosensitized Reactions. *Photochem. Photobiol.* **2012**, *88* (5), 1048–1065.

(129) El-Yazbi, A. F.; Loppnow, G. R. Detecting UV-Induced Nucleic-Acid Damage. *TrAC - Trends Anal. Chem.* **2014**, *61*, 83–91.

(130) Cadet, J.; Weinfeld, M. Detecting DNA Damage. *Anal. Chem.* **1993**, *65* (15), 675–682.

(131) Cadet, J.; Sage, E.; Douki, T. Ultraviolet Radiation-Mediated Damage to Cellular DNA. *Mutat. Res. - Fundam. Mol. Mech. Mutagen.* **2005**, *571* (1-2 SPEC. ISS.), 3–17.

(132) El-Yazbi, A. F.; Loppnow, G. R. Chimeric RNA–DNA Molecular Beacons for Quantification of Nucleic Acids, Single Nucleotide Polymophisms, and Nucleic Acid Damage. *Anal. Chem.* **2013**, *85* (9), 4321–4327. https://doi.org/10.1021/ac301669y.

(133) Nair, S. G.; Loppnow, G. R. Multiplexed, UVC-Induced, Sequence-Dependent DNA Damage Detection. *Photochem. Photobiol.* **2013**, *89* (4), 884–890.

(134) Nair, S. G.; Loppnow, G. R. Comparison of K- Ras and N- Ras Mutagenic Hot Spots for UVC Damage. *ACS Omega* **2019**, *4* (2), 3469–3475.

(135) Shoute, L. C. T.; Loppnow, G. R. Characterization of the Binding Interactions between EvaGreen Dye and DsDNA. *Phys. Chem. Chem. Phys.* **2018**, *20* (7), 4772–4780.

(136) Khoe, C. V.; Chung, L. H.; Murray, V. The Sequence Specificity of UV-Induced DNA Damage in a Systematically Altered DNA Sequence. *J. Photochem. Photobiol. B Biol.* **2018**, *183* (March), 88–100.

(137) Patel, D. J.; Pardi, A.; Itakura, K. DNA Conformation, Dynamics, and Interactions in Solution. **1982**, *216* (May).

(138) Kastenholz, M. A.; Schwartz, T. U.; Hünenberger, P. H. The Transition between the B and Z Conformations of DNA Investigated by Targeted Molecular Dynamics Simulations with Explicit Solvation. *Biophys. J.* **2006**, *91* (8), 2976–2990.

(139) Charney, E.; Chen, H. H. Structure of A-DNA in Solution. *Proc. Natl. Acad. Sci. U. S. A.* **1987**, *84* (6), 1546–1549.

(140) Wood, B. R. The Importance of Hydration and DNA Conformation in Interpreting Infrared Spectra of Cells and Tissues. *Chem. Soc. Rev.* **2016**, *45* (7), 1980–1998.

(141) Svozil, D.; Kalina, J.; Omelka, M.; Schneider, B. DNA Conformations and Their Sequence Preferences. *Nucleic Acids Res.* **2008**, *36* (11), 3690–3706.

(142) Nielsen, P. E.; Møllegaard, N. E.; Jeppesen, C. DNA Conformational Analysis in Solution by Uranyl Mediated Photocleavage. *Nucleic Acids Res.* **1990**, *18* (13), 3847–3851.

(143) El-Yazbi, A. F.; Loppnow, G. R. Terbium Fluorescence as a Sensitive, Inexpensive Probe for UV-Induced Damage in Nucleic Acids. *Anal. Chim. Acta* **2013**, *786*, 116—123.

(144) Douki, T.; Court, M.; Sauvaigo, S.; Odin, F.; Cadet, J. Formation of the Main UV-Induced Thymine Dimeric Lesions within Isolated and Cellular DNA as Measured by High Performance Liquid Chromatography-Tandem Mass Spectrometry. *J. Biol. Chem.* **2000**, *275* (16), 11678–11685.

(145) Douki, T.; Cadet, J. Individual Determination of the Yield of the Main UV-Induced Dimeric Pyrimidine Photoproducts in DNA Suggests a High Mutagenicity of CC Photolesions. *Biochemistry* **2001**, *40* (8), 2495–2501.

(146) Vignard, J.; Mirey, G.; Salles, B. Ionizing-Radiation Induced DNA Double-Strand Breaks: A Direct and Indirect Lighting Up. *Radiother. Oncol.* **2013**, *108* (3), 362–369.

(147) Kumari, S.; Rastogi, R.; Singh, K.; Singh, S.; Sinha, R. DNA Damage: Detection Strategies. *Excli J* **2008**, *7*, 44–62.

(148) Tommasi, S.; Pfeifer, G. P. Sunlight Induces pyrimidine dimers preferentially at 5-methylcytosine bases**.** *Cancer Res,* **1997**, *57*, 4727–4730.

(149) Wang, G.; Hallberg, L. M.; Saphier, E.; Englander, E. W. Short Interspersed DNA Element-Mediated Detection of UVB-Induced DNA Damage and Repair in the Mouse Genome, in Vitro, and in Vivo in Skin. *Mutat. Res. - DNA Repair* **1999**, *433* (3), 147–157.

(150) Kligman, L. H. Photoaging. Manifestations, Prevention, and Treatment. *Dermatol. Clin.* **1986**, *4* (3), 518–528.

(151) D'Orazio, J.; Jarrett, S.; Amaro-Ortiz, A.; Scott, T. UV Radiation and the Skin. *Int. J. Mol. Sci.* **2013**, *14* (6), 12222–12248. https://doi.org/10.3390/ijms140612222.

(152) Kumari, S.; Rastogi, R.; Singh, K.; Singh, S.; Sinha, R. DNA Damage: Detection Strategies. *Excli J* **2008**, *7*, 44–62.

(153) El-Yazbi, A. F.; Loppnow, G. R. Detecting UV-Induced Nucleic-Acid Damage. *TrAC Trends Anal. Chem.* **2014**, *61*, 83–91. https://doi.org/https://doi.org/10.1016/j.trac.2014.05.010.

(154) El-Yazbi, A. F.; Loppnow, G. R. 2-Aminopurine Hairpin Probes for the Detection of Ultraviolet-Induced DNA Damage. *Anal. Chim. Acta* **2012**, *726*, 44–49. https://doi.org/10.1016/j.aca.2012.03.021.

(155) El-Yazbi, A. F.; Loppnow, G. R. Chimeric RNA–DNA Molecular Beacons for Quantification of Nucleic Acids, Single Nucleotide Polymophisms, and Nucleic Acid Damage. *Anal. Chem.* **2013**, *85* (9), 4321–4327. https://doi.org/10.1021/ac301669y.

(156) Nair, S. G.; Loppnow, G. R. Multiplexed, UVC-Induced, Sequence-Dependent DNA Damage Detection. *Photochem. Photobiol.* **2013**, *89* (4), 884–890. https://doi.org/10.1111/php.12066.

(157) El-Yazbi, A.; Loppnow, G. R. Locked Nucleic Acid Hairpin Detection of UV-Induced DNA Damage. *Can. J. Chem.* **2011**, *89* (3), 402–408. https://doi.org/10.1139/V10-165.

(158) Oladepo, S. A.; Loppnow, G. R. Self-Quenching Smart Probes as a Platform for the Detection of Sequence-Specific UV-Induced DNA Photodamage. *Anal. Bioanal. Chem.* **2010**, *397* (7), 2949–2957. https://doi.org/10.1007/s00216-010-3896-0.

(159) El-Yazbi, A. F.; Loppnow, G. R. A Selective, Inexpensive Probe for UV-Induced Damage in Nucleic Acids. *Can. J. Chem.* **2012**, *91* (5), 320–325. https://doi.org/10.1139/cjc-2012-0417.

(160) El-Yazbi, A. F.; Loppnow, G. R. Terbium Fluorescence as a Sensitive, Inexpensive Probe for UV-Induced Damage in Nucleic Acids. *Anal. Chim. Acta* **2013**, *786*, 116–123. https://doi.org/10.1016/j.aca.2013.04.068.

(161) El-Yazbi, A. F.; Wong, A.; Loppnow, G. R. A Luminescent Probe of Mismatched DNA Hybridization: Location and Number of Mismatches. *Anal. Chim. Acta* **2017**, *994*, 92–99. https://doi.org/10.1016/j.aca.2017.09.036.

(162) Kumari, S.; Rastogi, R.; Singh, K.; Singh, S.; Sinha, R. DNA Damage: Detection Strategies. *Excli J* **2008**, *7*, 44–62.

(163) Figueroa-González, G.; Pérez-Plasencia, C. Strategies for the Evaluation of DNA Damage and Repair Mechanisms in Cancer. *Oncol. Lett.* **2017**, *13* (6), 3982–3988. https://doi.org/10.3892/ol.2017.6002.

(164) Shoute, L. C. T.; Loppnow, G. R. Characterization of the Binding Interactions between EvaGreen Dye and DsDNA. *Phys. Chem. Chem. Phys.* **2018**, *20* (7), 4772–4780. https://doi.org/10.1039/C7CP06058K.

(165) Nair, S. G.; Loppnow, G. R. Comparison of K-Ras and N-Ras Mutagenic Hot Spots for UVC Damage. *ACS Omega* **2019**, *4* (2), 3469–3475. https://doi.org/10.1021/acsomega.8b03017.

(166) Horspool, M. W.; Song, P.-S. *CRC Handbook of Organic Photochemistry and Photobiology*, 1st ed.; Horspool, W., Song, P.-S., Eds.; CRC-Press: New york, 1995.

(167) Rastogi, R. P.; Richa; Kumar, A.; Tyagi, M. B.; Sinha, R. P. Molecular Mechanisms of Ultraviolet Radiation-Induced DNA Damage and Repair. *J. Nucleic Acids* **2010**, 592980. https://doi.org/10.4061/2010/592980.

(168) Shoute, L. C. T.; Loppnow, G. R. Characterization of the Binding Interactions between EvaGreen Dye and DsDNA. *Phys. Chem. Chem. Phys.* **2018**, *20* (7), 4772–4780. https://doi.org/10.1039/c7cp06058k.

(169) Nair, S. G.; Loppnow, G. R. Multiplexed, UVC-Induced, Sequence-Dependent DNA Damage Detection. *Photochem. Photobiol.* **2013**, *89* (4), 884–890. https://doi.org/10.1111/php.12066.

(170) Markman, M. Diagonising skin cancer https://www.cancercenter.com/cancer-types/skin-cancer/diagnosis-and-detection (accessed Dec 10, 2020).

(171) Oliveira Brett, A. M.; Serrano, S. H. P.; Piedade, A. J. P. Chapter 3 - Electrochemistry of DNA. In *Applications of Kinetic Modelling*; Compton, R. G., Hancock, G. B. T.-C. C. K., Eds.; Elsevier, 1999; Vol. 37, pp 91–119. https://doi.org/https://doi.org/10.1016/S0069-8040(99)80008-9.